Dissertation

submitted to the

Combined Faculty of Natural Sciences and Mathematics

of the Ruperto Carola University of Heidelberg, Germany

for the degree of

Doctor of Natural Sciences

Presented by

M.Sc. Nuttarak Sasipong

Born in: Bangkok, Thailand

Oral examination: 10th October 2019

Targeted overexpression of relaxin receptor 1 (RXFP1) with chronic administration of relaxin as a novel inotropic approach for heart failure treatment

Referees: Prof. Dr. rer. nat. Markus Hecker

Prof. Dr. med. Patrick Most

Table of Contents

Abbreviations and Symbols

List of Figures

List of Tables

1 Abbreviations and Symbols

AAV	Adeno-associated virus	**Prefixes**	
AC	Adenylyl cyclase	k	kilo-10^3
Ad	Adenovirus	c	centi-10^{-2}
Akt	Protein kinase B	m	milli-10^{-3}
ANP	Atrial natriuretic peptide	μ	micro-10^{-6}
AP	Action Potential	n	nano-10^{-9}
BNP	B-type natriuretic peptide	p	pico-10^{-12}
cAMP	Cyclic adenosine monophosphate		
cDNA	Complementary DNA		
cGMP	Cyclic guanosine monophosphate		
CMV	Cytomegalovirus		
DMEM	Dulbecco's Modified Eagle Medium		
DNA	Deoxyribonucleic acid		
E. coli	Escherichia coli		
eGFP	Enhanced green fluorescent protein		
ER	Endoplasmic reticulum		
ERK	Extracellular signal regulated kinase		
FCS	Fetal calf serum		
GAPDH	Glyceraldehyde 3-phosphate dehydrogenase	**Symbols**	
GPCR	G-protein coupled receptor	~	Approximately
HEK	Human embryonic kidney cell	°C	Degree Celsius
HF	Heart failure	ANOVA	Analysis of variance
ISO	Isoproterenol	Ca^{2+}	Calcium
ITR	Inverted terminal repeat	CO_2	Carbon dioxide
LB	Luria-Bertani medium	ddH_2O	Double-distilled water
LV	Left ventricle	EtOH	Ethanol
LVEF	Left ventricular ejection fraction	g	Gram
MMPs	Matrix metalloproteinases	h	Hour
mRNA	Messenger RNA	H_2O	Water
NOS	Nitric oxide synthases	i.p.	Intraperitoneal
NRACM	Neonatal rat atrial cardiomyocytes	I.U.	International unit
NRVCM	Neonatal rat ventricular cardiomyocytes	i.v.	Intravenous
PBS	Phosphate buffered saline	kb	Kilo bases
PCR	Polymerase chain reaction	kDa	Kilodalton
PEI	Polyethylenimine	L	Liter

PFA	Paraformaldehyde	M	Molar (mol/L); also molar mass (g/mol)
PI3K	Phosphoinositide 3-kinase	m	Meter
PKA	Protein kinase A	Max	Maximum
PKC	Protein kinase C	Min	Minute
PLB	Phospholamban	MOI	Multiplicity of infection
P-PLB(S16)	Phosphorylated phospholamban at serine 16	mol	Mole
P-PLB(T17)	Phosphorylated phospholamban at threonine 17	n	Number of experimental replicates
RLN	Relaxin	NaCl	Sodium Chloride
RNA	Ribonuclic acid	NO	Nitric oxide
RV	Right ventricle	OD	Optical density
RXFP1	Relaxin family peptide receptor 1	P/S	Penicillin-streptomycin
RyR2	Ryanodine receptor	pH	Negative decimal logarithm of the hydrogen ion concentration
SERCA2a	Sarco/endoplasmic reticulum Ca^{2+}-ATPase	RPM	Rounds per minute
SR	Sarcoplasmic reticulum	s.c.	Subcutaneous
SV40	Simian vacuolating virus 40	V	Volt
TAC	Trans-aortic constriction	vg	Viral genome
βAR	β-adrenergic receptor	Δ	Difference

2 Summary

2.1 German

Trotz des Fortschritts in der modernen Medizin ist die Herzinsuffizienz nach wie vor eine der häufigsten Todesursachen in den Industrieländern. Die Herzinsuffizienz ist eine fortschreitende Erkrankung, die das Herz allmählich beeinträchtigt. Sie ist allgemeiner Endpunkt aller Herzerkrankungen und es gibt derzeit keine ursächliche Behandlung. Therapeutische Ansätze zur Behandlung der Herzinsuffizienz konzentrieren sich lediglich darauf, das Fortschreiten der Erkrankung zu verlangsamen oder zu verhindern, aber sie zielen nicht auf die zugrunde liegenden molekularen Veränderungen im Herzen ab. Daher sind neuartige therapeutische Ansätze erforderlich, um die zugrunde liegenden Ursachen der Herzinsuffizienz wirksam zu behandeln. Relaxin (RLN) und dessen Rezeptor, RXFP1, haben in letzter Zeit aufgrund zahlreicher vorteilhafter Effekte besonders im Zusammenhang mit kardiovaskulären Erkrankungen Aufmerksamkeit erregt. Es wurde beobachtet, dass die Aktivierung von RXFP1 durch RLN neben vasodilativen, antifibrotischen und antiapoptotischen Effekten auch positiv intrope Wirkungen sowohl im insuffizienten als auch im gesunden Vorhof-Myokard hat. Interessant ist dabei, dass Vorhöfe und Ventrikel ein unterschiedliches RXFP1-Expressionsmuster aufweisen und ventrikuläre Kardiomyozyten daher nicht auf eine RLN-Behandlung ansprechen.

Ziel dieser Arbeit war es daher, die Effekte einer Kombinationstherapie aus ektoper ventrikulärer RXFP1-Expression und exogener RLN-Stimulation in einem Herzinsuffizienz-Modell zu untersuchen. Hierzu wurden Mäuse einer transaortalen Konstriktion (TAC) unterzogen, um eine Herzinsuffizienz herbeizuführen. Anschließend wurde bei den Mäusen zunächst ein Gentransfer mittels Adeno-assoziierter Viren (AAV) durchgeführt und schließlich durch Implantation osmotischer Pumpen eine chronische RLN-Gabe erreicht.

Durch den AAV-vermittelten Gentransfer wurde eine stabile Überexpression von RXFP1 im ventrikulären Myokard erreicht. Nebenwirkungen der viralen Behandlung konnten weder in gesunden noch in insuffizienten Tieren beobachtet werden. Die Kombination aus RXFP1-Gentherapie und chronischer RLN-Gabe erzielte eine deutliche Verbesserung der TAC-induzierten Herzinsuffizienz, während die alleinige RXFP1-Gentherapie die Tiere zumindest vor der Entwicklung einer schweren Herzinsuffizienz schützte. Die Aktivierung von RXFP1 hatte einen signifikanten Einfluss auf die cAMP-Akkumulation und die Phosphorylierung von Phospholamban (PLB) an Serin-16. Dies führte

zu einem höheren Ca^{2+}-Gehalt im Sarkoplasmatischen Retikulum (SR), was wiederum die positive Inotropie bedingt haben könnte.

Insgesamt konnte in der vorliegenden Arbeit gezeigt werden, dass ein gentherapeutischer Ansatz, bestehend aus RXFP1-Überexpression und gleichzeitiger RLN-Gabe, eine Aktivierung inotroper Signalwege im ventrikulären Myokard induziert, was schließlich zu einer deutlichen Verbesserung der Pumpfunktion in einem murinen Herzinsuffizienz-Modell geführt hat.

2.2 English

Despite advances in modern medicine, heart failure (HF) is one of the leading causes of death in developed countries. HF is a progressive condition that gradually affects the heart. It is a common end point for all heart diseases. There is no definite treatment currently available. Therapeutic approaches focus on slowing the progress of the disease but do not treat the underlining molecular changes in the heart. Therefore, a novel approach is needed to effectively treat the underlining molecular causes of HF. Relaxin (RLN) and its cognate receptor, RXFP1, have recently gained recognition in the setting of cardiovascular disease because of their beneficial vasodilator, anti-fibrotic, anti-apoptotic, and other properties. Furthermore, studies have shown that activation of RXFP1 by RLN induces positive inotropic effects from both failing and non-failing atrial myocardium. Interestingly, ventricular cardiomyocytes do not respond to RLN treatment due to a distinct RXFP1 expression pattern between atria and ventricles.

Thus, the aim of this study was to investigate the effects of a combined RXFP1 gene transfer with RLN stimulation in the setting of a murine HF model. A trans-aortic constriction (TAC) operation was performed on mice to induce HF. Adeno-associated virus (AAV) was used for gene transfer followed by chronic RLN administration via osmotic pumps. Further investigation of the RXFP1 signaling pathway was also performed in an *in vitro* setting to support the findings from the *in vivo* model.

AAV transduction achieved a stable overexpression of RXFP1 in the ventricle. No adverse effect from the viral treatment was detected in either healthy or HF animals. RXFP1 gene therapy with chronic RLN administration was able to rescue TAC induced HF, while RXFP1 gene therapy alone only protected the animals from the development of severe HF. RXFP1 activation significantly affected cAMP accumulation and phosphorylation of phospholamban (PLB) at serine 16 leading to an increase in sarcoplasmic reticulum (SR) Ca^{2+} content which might explain the observed positive inotropy. Prolonged RXFP1 activation did not result in detrimental Ca^{2+} mishandling like other inotropic stimuli. Finally, the RXFP1-RLN signaling pathway resembled that of other β-adrenergic signaling pathways but with a significant reduction in initial activation strength, which seemed to be pivotal for prolonged inotropic effects and favorable molecular changes.

In conclusion, gene therapy treatment consisting of RXFP1 overexpression and chronic RLN administration could rescue HF by artificially inducing inotropic responses in the ventricle through ectopic expression of RXFP1 with RLN administration.

3 Introduction

3.1 Heart failure

3.1.1 Epidemiology and definition of heart failure

Heart failure (HF) is one of the leading causes of death in developed countries [1]. It is responsible for 17 million deaths worldwide and 23 million adults are currently living with HF [2]. In Germany, approximately 26,000 new cases of HF are diagnosed annually [3].

HF is a chronic progressive condition that affects the pumping power of the heart muscles. The condition is defined by a reduced ability of the heart to pump sufficient oxygenated blood to meet the body's requirements [4]. Symptoms attributed to the progression of HF include reduced contractility, reduced energy metabolism, chronic neuroendocrine activity and increase incidence of both atrial and ventricular arrhythmias [5, 6].

3.1.2 Causes of HF

HF is a result of trigger events that damages cardiac muscle and impairs cardiac myocytes. This initial trigger event can have a sudden onset (e.g. myocardial infraction) or a gradual insidious onset (e.g. volume overloading or hemodynamic pressure) or hereditary [7]. Conditions such as hypertension, faulty valve conditions, cardiomyopathy, congenital heart defects and coronary artery disease may result in HF if left untreated [8]. Chronic diseases such as diabetes, obesity, and sleep apnea may increase the risk of HF [8, 9]. Chronic drug, tobacco, and alcohol use also increase the risk of HF at an earlier age [9].

3.1.3 Different types of HF

Left ventricular heart failure can be classified into two types which are heart failure with reduced ejection fraction (HFrEF), and heart failure with preserved ejection fraction (HFpEF). In HFrEF, the left ventricle loses its ability to properly contract. This leads to insufficient pumping force to push blood through the circulatory system [10, 11]. To compensate for the insufficient output, the left ventricle pumps harder and grows weaker and thinner. As a consequence, blood flows backwards into organs leading to fluid buildup in the lungs and/or swelling (edema) in other parts of the body [6]. In contrast, HFpEF, occurs when the left ventricle becomes stiffened and loses its ability to properly relax. This leads to insufficient filling of blood into the LV during the resting period and ultimately results in a reduction of blood pumped out to the body [5, 12]. Overtime this causes blood to build up

inside the left atrium and lung leading to fluid congestion and classical symptoms of HF [13, 14].

3.1.4 Molecular alteration leading to heart failure

Cardiac remodeling, inflammation, and oxidative stress all play a role in altering transcriptional regulator networks that could consequently lead to the development of HF [15, 16]. HF is a progressive disease that gradually develops after the initial triggering event. The body will activate compensatory mechanisms to oppose the declined cardiac output [17, 18]. One prominent compensatory mechanism is the activation of the sympathetic nervous system and stimulation of β-Adrenergic Receptors (β-AR) [19, 20]. These receptors respond to a variety of stimuli (e.g. exercise, blood loss, increased sympathetic tone, etc.) to increase cardiac output, by altering cardiac rate (chronotropism), cardiac contraction (inotropism) and cardiac relaxation (lusitropism). The two types of β-ARs, β_1 and β_2, are expressed in the heart
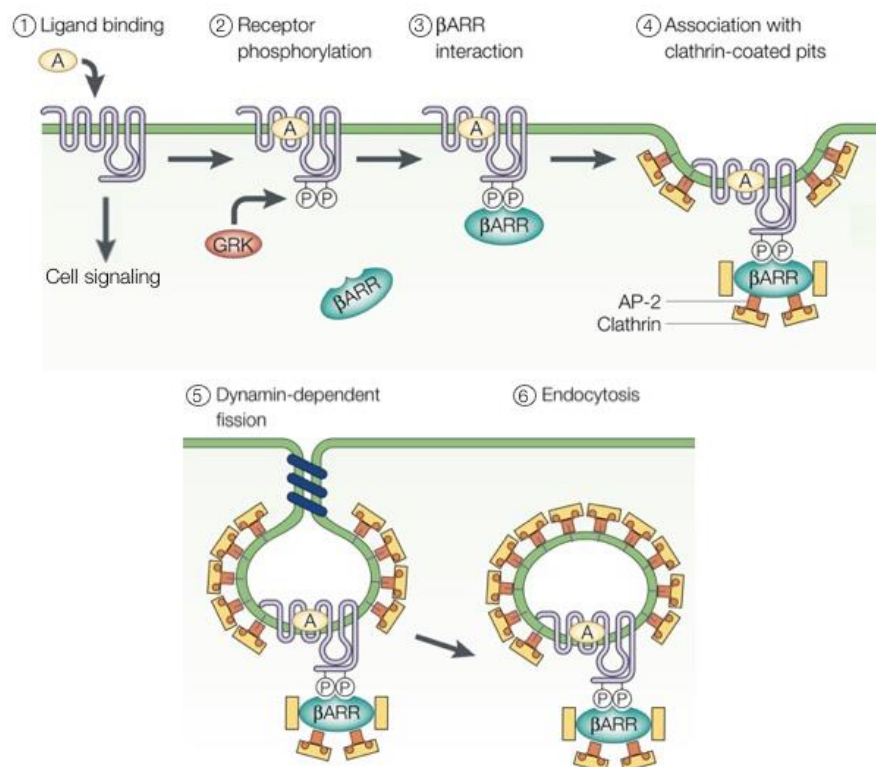
Figure 1: Prolonged activation of β-Adrenergic receptors leads to HF.
(1) After ligand (A) binds to GPCR, normal cell signaling occurs, **(2)** After a prolonged period of activation, GRKs phosphorylate residues in the carboxyl tail of GPCRs, **(3)** Phosphorylation of carboxyl tail leads to recruitment of β-arrestin (βARR), **(4)** β-arrestins recruit clathrin and AP-2 complex, **(5)** GPCRs are targeted for clathrin-mediated endocytosis, **(6)** Endocytosis GPCRs can be recycled or reinserted into the membrane. The figure was modified from Pierce et al. [21].

in a ratio of 70%:30% [22, 23]. Both types of receptors are responsible for increased cardiac contractility and heart rate [24]. After cardiac remodeling starts to manifest and cardiac output declines, the body will increase cardiac output by increasing sympathetic tone leading to hyper-activation of β-ARs. Prolonged activation of β-ARs leads to desensitization and internalization of the β-receptors by β-arrestins (βARRs), which results in a blunted cardiac contractile response to β-adrenergic activation [18, 20] (Figure 1). Accompanying the reduction in βARs density is the alteration of β-adrenergic signaling [25]. Moreover, marked increase in $G\alpha_i$ expression leads to a decrease in $G\alpha_s$:$G\alpha_i$ ratio [26]. A down regulation of AC V and AC VI has also been reported [27]. These changes in the β-adrenergic signaling pathway lead to a decrease in cAMP production, PKA activation and PLB phosphorylation. These alterations result in SERCA2a inactivation which decreases cardiac relaxation. Hajjar et al. reported that a decrease in SERCA2a expression and activity in HF could impair SR Ca^{2+} reuptake and consequently diastolic dysfunction. Altogether these changes in βAR signaling pathway and effector proteins gradually blunt and worsen cardiac responses upon adrenergic stimulation. As a result, left ventricular function deteriorates, leading to subsequent cardiac decompensation, and ultimately symptomatic HF [28].

3.1.5 Current treatments and prognosis

While mild HF can be treated with lifestyle changes and medications, current therapeutic options for treating advanced HF are limited to preventive and supportive treatments. Figure 2 shows therapeutic algorithm for patients with symptomatic HFrEF. The most common treatment for advanced HF is pharmacological treatment using a combination of different medications that target renin-angiotensin-aldosterone and the sympathetic nervous system to reduce neuroendocrine activity and increase cardiac output [29, 30]. The treatment usually starts with an Angiotensin-converting enzyme inhibitor (ACE-I) and a β-blocker. If still symptomatic, mineralocorticoid receptor (MR) antagonist can be added, and ACE-I can be replaced with an angiotensin receptor neprilysin inhibitor (ARNI) [6, 31]. In severe cases, implantation of an automatic implantable cardioverter defibrillator (AICD) might be indicated to prevent sudden cardiac death, and in terminal HF cases, implantation of ventricular assist device or heart transplantation could be indicated [32].
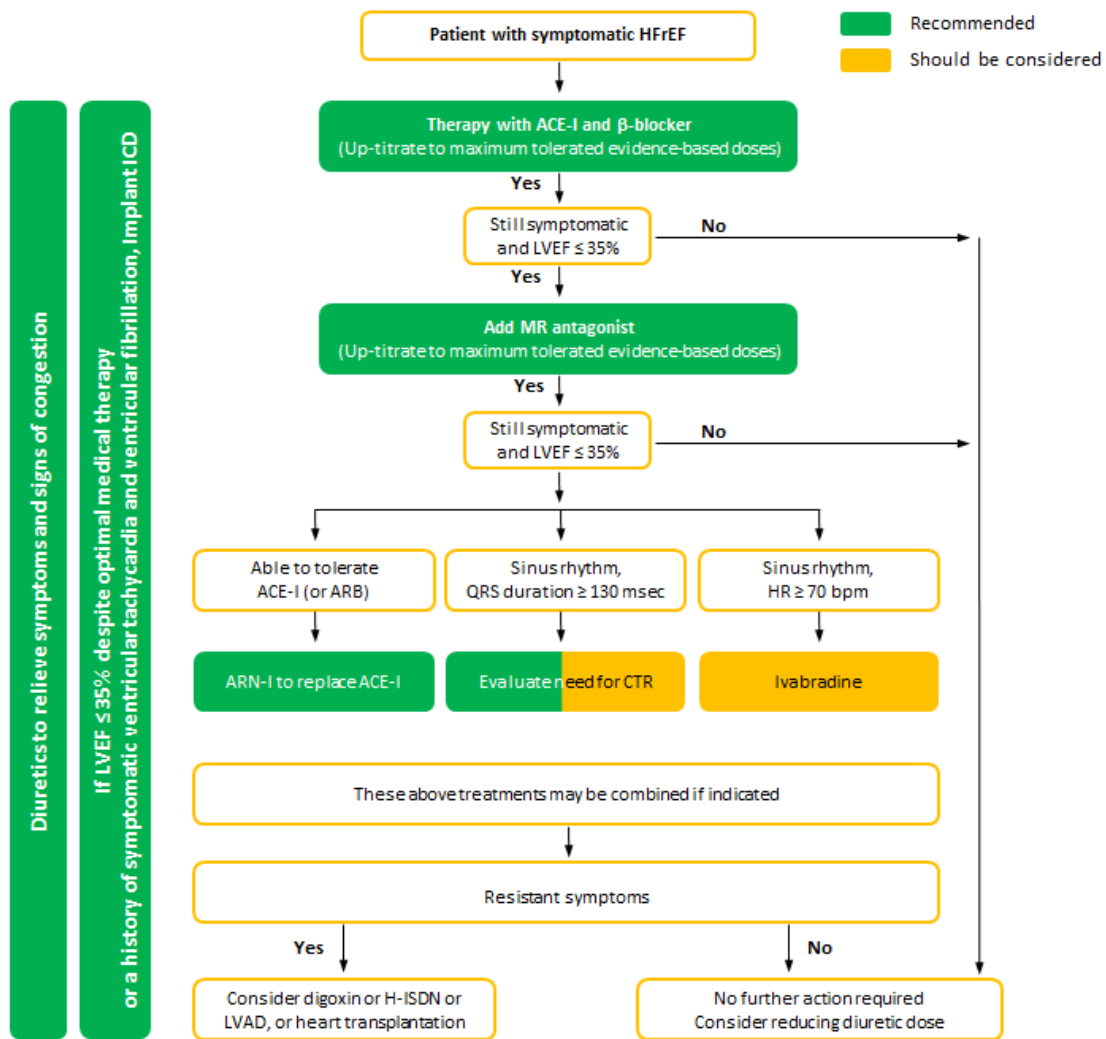
Figure 2: Therapeutic algorithm for a patient with symptomatic HFrEF.
Green indicates recommended treatments and yellow indicates treatments that should be considered. ACEI = angiotensin-converting enzyme inhibitor; ARB = angiotensin receptor blocker; ARNI = angiotensin receptor neprilysin inhibitor; CRT = cardiac resynchronization therapy; H-ISDN = hydralazine and isosorbide dinitrate; ICD = implantable cardioverter defibrillator; MR = mineralocorticoid receptor. The figure was modified from Panikowski et al. [6].

These pharmacological and surgical treatments for HF are designed to only correct the body's compensatory mechanisms and pathways to decelerate the progression of the disease and increase the lifespan for patients. However, they do not correct the underlying molecular causes of HF which are the pathological changes within the cardiomyocytes. A recent study also revealed that these treatments do not increase the quality of life for the patients because a high rate of re-hospitalization is still observed (up to 20% re-hospitalize within 1 month and 50% within 1 year [33]). This frequent hospitalization also leads to a heavy financial burden on the healthcare system which will only increase overtime [34].

Therefore, there is a need for novel therapeutic approaches in order to stop, treat, and, reverse the progression of HF. For the past two decades, researches and doctors have discovered numerous molecular mechanisms that control cardiac function in both the physiological and pathophysiological states. These discoveries couple with recent advancement in gene therapy techniques could potentially be used to develop a novel gene therapy treatment that can correct the underlying molecular causes of HF.

3.2 Relaxin

3.2.1 Relaxin structure and expression pattern
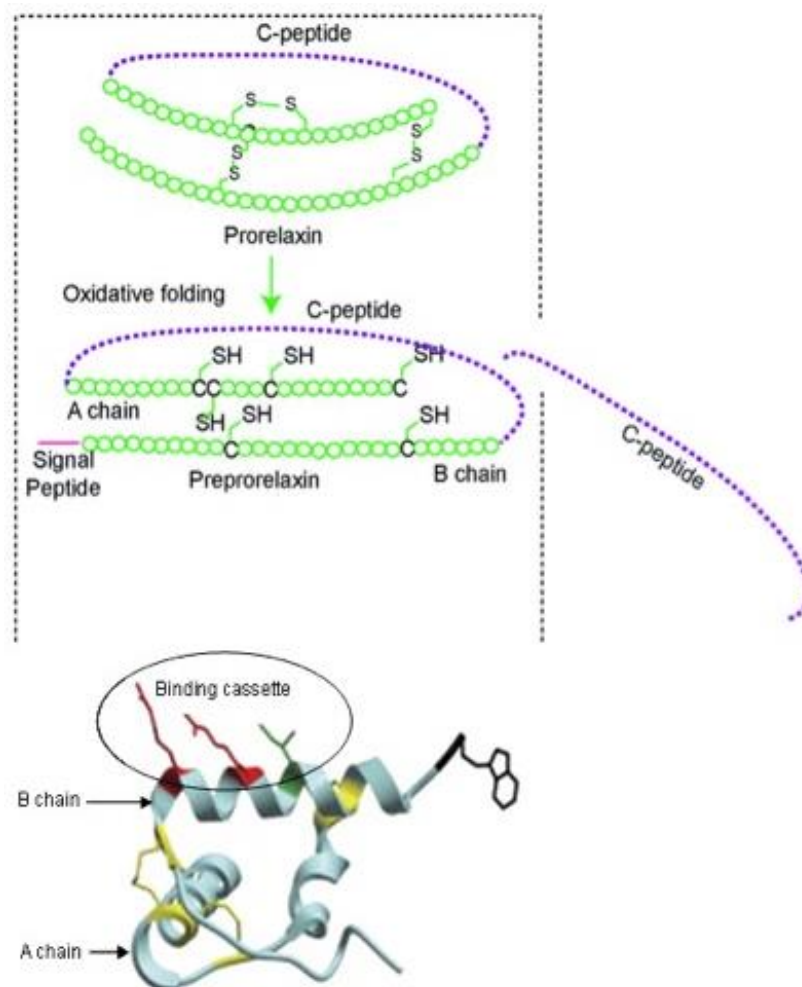
Figure 3: Structure of RLN H2.
RLN H2 is synthesized as a prorelaxin consisting of 3 chains: A, B, and C. When the peptide matures, the C chain is cleaved, and the A and B chains are linked together with disulfide bonds. The binding site of RLN H2 resides on the B chain as depicted. The figure was modified from Hossain et al. and Westhuizen et al. [35, 36].

Relaxin (RLN) is a 6 kDa hormone (Figure 3). It was formerly known as a pregnancy hormone, secreted during pregnancy to adjust the cardiovascular system and prepare the uterus for the process of birth [37-39]. Similar to insulin, RLN is a heterodimeric protein consisting of two peptide chains, A-(24 amino acids) and B-(29 amino acids) linked by 2 disulfide bonds [40, 41].

The relaxin gene is located on chromosome 9. The encoded protein is synthesized as a single chain called prorelaxin [42]. Prorelaxin contains an additional C-chain that connects the two active chains, A and B. Upon secretion, the additional C-chain is cleaved and the disulfide bonds form, turning the prorelaxin into mature RLN with A- and B-chains connected [43]. There are a total of 3 disulfide bonds in a mature RLN. The disulfide bonds are located between: 1) Cysteine 10 and 15 of the A and B chains, 2) Cysteine 11 of the A and the B chains, and 3) Cysteine 24 of the A chain and Cysteine 23 of the B chain [44]. The concentration of RLN is increased in the female reproductive organs during menstruation and pregnancy [45]. However, RLN mRNA is also detectable in other organs such as the heart, kidneys, brain, lung, liver and blood vessels [37, 46, 47]. In humans, the insulin superfamily contains three isoforms of relaxin (RLN H1-H3) [48, 49]. RLN H2 is the only prominent form that can be detected within the circulatory system [50]. In mice, there are two isoforms which are RLN H1 and RLN H3 [50]. RLN H1 in mice is comparable to RLN H2 in humans.

Studies on the RLN H2 structure have shown that the active site of RLN H2 most likely consists of the mid region of the B chain and the C-terminal region of the A chain [51]. Moreover, a comparison study of the structure of RLN H2 in different species revealed a remarkable sequence similarity in the mid region of the B chain, where two arginine residues are located [52]. Studies have shown that the two arginine residues, along with isoleucine at position 20 on the B chain, are important for interaction with RXFP1 [53, 54].

3.2.2 Role of relaxin in the cardiovascular system

In the cardiovascular system, RLN is an effective regulator of hemodynamics and contributes to positive inotropic, positive chronotropic, and lusitropic responses only in the atria of the heart [55]. RLN regulates vascular tone by increasing nitric oxide production leading to a decrease in systemic pressure [38].

Introduction
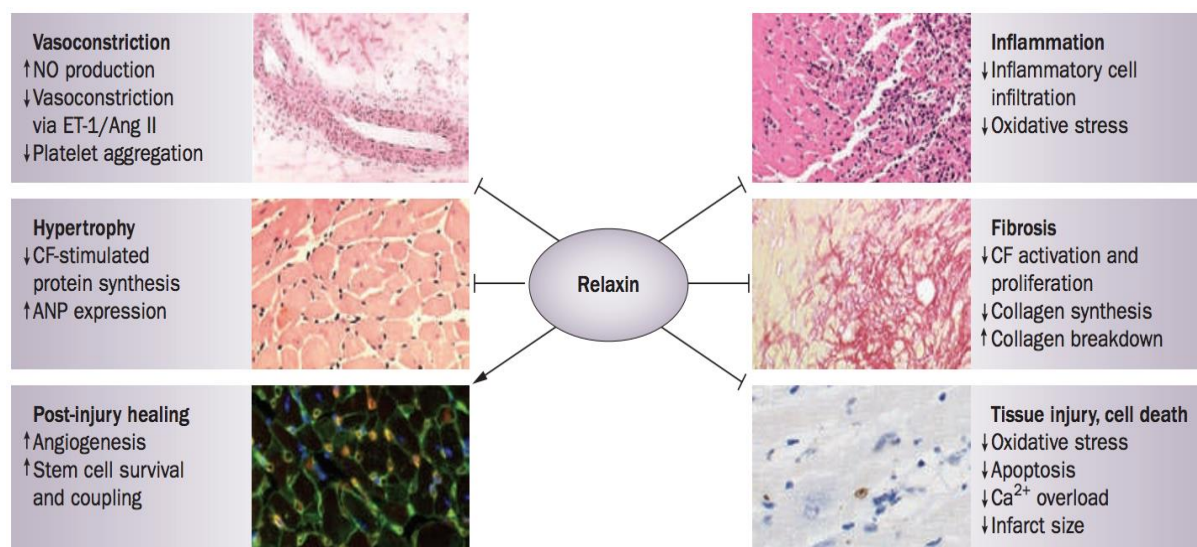
Figure 4: Effects of RLN in the cardiovascular system.
Summary of the RLN effects in the cardiovascular system based on experimental studies using a variety of animal models. In the diagram, ↑ and ↓ indicate increase and decrease, respectively. *Abbreviations*: Ang II, angiotensin II; ANP, atrial natriuretic peptide; CF, cardiac fibroblast; ET-1, endothelin-1; NO, nitric oxide [56].

RLN exerts its cardioprotective effects during myocardia injury by preventing fibroblast differentiation into myofibroblast and decreasing myocytes apoptosis after cardiac damage [57]. The study done by Debrah et al. also revealed that RLN can induce favorable hemodynamic changes (i.e. it reduced afterload and increased cardiac index) in an experimental hypertensive HF model [58]. Figure 4 summarizes the effects of RLN in the cardiovascular system. Boccalini et al. showed that RLN also has anti-ischemic and anti-inflammatory effects and could stimulate angiogenesis in ischemia reperfusion models by upregulation of VEGF to protect the heart from ischemia and reperfusion injury [59]. One study also showed that RLN could promote maturation of neonatal-cardiomyocytes in mouse [60]. Finally, RLN also produces strong positive inotropic effects in the atrial myocardium from both failing and non-failing heart by affecting PKA activation, transient potassium current, and calcium accumulation within the sarcoplasmic reticulum [61, 62].

3.2.3 Secretion of relaxin during decompensated HF

In 2001, Dschietzig et al. reported that the plasma levels of RLN in HF patients correlated to the severity of the disease, especially during the decompensation period [46] (Figure 5). Several follow up studies with larger cohorts also confirmed the elevated levels of RLN during the decompensation period but could not find a correlation between RLN concentration and the severity of HF [63-65]. Additional studies identified RLN as a

compensatory mediator of HF [46, 64]. During the decompensation period, the heart upregulates the RLN gene to produce and release RLN into the circulatory system; as a consequent, systemic concentration of RLN increases during decompensated HF, and might lead to an increase in cardiac output and a decrease systemic vascular resistant [46, 64].
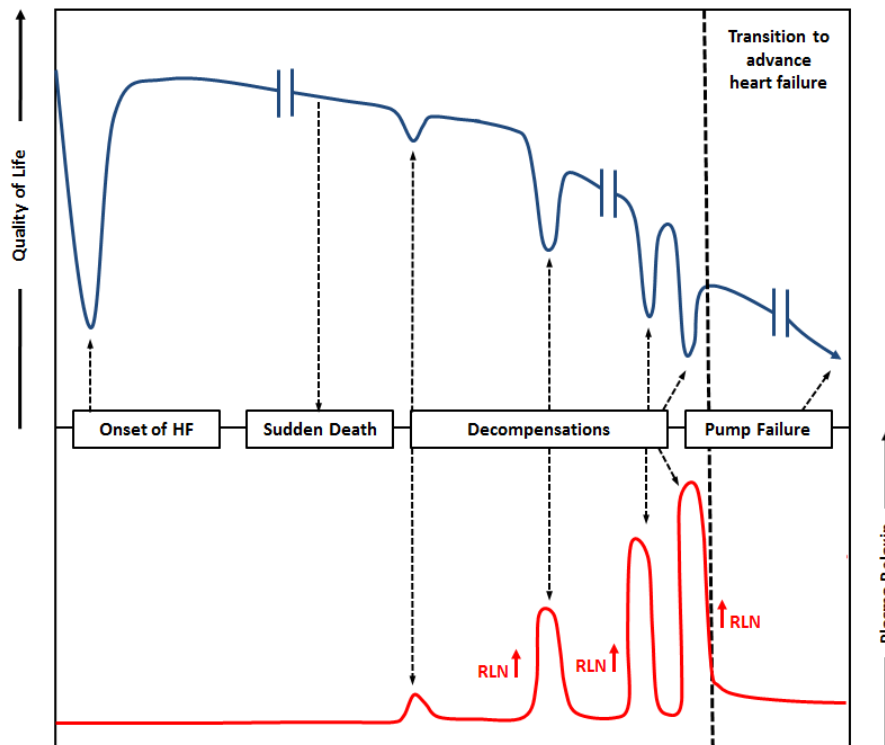
Figure 5: Secretion of RLN during decompensated HF.
RLN plasma levels increase depending on the severity of HF decompensations. Severe decompensation leads to high increase in RLN plasma levels. Figure adapted and modified from Dschietzig et al. and Allen et al. [46, 66].

In summary, RLN is physiologically secreted during pregnancy, but it is widely believed that it is also secreted during the decompensation period of HF [46]. Clear evidences for the effects of RLN secreted during decompensated HF is still missing, but it is considered to be beneficial [49]. As such, there is a great interest in using RLN as a medication specific to the treatment of decompensated HF.

3.3   Relaxin Receptor (RXFP1)

3.3.1   Relaxin receptor structure and expression pattern

The receptor for RLN is found in different tissues throughout the body. RNA and protein expression of RXFP1 could be detected in organs such as the brain, lung, kidneys, reproductive tissues, liver, adrenal gland, and atria of the heart. RLN exerts its physiological

effects by primarily binding to its cognate receptor RXFP1 previously known as LGR7 [67, 68]. The receptor contains an N-terminal low-density lipoprotein receptor class A (LDLa) module, and it is the only GPCR that contains such a domain [69]. The LDLa module on RXFP1 is crucial for receptor activation through ligand-stimulated cAMP signaling. Additionally, the receptor also contains a large ectodomain with 10 leucine-rich repeats (LRRs) that is important for high affinity ligand binding [54, 70]. This primary ligand binding between RLN and RXFP1 is mediated through the interaction of Arg[13], Arg[17], Ile[20] residues on the RLN B-chain α-helix and several pockets of surface-exposed amino acids located in LRR 4–8 on RXFP1 [71]. Like many GPCRs, RXFP1 also contains 7 transmembrane regions which form loops that embed the receptor into the plasma membrane [72, 73]. The extracellular parts of loop 1, 2, and 3 are important for the interaction between the receptor and the A-chain of RLN [74]. The C-terminal of the receptor resides within the membrane [75]. Figure 6 describes different structural features of RXFP1 in detail.
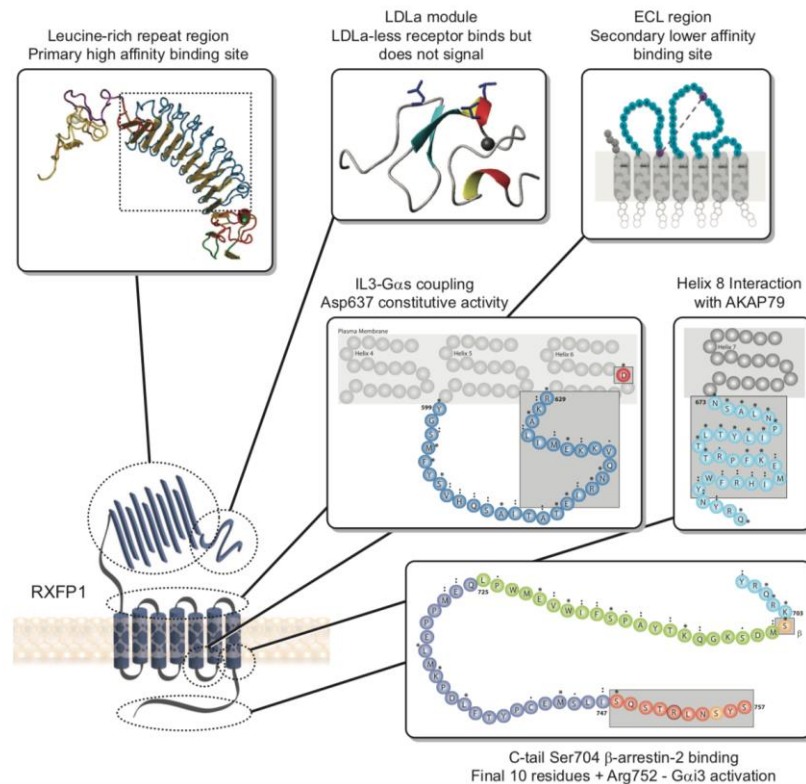
Figure 6: Structural features of the RXFP1.
RXFP1 has a large extracellular domain that contains a low-density lipoprotein receptor type A (LDLa) module connected to a leucine-rich repeat (LRR) region linked to the transmembrane domains of the receptor. The primary high affinity binding site for RLN is located in the LRR region, but the peptide also interacts with a lower affinity binding site located on the extracellular loops [37].

3.3.2 Relaxin receptor signaling pathway in cardiomyocytes

RLN and its receptor exert various effects through several pathways, especially in vascular, renal, and reproductive organs. In this work, the focus will be on RLN effects on the cardiovascular system.

In RXFP1 expressing cell lines, activation of RXFP1 leads to a biphasic cAMP response. Figure 7 describes the different pathways involved in RXFP1 signaling by RLN. At nanomolar levels of RLN, RXFP1 activates three distinct Gα proteins – $G\alpha_s$, $G\alpha_{oB}$, and $G\alpha_{i3}$. Activation of $G\alpha_s$ leads to an initial increase of cAMP, which is restricted by $G\alpha_{oB}$ and late maintained by $G\alpha_{i3}$ [47, 76, 77]. To maintain the high amount of cAMP needed, the second surge of cAMP comes from the activation of PI3K through $G\alpha_{i3}$ and $G\beta\gamma$ [78, 79]. In healthy cardiomyocytes, RLN would preferably signal primarily through $G\alpha_s$, since only a small amount of $G\alpha_{i3}$ is expressed leading to a limited inotropic response [26]. During HF $G\alpha_{i3}$ is upregulated in cardiomyocytes while $G\alpha_s$ stays unchanged. Thus RLN could potentially utilizes both $G\alpha_s$ and $G\alpha_{i3}$ for downstream signaling [26], which could significantly increase cAMP production resulting in a positive inotropic response.
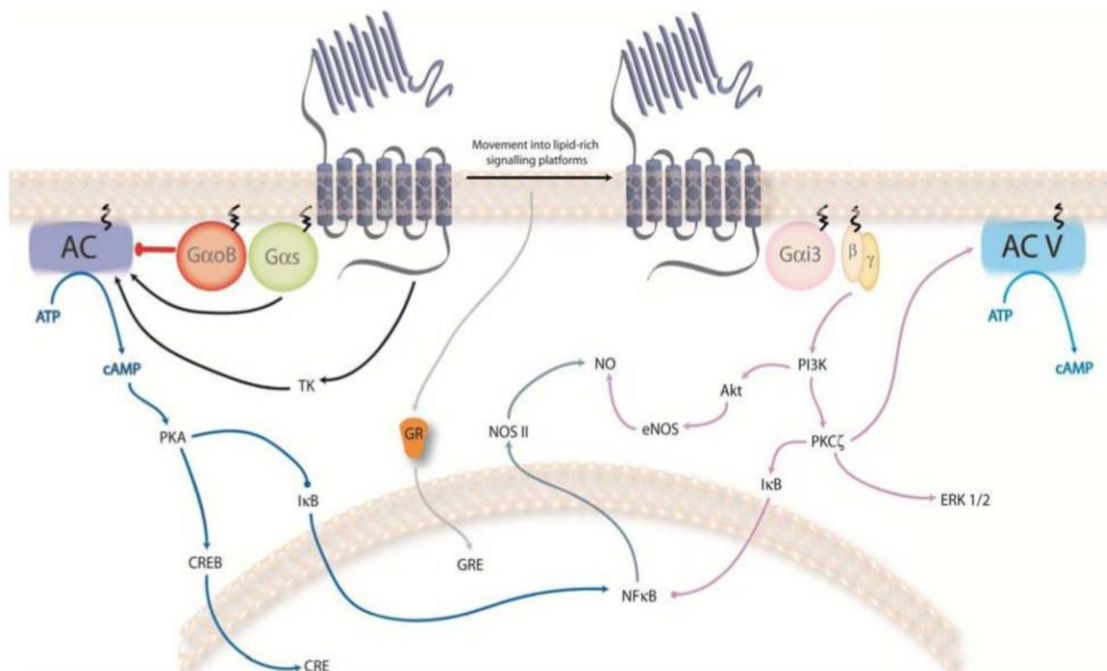
Figure 7: RXFP1 signaling pathway previously described.
RXFP1 activation by RLN induces signaling transduction through both $G\alpha_s$ and $G\alpha_{i3}$ subunits of the heterotrimeric G protein. Activation of the receptor classically increases cAMP production and PKA activity resulting in changes in genes expression profile and protein phosphorylation states [80].

The positive inotropy of RLN was initially described in isolated atrial cardiomyocytes of rats. This was later confirmed in atrial cardiomyocytes from failing human hearts [55, 77]. In contrast to atrial cardiomyocytes, ventricular cardiomyocytes isolated from the same human hearts did not respond to RLN treatment, which could be reasonably explained by the distinct RXFP1 expression pattern between the atria and the ventricle [81]. In both rats and humans, RXFP1 mRNA and protein are predominantly expressed in the atria while a minimal of RXFP1 mRNA is detected in the ventricle. Thus, it might be possible to produce inotropic responses in the ventricle, if gene therapy could be utilized to ectopically express RXFP1.

In summary, RXFP1 is a G-protein coupled receptor. In cardiovascular system, it is highly expressed in the atria of the heart. Upon activation, it preferably couples to $G\alpha_s$ and $G\alpha_{i3}$ sub-units of the heterotrimeric G-protein to increase cAMP production and PKA activation leading to positive inotropy.

3.3.3 Positive inotropic potential from activation of RXFP1 in HF

A hallmark of β-AR activation is an increase in cAMP production [82]. Increased cAMP leads to activation of PKA and Epac resulting in phosphorylation of PLB at both serine 16 and threonine 17 which activates SERCA2a [83-85]. Activation of SERCA2a influences intracellular calcium handling by increasing the rate of calcium being transported back into the SR, which contributes to positive inotropic effects [86]. Nonetheless, the positive inotropic effects from β-AR is only short lived and a prolonged β-AR stimulation leads to desensitization of the receptor. In HF, global desensitization of β-AR by β-arrestins occurs, leading to a lack of response to β agonists and rendering HF patients irresponsive to inotropic stimuli [87]. Modern treatment for HF focuses on preventing desensitization of β-AR using β-blockers in order to preserve sufficient cardiac functions. Similar to β-AR activation, RXFP1 activation by RLN also induces positive inotropy by increasing cAMP production and phosphorylation of its downstream target such as PLB [88]. However, there are two major differences between the two receptors: 1) RXFP1 is barely desensitized, which leads to a prolonged increase in cAMP, and 2) RXFP1 is shown to retain its function in the failing heart [55, 89]. This suggests that β-AR and RXFP1 are independent receptors that work through similar pathways [61, 62]. They might share some parts of the intracellular pathway such as cAMP production and PKA activation, but in the presence of desensitized β-AR, the signal from RXFP1 will dominate the overall downstream signal produced since minimal signal can go through a desensitized β-AR pathway. Thus, when β-AR is

desensitized in HF, RXFP1 and RLN could potentially be used to induce positive inotropic effects to increase cardiac output.

3.3.4 Beneficial effects of ectopic expression of RXFP1

It has been shown that RXFP1 retains its function regardless of the heart conditions [55]. Utilizing gene therapy technology, RXFP1 could be ectopically expressed in the ventricle upon HF. RXFP1 gene with cardiac specific promoter could be packed into a single strand AAV recombinant vectors to infect the ventricular cardiomyocytes. After infection, the beneficial effects of RXFP1 could be harnessed by a controlled administration of RLN. This treatment would create a new inducible inotropic pathway in a failing ventricle apart from the desensitized β-AR. Thus, the method could lead to a new mean of stimulating failing cardiomyocytes for positive inotropy.

3.4 Viral assisted human gene transfer

3.4.1 Definition of human gene transfer

The concept of human gene transfer (or gene therapy) is defined as the transfer of foreign genetic material (DNA or RNA) into a cell, tissue, or organ in order to treat a disease caused by defective genes. Human gene transfer according to the definition of the European Medicines Agency (EMA) includes any products that use foreign genetic material to add, delete, replace, repair, or regulate genetic sequences, which use results in the correction, restoration, or modification of the physiological function of humans.

3.4.2 AAV serotypes

AAV was discovered as a contaminant of an Adeno production in 1965 [90, 91]. A hallmark character of an AAV is its inability to replicate in the absence of a co-infecting virus. Potential helper viruses include: adenovirus, herpes simplex virus type 1 and 2, vaccinia virus, human Papilloma virus type 16, and human cytomegalovirus [92-95].

At present, several serotypes of AAV have been discovered. They are characterized by distinct variations of antigenic properties. There are 12 different serotypes of AAVs identified as AAV1 to AAV12. Serotypes 2, 3, 5, 6, and 9 were isolated from humans [96-100]. Serotypes 1, 4, 7, 8, 10, 11, 12 were isolated from primates [101-105]. Table 1 shows the targeted tissues of different AVV serotypes and their expression levels. All AAV serotypes are capable of infecting human cultured cells regardless of their *in vivo* tropism.

Introduction

Interest in the field of gene therapy led to extensive studies on several different AAV serotypes. Due to its remarkable ability to cross the blood brain barrier (BBB), and its strong transduction efficiency, AAV9 has recently gained interest in gene therapy studies [106]. In cardiac research, AAV9 is the vector of choice due to its strong *in vivo* cardiac transduction in mice.

Serotypes	Isolated from	Primary tropism	Expression level	Description
AAV1	Primate	Muscle	Medium	Best for cardiac and skeletal muscle
AAV2	Human	Muscle, Liver, retina	Low	Best for neurons, muscle, and brain
AAV3	Human	Megakaryocytes	Low	Best for megakaryocytes, muscle, liver, lung and retina
AAV4	Primate	Retina	Low	Best for neurons, muscle, brain and retina
AAV5	Human	Lung	Medium	Best for lung, neurons, synovial joint, retina, and pancreas
AAV6	Human	Muscle, Lung	Medium	Best for lung, liver, and heart
AAV7	Primate	Muscle, retina, neurons	High	Best for muscle, neurons, and liver
AAV8	Primate	Liver	High	Best for muscle, brain, liver, and retina
AAV9	Human	Various	High	Best for muscle, heart, liver, lung, and brain
AAV10	Primate	Pleura, CNS	Medium	Best for lung, muscle, heart, CNS, and liver
AAV11	Primate	Various	Low	Unknown, likely similar to AAV4
AAV12	Primate	Various	Low	Unknown, likely similar to AAV4

Table 1: AAV serotypes with tropology and expression level [107]

Out of the 12 serotypes, AAV1, 6, 8, and 9 have shown cardiac tropism [108]. Recombinant AAVs used for gene therapy are non-pathogenic, have low genome integration ratio and offer a long-term transgene expression in non-dividing cells after a single delivery; therefore making them generally very safe [109, 110]. Moreover, the small size of AAV allows it to be delivered to the myocardium by both direct and systemic injection [110].

However, there are three serious drawbacks of using AAV in gene therapy: 1) the limited packaging capacity of ~ 4.7 kbp for a single strain virus and ~ 2.3 kbp for a double strain virus, 2) the widely spread neutralizing antibodies against the AVV serotype in humans, and 3) the inevitable production of neutralizing antibodies upon single or repeated treatments with the same serotype, thereby limiting the number of viral treatments a single individual can receive [109, 111]. Scientists are currently working to overcome these setbacks by creating AAV vectors capable of coinfection and by generating a chimeric AAV vector that is not recognized by the immune system [112, 113].

AAV capsid is build up from 60 subunits of capsid proteins VP1, VP2, and VP3 that form an icosahedral viral particle with a diameter of ~ 25 nm [114]. The capsid proteins exist in the ratio of 1:1:10 (VP1:VP2:VP3) with 5 copies of VP1 and 2, and 50 copies of VP3 per particle (22) [115]. Twenty triangular faces were arranged from trimmers of all three capsid proteins.

3.4.3 AAV gene transfer

Delivery of AAV vectors in mice can be done through intravenous injection, but for larger animals such as pig or human, a cardiac specific delivery is required because of it minimally invasive nature [116]. In the first human clinical trial of gene therapy in the setting of HF (CUPID Trial), an antegrade intracoronary injection was employed [117].

After entering the body, AAV vectors gain entry into the cells using different cellular receptors such as heparan sulfate proteoglycan, N-linked sialic acid, O-linked sialic acid, and O-linked galactose [103, 118, 119]. Internalization is enhanced by interactions with one or more of at least 6 known coreceptors including $\alpha_V\beta_5$ integrins, fibroblast growth factor receptor 1 hepatocyte growth factor receptor, $\alpha_v\beta_1$integrin, and laminin receptor [118, 119]. AAVs are able to utilize several pathways such as clatherin-mediated, RacI-mediated or CLIC/GEEC mediated for cellular uptake [120-122]. After endocytosis AAV virions are trafficked in vesicles along the cellular cytoskeleton [121]. Low pH inside the endocytic vesicles triggers a conformational change in the capsid VP1 protein and facilitates its release from the endosomes [123]. Next AAVs enter the nucleus through the nuclear pore complex or other alternative pathways [121, 124, 125]. Then without the helper virus or the Rep protein the viral genomes cannot replicate and persist in the nucleus extrachromosomally as episomes [126]. Ribosomes can bind to the episomes to transcript mRNA for protein production. Figure 8 shows the process of AAV particles infecting in the cell.
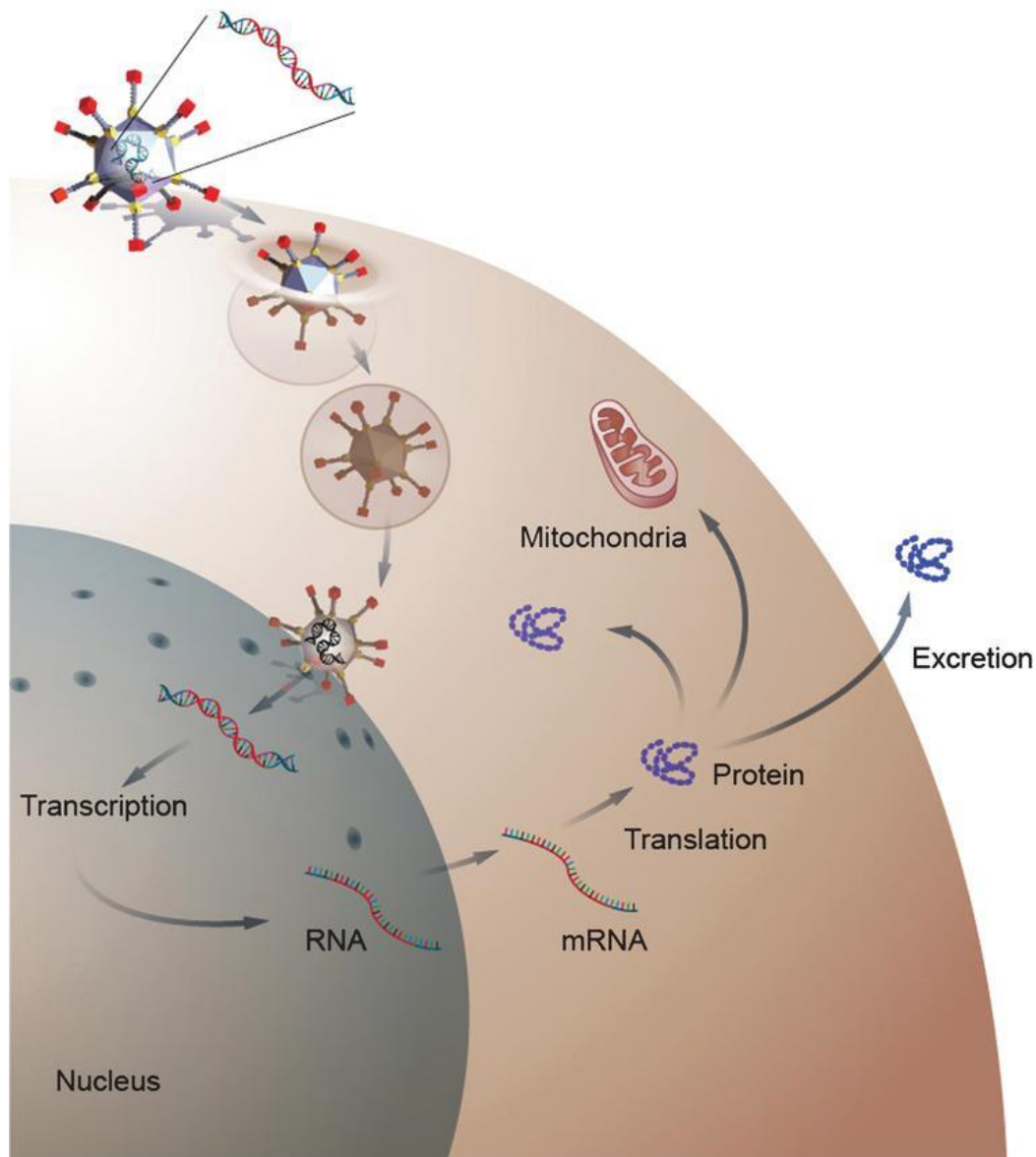
Figure 8: Gene Therapy using AAV vectors.
The diagram depicts gene delivery to a cell by an AAV vector. First, the gene of interest is cloned into a recombinant AAV genome and packed into an AAV capsid. The AAV particle binds to the cell membrane through several specific receptors and enters the cells cytoplasm. After entering the cell, the virus traffics to the nucleus, where the transgene is delivered. The transgene remains as an episome and IS transcribed into mRNA. The mRNA is modified and transported to the cytoplasm before being translated into protein. The newly formed protein can be modified or transported to different compartments within the cell depending on the function of the protein [127].

3.4.4 AAV for cardiac gene therapy

Collectively AAVs display a very broad tropism, but none of the currently available AAVs has shown tropism exclusive in one tissue [116]. Although AAV serotype 1, 6, 8 and 9 are the more promising serotypes for cardiac gene transfer [107], high specificity is still required for a targeted cardiac gene transfer. To further increase cardiac specificity, different

cardiac specific promoters can be added to further control the expression of the gene of interest [128]. Ventricular specific promoters such as Troponin T (TnT), myosin light chain-2v (MLC-2v), and α-myosin heavy chain (α-MHC) were previously used in numerous studies to achieve high cardiac specificity expression need for gene therapy [128-131].

In summary, a combination of a cardiac specific promoter and a targeted HF gene construct packing into a recombinant AAV vector can be used to correct molecular changes in cardiomyocytes to treat HF from within the cells. This treatment is different from conventional treatments because it addresses the underlying molecular changes of HF rather than treating the body's compensation mechanisms which are the result of the molecular changes. In the past decades many HF gene therapy targeted proteins have been identified and tested for their effectiveness at correcting the underlying molecular changes of HF in a gene therapy setting. Several proteins including the one from this study have emerged as potential candidate for further testing.

3.5 Aims of the study

Traditionally, RLN and its receptor RXFP1 have been associated with the reproductive system. Their role in preparing the cardiovascular system and renal system during pregnancy is well established. Interestingly, recent evidence suggests that RLN and RXFP1 might also play a much more complex role in the cardiovascular system in HF patients, as elevated levels of RLN were detected in decompensated HF patients. However, clinical trials using recombinant RLN to treat acute heart failure (AHF), exploiting its vasodilatory properties, failed to improve mortality [132]. Expression of RXFP1 has been detected in the atria of HF patients and is known to induce positive inotropy under RLN stimulation. As expression of RXFPI in the ventricular cardiomyocytes is negligible, no positive inotropy was detected in ventricular cardiomyocytes upon RLN stimulation. It is unknown if ectopic RXFPI expression alone or in combination with exogenous RLN delivery can induce positive inotropy in failing hearts.

Gene therapy could help combine the benefit of RLN and RXFP1 interaction by mediating RXFP1 expression.

As such the hypothesis of this thesis is:

Cardiac gene therapy with AAV-mediated expression of RXFPI alone or in combination with exogenous RLN treatment improves cardiac function in murine HF.

Therefore, the aims of this thesis are:

1) To explore the possibility of ectopically overexpressing a functional RXFP1 in the left ventricle using AAV vectors.
2) To translate RXFP1 overexpression into a treatment for HF in an animal model.
3) To dissect the molecular signaling pathway of RXFP1 and RLN in left ventricular cardiomyocytes.
4) To differentiate RXFP1 and β-adrenergic signaling pathways.

4 Materials and Methods

4.1 Organisms and animals

4.1.1 Bacteria

E. coli **DH5α**

F– Φ80lacZΔM15 Δ(lacZYA-argF) U169 recA1 endA1 hsdR17 (rK–, mK+) phoA supE44 λ– thi-1 gyrA96 relA1

E. coli **Top10**

F- mcrA Δ(mrr-hsdRMS-mcrBC) φ80lacZΔM15 ΔlacX74 nupG recA1 araD139 Δ(ara-leu)7697 galE15 galK16 rpsL(Str^R) endA1 λ$^-$

E. coli **SURE2**

endA1 glnV44 thi-1 gyrA96 relA1 lac recB recJ sbcC umuC::Tn5 uvrC e14- Δ(mcrCB-hsdSMR- mrr)171 F'[proAB$^+$ lacI^q lacZΔM15 Tn10 Amy Cm^R]

4.1.2 Eukaryotic cell line

HEK 293T STR Profil: Amelogenin: X

        CSF1PO: 11,12

        D13S317: 12,14

        D16S539: 9,13

        D5S818: 8,9

        D7S820: 11,12

        THO1: 7,9.3

        TPOX: 11

        vWA: 16,19

4.1.3 Animals

In vivo **TAC RXFP1 gene therapy model:** C57/Bl6NRj (Janvier Labs)

Neonatal rat ventricular cardiomyocytes isolation: Wistar (Janvier Labs)

4.2 Chemicals and reagents

Denotation	Source
2-Mercaptoethanol	Sigma Aldrich, Munich, Germany
Acetic Acid	VWR, Darmstadt, Germany
Aqua ad injectabilia	B. Braun, Melsungen, Germany
Agarose	Sigma Aldrich, Munich, Germany
Ampicilin	Carl-Roth, Karlsruhe, Germany
Bacteriological Agar	BD, Franklin Lakes, USA
Bacto Trypton -pancreatic digest of Casein	BD, Franklin Lakes, USA
Bromophenol Blue	Sigma Aldrich, Munich, Germany
BSA	Sigma Aldrich, Munich, Germany
Chloroform	Sigma Aldrich, Munich, Germany
Collagen Type I rat tail	Merck, Darmstadt, Germany
Collagenase Type 2	Worthington, Lakewood, USA
DEPC H_2O	Carl-Roth, Karlsruhe, Germany
Disodium hydrogen phosphate-2-hydrate	Grüssing GmbH Analytic, Filsum, Germany
DTT	Sigma Aldrich, Munich, Germany
EDTA	AppliChem GmbH, Darmstadt, Germany
Ethanol 99%	Sigma Aldrich, Munich, Germany
Ethidiumbromide	Carl-Roth, Karlsruhe, Germany
Fetal Calf Serum (FCS)	GE healthcare, Chicago, USA
Formaldehyd (37 %)	Sigma Aldrich, Munich, Germany
Gallein	Santa Cruz Biotechnology, Heidelberg, Germany
Glycerin	Carl-Roth, Karlsruhe, Germany
Glycin	AppliChem GmbH, Darmstadt, Germany
H89	Tocris, Wiesbaden, Germany
HEPES	Carl-Roth, Karlsruhe, Germany
Hydrochloric acid	VWR, Darmstadt, Germany
iBlock Reagent (Tropix I-Block)	AppliedBiosystems, Carlsbad, USA
iQ SYBR Green Supermix	Bio-Rad, Munich, Germany
iScript cDNA Synthesis Kit	Bio-Rad, Munich, Germany
Isopropanol	AppliChem GmbH, Darmstadt, Germany
Isoproterenol hydrochloride	Sigma Aldrich, Munich, Germany
Kanamycin	Carl-Roth, Karlsruhe, Germany
KN92	Tocris, Wiesbaden, Germany
KN93	Tocris, Wiesbaden, Germany
Laminin	Sigma Aldrich, Munich, Germany
Magnesium sulfate-7-hydrate	Merck, Darmstadt, Germany
Melittin	Tocris, Wiesbaden, Germany
Methanol	Sigma Aldrich, Munich, Germany
NP40 (Nonidet P40)	Sigma Aldrich, Munich, Germany

Optiprep	GE healthcare, Chicago, USA
Pancreatin	Sigma Aldrich, Munich, Germany
Percoll	GE healthcare, Chicago, USA
Pertussis toxin	Tocris, Wiesbaden, Germany
Phosphatase Inhibitor Cocktail 2,3	Sigma Aldrich, Munich, Germany
Polyacryl-Carrier	Molecular Research Center, USA
Potassium chloride	AppliChem GmbH, Darmstadt, Germany
Potassium dihydrogen phosphate	Merck, Darmstadt, Germany
Propranolol hydrochloride	Sigma Aldrich, Munich, Germany
Proteaseinhibitor Complete Mini EDTA- free	Roche, Mannheim, Germany
Proteinase K	AppliChem GmbH, Darmstadt, Germany
Recombinant Relaxin H2	R&D Systems, Minneapolis, USA
SDS in Pellets	SERVA GmbH, Heidelberg, Germany
Sodium Acetate	Sigma Aldrich, Munich, Germany
Sodium chloride	Carl-Roth, Karlsruhe, Germany
Sodium chloride 0,9% intravenous	B. Braun, Melsungen, Germany
Sodium hydroxide	Sigma Aldrich, Munich, Germany
SQ22536	Tocris, Wiesbaden, Germany
Stauroporine	Tocris, Wiesbaden, Germany
Taurin	Carl-Roth, Karlsruhe, Germany
Tris	Carl-Roth, Karlsruhe, Germany
Triton X100	Sigma Aldrich, Munich, Germany
Trizol®	Invitrogen, Karlsruhe, Germany
Tryptone	BD, Franklin Lakes, USA
Tween 20	Carl-Roth, Karlsruhe, Germany
Vectashield® Hard Mounting Medium/Dapi	Linaris Biologische Produkte
Wortmannin	Sigma Aldrich, Munich, Germany
Yeast Extract	Carl-Roth, Karlsruhe, Germany

Materials and Methods

4.3 Buffers and solutions

4.3.1 Solution for molecular biology

Denotation	Composition	Source
6x Agarose Gel loading buffer	30 % Glycerol (v/v), 0.25 % Bromophenol Blue (w/v), 0.05 % SDS (w/v)	Prepare in the lab
RIPA lysis buffer	150 mM NaCl, 50 mM Tris, 50 mM EDTA, 1 % NP40 (v/v), 0.5 % Desoxychola, 10 mM NaF, 10 mM Na_2-Pyrophosphate, phosphatase inhibitor 2 and 3, 1 tablet protease inhibitor in 10ml	Prepare in the lab
i-Block blocking buffer	10% 10x TBS, 0.2% i-Block (w/v), 0.1% Tween 20 (v/v)	Prepare in the lab
Semi-Dry transfer buffer	48 mM Tris, 39 mM Glycin, 20 % Methanol (v/v)	Prepare in the lab
10x TBS	0.25 M Tris, 1.5 M NaCl, 10 mM CaCl2, pH 7.5 fill up to 2.5 L with ddH_2O	Prepare in the lab
10x Anode buffer	1 M Tris, fill up to 1 L with ddH_2O	Prepare in the lab
1x Cathode buffer	0.1 M Taurin, 0.1 M Tris, 0.1% SDS, fill up to 2.5 L with ddH_2O	Prepare in the lab
10x TAE	400 mM Tris (pH 7.6), 200 mM acetic acid, 10 mM EDTA	Prepare in the lab
1x TBS-T	20 % 10x TBS (v/v), fill up to 0.5 L with ddH_2O, 0.1 % Tween 20 (v/v)	Prepare in the lab
5x SDS-PAGE loading buffer	30 % Glycerol (v/v), 50 mM TRIS, 10 % SDS (v/v), 250 mM DTT, 10 mM EDTA, 0.1 % Bromophenol Blue (w/v), pH 6.8; fill up to 1 L with ddH2O	Prepare in the lab
4 % Paraformaldehyd	4 % PFA (w/v), 4 % Sacharose, 1x PBS, heat to 60° C, pH 7-8	Prepare in the lab
0.5M EDTA (pH 8.0)		Prepare in the lab
1M Tris-HCl (pH 7.4)		Prepare in the lab
3M SodiumAcetate (pH 6.2)		Prepare in the lab
1% SDS lysis buffer	PBS, 1 mM EDTA, 1 mM EGTA, 1% SDS, 1% phosphatase inhibitor 2 and 3, 1 tablet protease inhibitor in 10ml	Prepare in the lab

4.3.2 Solution for microbiology

Denotation	Composition	Source
10x LB Medium 1L [Bertani, 1951]	100 g Bacto trypton, 50 g yeast extract, 50 g NaCl, pH 7.2 (adjusted with 2M NaOH)	Prepare in the lab
LB Medium 1L [Bertani, 1951]	10 g Bacto trypton, 5 g yeast extract, 5 g NaCl, pH 7.2 (adjusted with 2M NaOH), for solid nutrient media 20 g/L of agar was added before autoclaving	Prepare in the lab
Cyro preservation medium	57.5 ml 87 % Glycerol in H_2O, 42.5 ml TY medium	Prepare in the lab
TSS Medium (100 ml) [Chung et al., 1989]	82,5 ml LB0 (pH 6.5), 10 g PEG 6000, 5 ml DMSO, 2.5 ml 2 M $MgCl_2$ mixed before autoclaving	Prepare in the lab
TY Medium (500 ml)	5 g Bacto trypton, 2,5 g yeast extract, pH 7.2 (adjusted with 2M NaOH)	Prepare in the lab

4.3.3 Solutions for cell culture

Denotation	Source
0.25% Trypsin-EDTA (1x)	Gibco (Thermo Fisher Scientific), Waltham, USA
DMEM with High Glucose	Sigma Aldrich, Munich, Germany
FCS Superior	Biochrom, Berlin, Germany
HBSS	Gibco (Thermo Fisher Scientific), Waltham, USA
HEPES Buffer Solution 1(M)	Gibco (Thermo Fisher Scientific), Waltham, USA
L-Glutamin 200mM 100x	Gibco (Thermo Fisher Scientific), Waltham, USA
Medium 199, HEPES Modification	Sigma Aldrich, Munich, Germany
PBS	Sigma Aldrich, Munich, Germany
Penicillin/Streptomycin (5000U/ml)	Gibco (Thermo Fisher Scientific), Waltham, USA
Percoll	GE Healthcare, Freiburg, Germany

4.3.4 Media for cell culture

Denotation	Composition
Collagenase digestion solution	80 U/mL collagenase type 2, 0.06 % pancreatin (w/v) dissolved in 120 mL Aqua ad injectabilia for 45 minutes with maximum stirring, 20 mL 10x ADS, and fill up to 200 ml with Aqua ad injectabilia, filtered sterile
Digestion stop solution	25% FCS-Gold by adding 10 mL to 30 mL of digested solution
Culture medium NRVCMs (10 % FCS)	Medium 199, 10 % FCS Superior (v/v), 1 % P/S (v/v), 1 % L-Glutamin (v/v), 1 mM $CaCl_2$, filtered sterile and store at 4° C
Culture medium NRVCMs (0.5 % FCS)	Medium 199, 0.5 % FCS Superior (v/v), 1 % P/S (v/v), 1 % L-Glutamin (v/v), 1 mM $CaCl_2$, filtered sterile and store at 4° C
Culture medium for HEK293T (10% FCS)	DMEM (with High Glucose), 1% P/S, 10% FCS Superior, store at 4° C
Culture medium for HEK293T (0% FCS)	DMEM (with High Glucose), 1% P/S, 0.0% FCS Superior, store at 4° C
10x ADS (for isolation of NRVCMs)	1163.3 mM NaCl, 197.2 mM HEPES, 94.2 mM NaH_2PO_4 x H_2O, 55.5mM Glucose, 53.6 mM KCl, 8.3 mM $MgSO_4$ x 7 H_2O, adjusted pH with (5M NaOH) to 7.4
1x ADS with phenol red (for isolation of NRVCMs)	450 ml H_2O (Aqua ad injectabilia), 50 ml 10x ADS, 50 mg of phenol red, filtered sterile and store at 4° C
1x ADS colorless (for isolation of NRVCMs)	450 ml H2O (Aqua ad injectabilia), 50 ml 10x ADS, filtered sterile and store at 4° C
Percoll-Gradient stock solution (for 6 gradients)	36 ml Percoll, 4 ml 10x ADS, store at 4° C 4°C
Percoll-Gradient Top-layer	13.5 ml stock solution, 16.5ml 1x ADS with phenol red, stored at 4° C
Percoll-Gradient Bottom-layer	19.5 ml stock solution, 10.5ml 1x ADS colorless, stored at 4° C

4.4 Primers

Primers for quantitative real time PCR (qRT-PCR) were ordered from Life Technologies and they were delivered lyophilized and desalted.

Gene	Sequence (5' - 3')	Temp.	Sp.	Template
ANP Forward	TGCCGGTAGAAGATGAGGTC	63.5° C	Rat, Mouse	NM_008725.3
ANP Reverse	TGCTTTTCAAGAGGGCAGAT			
β-MHC Forward	GCCAACACCAACCTGTCCAAGTTC	63.5° C	Rat, Mouse	NM_080728.3
β-MHC Reverse	TGCAAAGGCTCCAGGTCTGAGGGC			
BNP Forward	CTGAAGGTGCTGTCCCAGAT	57° C	Rat, Mouse	NM_008726.5
BNP Reverse	CCTTGGTCCTTCAAGAGCTG			
Col1a1 Forward	GTGTTCCCTACTCAGCCGTC	57° C	Mouse	NM_007742.4
Col1a1 Reverse	ACTCGAACGGGAATCCATCG			
Col3a1 Forward	TGACTGTCCCACGTAAGCAC	57° C	Mouse	NM_009930.2
Col3a1 Reverse	GAGGGCCATAGCTGAACTGA			
GNAi2 Forward	AGCGTGCGGATGATGCC	61° C	Mouse	NM_008138.5
GNAi2 Reverse	TGCGCTCCAGATCATTCAGG			
HPRT1 Forward	GAGGAGTCCTGTTGATGTTGCCAG	55-65° C	Mouse	NM_013556.2
HPRT1 Reverse	GGCTGGCCTATAGGCTCATAGTGC			
HPRT1 Forward	CTCATGGACTGATTATGGACAGGAC	55-65° C	Rat	NM_012583.2
HPRT1 Reverse	GCAGGTCAGCAAAGAACTTATAGCC			
POSTN Forward	ACAAAAGGGTTCAAGGGCCTA	60° C	Mouse	NM_009071.2
POSTN Reverse	TTGGCTTCTGTTGGTTGTCA			
Rel1 Forward	CCATGCATTGTTTGTGCCGA	61° C	Rat	NM_201417.1
Rel1 Reverse	TTTGCAGGCACAGCTTTTGG			
Rel1 Forward	CGAATGCTTGGTTGGCTCTG	59° C	Mouse	NM_212452.2
Rel1 Reverse	AAGACGCTCACGGAGTGAATC			

Materials and Methods

4.5 Antibodies

4.5.1 Primary antibodies

Name of Protein	Ratio	Sp.	System	Source
AKT	1:1000	Rabbit	LiCor	Cell Signaling Technology, Inc. Frankfurt am Main, Germany
ERK 1/2	1:2000	Rabbit	LiCor	Cell Signaling Technology, Inc. Frankfurt am Main, Germany
FLAG M2	1:1000	Mouse	LiCor	Sigma Aldrich, Munich, Germany
GAPDH	1:10000	Mouse	LiCor	Merck Millipore, Darmstadt, Germany
P-Akt (Ser473)	1:1000	Mouse	LiCor	Cell Signaling Technology, Inc. Frankfurt am Main, Germany
P-ERK 1/2	1:2000	Mouse	LiCor	Cell Signaling Technology, Inc. Frankfurt am Main, Germany
P-PLB (S16)	1:5000	Rabbit	LiCor	Merck Millipore, Darmstadt, Germany
P-PLB (T17)	1:5000	Rabbit	LiCor	Badrilla, Leeds, UK
PLB	1:7500	Mouse	LiCor	Thermo Fisher Scientific, Waltham, USA
α-Actinin (sarcomeric)	1:2000	Mouse	LiCor	Sigma Aldrich, Munich, Germany

4.5.2 Secondary antibodies

Name	Ratio	Sp.	System	Source
Goat anti-mouse IgG (H+L) Alexa Fluor® 680	1:10000	Mouse	LiCor	Invitrogen, Karlsruhe, Germany
Anti-rabbit IgG (H+L) DyLight(TM)800	1:10000	Rabbit	LiCor	Cell Signaling Technology, Inc. Frankfurt am Main, Germany

4.5.3 Secondary antibodies for immunofluorescence

Name	Ratio	Sp.	System	Source
Goat anti-rabbit IgG (H+L) Alexa Fluor® 568	1:200	Rabbit	Olympus	Invitrogen, Karlsruhe, Germany
Goat anti-mouse IgG (H+L) Alexa Fluor® 488	1:200	Mouse	Olympus	Invitrogen, Karlsruhe, Germany

4.6 Plasmids

Denotation	Description	Antibiotic Resistant
pSSV9 CMV MLC260 FLAG RXFP1	FLAG RXFP1 recombinant plasmid for viral production	Amp
pSSV9 CMV MLC260 FLAG LUC	FLAG Luciferase recombinant plasmid for viral production	Amp
pDP9rs	Helper plasmid for virus production	Amp
pDP6rs	Helper plasmid for virus production	Amp
pCDNA3.1 FLAG RXFP1	Sub-clone plasmid	Amp
pCDNA3.1 FLAG LUC	Sub-clone plasmid	Amp

4.7 Equipment

Denotation	Source
ADVANTAGE PV Loop system	Scisense, Ontario, Canada
Agarose-Gel Chamber	Bio-Rad, Munich, Germany
Autocalve VX-150	Systec, Linden, Germany
Bacterial Incubator	HEREUS, Kleinostheim, Germany
CFX96 Real-Time system C1000 Touch™ Thermal Cycler	Bio-Rad, Munich, Germany
ChemiDoc ECL Scanner	Bio-Rad, Munich, Germany
Echo Vevo 2100	FUJIFILM Sonosite B.V., Amsterdam, Netherland
Electrophoresis unit	Bio-Rad, Munich, Germany
ELISA Reader Multiscan Spectrum	Thermo Scientific, Karlsruhe, Germany
Fluorescence microscope IX81; CellR MT20	Olympus, Hamburg, Germany
Freezer (-20° C)	Liebherr, Kirchdorf an der Iller, Germany
Gel Doc XR System	Bio-Rad, Munich, Germany
Hera Safe Laminar Flow	Thermo Scientific, Karlsruhe, Germany
Heracell™ 150i CO_2 Incubators with Copper Chambers	Thermo Scientific, Karlsruhe, Germany
Heraeus Multifige 4 UR	Thermo Scientific, Karlsruhe, Germany
Light microscope AXIO Vert.A1	Carl Zeiss, Oberkochenm, Germany
Luminometer	Berthold, Bad Wildbach, Germany
Magnetic stirrer Model L-71	Labor Brand, Gießen, Germany
Megafuge Sorvall RC6	Thermo Scientific, Karlsruhe, Germany
NanoDrop™ 2000	Thermo Scientific, Karlsruhe, Germany
Neubauer counting chamber	Hecht-Assistant, Sondheim/Rhön, Germany
Odyssey CLX	Licor, Bad Homburg, Germany
PCR cycler C1000 Touch™ Thermal Cycler	Bio-Rad, Munich, Germany
pH-Meter MP220	Mettler Toledo, Gießen, Germany
Pipetboy	Neo lab, Heidelberg, Germany
Pipets	Eppendorf, Hamburg, Germany

Scales EW 6000-1M	Kern, Balingen, Germany
SDS-Gel chamber XCell Surelock	Invitrogen, Karlsruhe, Germany
SemiDry Blotter	Bio-Rad, Munich, Germany
Shaker DRS-12	Neo lab, Heidelberg, Germany
Spectrophotometer U-2000	Hitachi, Mannheim, Germany
Table top centrifuge 1-15K	Sigma Aldrich, Osterode am Harz, Germany
Thermomixer 5436	Eppendorf, Hamburg, Germany
Transilluminator Alpha DigiDoc	Alpha Innotech, Santa Clara, USA
Ultracentrifuge Sorvall™ WX Untra Series	Thermo Scientific, Karlsruhe, Germany
Voltage regulator Power Pac HC	Bio-Rad, Munich, Germany
Vortex-Genie	Neo lab, Heidelberg, Germany
Water bath E100	Lauda, Lauda-Königshofen, Germany
Water purification system TKA-GenPure	Thermo Scientific, Karlsruhe, Germany

4.8 Software

Program	Source	Application
CFX Manager™	Bio-Rad	Analysis of qRT-PCR data
Echo Vevo 2.0	Visualsonics	Evaluation of echocardiography
G-power	University of Düsseldorf	*In vivo* experiments power analysis
Image J (Freeware)	National Institutes of Health, Bethesda, Maryland	Histology evaluation and quantification
Image Studio Lite	Licor	Odyssey Western Blots
ImageLab	Bio-Rad	ECL Western Blots and agarose gels
Labscribe 2.0	Iworx/scisense	Evaluation of pressure-volume loop
Office 2016	Microsoft	Word, Excel, Powerpoint, Outlook
Prism 6	GraphPad	Illustration of data and statistical analysis
Serial Cloner	SerialBasics	Analysis of plasmid sequences
EndNote X9	Clarivate Analytics	Reference management

4.9 Special materials, assays and kits

4.9.1 Special materials

Denotation	Description	Source
Surgical Tools	Surgical scissors	
	2 fine tip tweezers	Fine Science Tools GmbH, Heidelberg
	Scalpel	
	Surgical stapler	
PV Loop	PV catheter mouse 112-479 1.2F; 4.5mm electrode spacing	Transonic, Ithaca, USA
DNA Loading Standards	GeneRuler 100 bp DNA Ladder	Thermo Fisher Scientific, Waltham, USA
	100 bp Extended DNA Ladder	Carl-Roth, Karlsruhe, Germany
Protein Loading Standard	PageRuler Prestained Protein Marker 10 to 180 kDa	Thermo Fisher Scientific, Waltham, USA
Enzymes	Restriction enzymes and T4 DNA Ligase	New England Biolabs, Ipswich, USA
	Alkaline Phosphatase	New England Biolabs, Ipswich, USA
	Benzonase®	Sigma Aldrich, Munich, Germany

4.9.2 Assays and Kits

Denotation	Source
Human Relaxin-2 Quantikine Elisa Kit DRL200	R&D Systems, Minneapolis, USA
BioMix™ Red PCR Kit	Bioline, London, UK
DC™ (detergen compatible) Protein assay	Bio-Rad, Munich, Germany
GeneElute™ Plasmid Miniprep Kit	Sigma Aldrich, Munich, Germany
Phusion PCR Kit	New England Biolabs, Ipswich, USA
QIAGEN Plasmid Giga Kit (5).	Qiagen, Hilden, Germany
QIAGEN Plasmid Maxi Kit (10).	Qiagen, Hilden, Germany
QIAGEN Plasmid Midi Kit (25).	Qiagen, Hilden, Germany
QIAquick Gel Extraction Kit	Qiagen, Hilden, Germany
QIAquick PCR Purification Kit	Qiagen, Hilden, Germany
SignalFire ECL Detection Kit	Cell Signaling Technology, Inc. Frankfurt am Main, Germany

4.10 Consumables

Denotation	Source
12 and 24 Well Plate	Corning, Kaiserslautern, Germany
6 and 96 Well Plate	Greiner bio-one, Frickenhausen, Germany
96 Well Plate, Lumitrac white	Greiner bio-one, Frickenhausen, Germany
Cell culture dishes ø 145 cm, ø 6 cm	Greiner bio-one, Frickenhausen, Germany
Cell culture Flasks (T 75 cm^2, and T 175 cm^2)	Sarstedt, Nümbrecht, Germany
Cell scraper	Greiner bio-one, Frickenhausen, Germany
Cell stack (10 layers)	Corning, Kaiserslautern, Germany
Cell strainer 100 micron	BD, Heidelberg, Germany
Conical centrifuge tubes, 500 ml	Corning, Kaiserslautern, Germany
Cryotubes, 1.5 ml	Neo Lab, Heidelberg, Germany
Filter 0.45 μm, 0.22 μm, and 0.33 mm Millex GS	Merck Millipore, Darmstadt, Germany
Filter paper	LLG Lab Logistics Group, Meckenheim, Germany
Immobilon-FL PVDF membrane	Merck Millipore, Darmstadt
Magnetic stir bar	Neo Lab, Heidelberg, Germany
Microscope cover glass round, ø 15 mm	Neo Lab, Heidelberg, Germany
Microscope superfrost® slide plus	Menzel, Braunschweig, Germany
Microseal B film	Bio-Rad, Munich, Germany
Needles (Microlance: 20G, 21G, 23G, 26G, 27G)	BD, Heidelberg, Germany
Novex Tris Glycin Gele 4-20 %	Life Technologies, Darmstadt, Germany
PCR Tube 0.2 ml	Kisker Biotech, Steinfurt, Germany
PCR-Plate 96 Well	Bio-Rad, Munich, Germany
Plasma collection tube	Sarstedt, Nümbrecht, Germany
Quick seal tube 13 mL and 40 mL	Beckman Coulter, Indianapolis, USA
Reaction tubes 1.5 ml RNAse-, DNase-, Pyrogen free	Nerbe plus, Winsen/Luhe, Germany
Reaction tubes 1.5 ml, 2ml	Sarstedt, Nümbrecht, Germany
Reaction tubes 12 ml, 50 ml	Sarstedt, Nümbrecht, Germany
Serological Pipettes	Sarstedt, Nümbrecht, Germany
Silk and prolene suture	Harvard Apparatus, Holliston, USA
Sterile filter 0.22 μm, 0.45 μm and, 0.33 mm Millex GS	Merck Millipore, Darmstadt, Germany
Sterile pipette Tips	Sarstedt, Nümbrecht, Germany
Syringe 1 mL, 2 mL, 5 mL, 10 mL, 50 mL	BD, Heidelberg, Germany
Test tubes 5 ml	Sarstedt, Nümbrecht, Germany
Transfer membranes with 0.45 μm pore	Merck Millipore, Darmstadt, Germany
Whatman paper	GE Healthcare, Freiburg, Germany
Zeba Spin Desalting columns	Thermo Fisher Scientific, Waltham, USA

4.11 Methods

4.11.1 Cloning
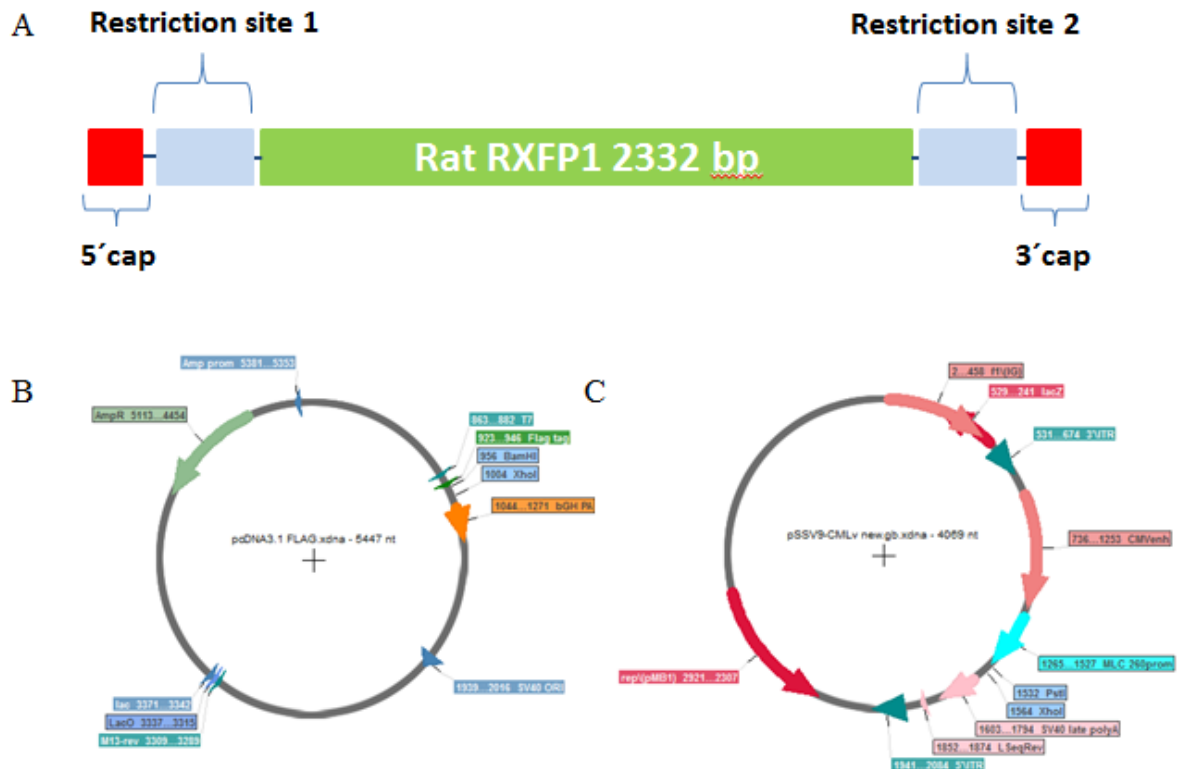
Figure 9: DNA fragments and plasmid construct used for cloning.
(A) Fragment of RXFP1 construct used to sub cloned into AAV transfer plasmid, **(B)** pCDNA3.1 FLAG plasmid with restriction sites of interest, and **(C)** AAV transfer plasmid with restriction sites of interest.

The recombinant AAV vectors of serotypes 6 and 9 CMV MLC260 FLAG *Rel1*Rattus (designated AAV6 RXFP1 or AAV9 RXFP1) were generated as follows. The FLAG-TAG Rattus Norvegicus *Rel1* cDNA [NM_201417.1, National Center for Biotechnology Information (NCBI)] was synthesized and sub-cloned into a pCDNA3.1 plasmid. After extensive testing in a cell line, the transgene cassette was subcloned into an AAV transfer plasmid between a synthetic cardiac myocyte-specific cytomegalovirus (CMV) enhancer, short (260bp) myosin light chain promoter and a bGH pA, which is flanked by two ITRs from AAV2. Figure 9 shows RXFP1 DNA fragment and different plasmid construct used for cloning.

Materials and Methods

4.11.1.1 DNA Digestion
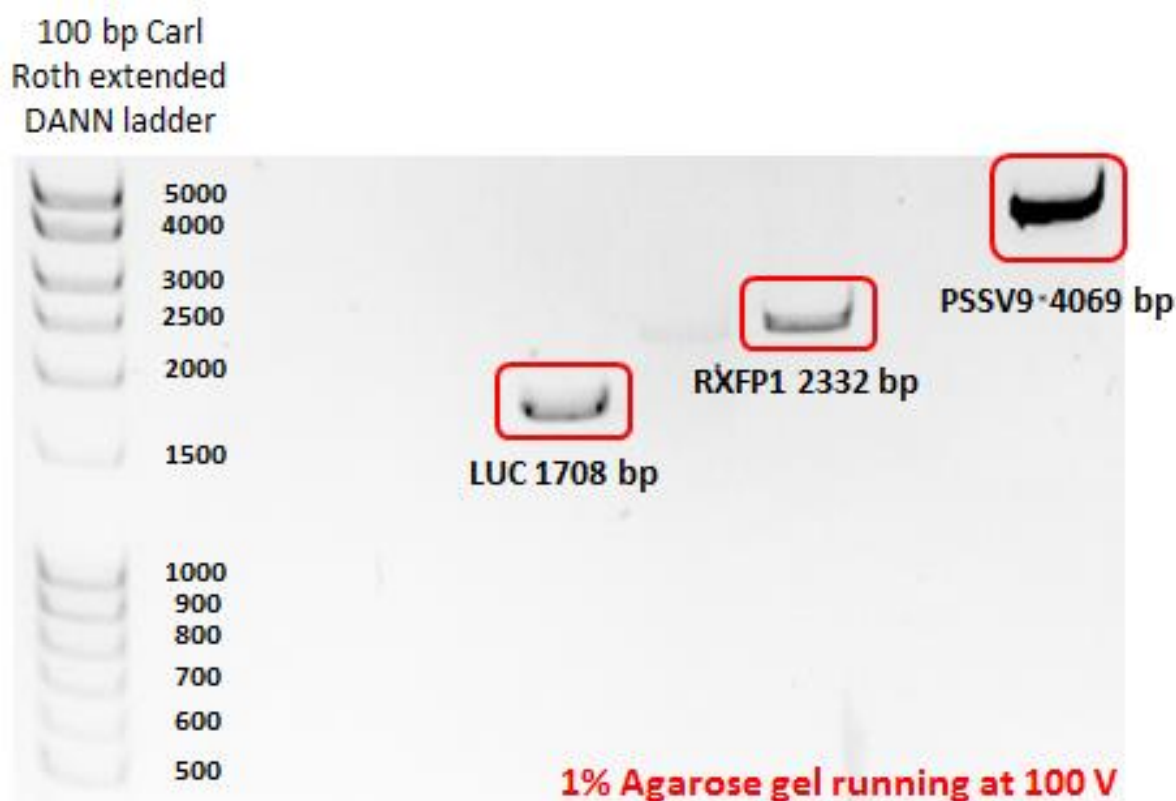
Figure 10: Agarose gel purification.
Agarose gel containing fragments of LUC, RXFP1 and PSSV9 AAV transfer plasmid

In general, 1 µg of DNA was used in all restriction digests. 1 unit of restriction endonuclease was used in order to complete DNA digestion. A 40 µL total digestion volume was set up for all digestions. To completely digest all the DNA, the solution was incubated at 37° C for 3 hours and the reaction was quenched at 80° C for 20 minutes. For the backbone plasmids, 10 unit of alkaline phosphatase was used in order to prevent re-ligation of the plasmids. The mixture was incubated for 1 hour and the enzyme was denatured for 20 minutes at 95° C. Gel electrophoresis was used to separate the correct DNA fragments. 1 percent agarose gel was run at 100 V for 1 hour 30 minutes. A correct DNA fragment was excised from the gel under UV lamp and a gel isolation kit was used in order to recover the fragment from the gel (Figure 10). A final clean up step using a PCR clean up kit was performed in order to remove as much agarose as possible. DNA was eluted in sterile water and used for cloning afterward. The DNA was kept as concentrated as possible after the digestion step. For long term storage, the DNA was frozen in a TE buffer with low EDTA in order to prevent degradation.

4.11.1.2 DNA Ligation

An Online ligation calculator from New England Biolab (NEB) was used to set up all ligation reactions. 100 ng of backbone plasmid was used in every reaction. The amount of insert used was varied from reaction to reaction due to the different ratios between the backbone and insert. Generally, the ratio of 1:3 (backbone to insert) was kept in all reactions. 1 unit of DNA ligase was used for a 20 µL reaction. The reaction was incubated at 16° C overnight and the ligase was denatured at 85° C for 20 minutes before transformation.

4.11.1.3 Transformation

Chemically competent *E. coli* (DH5α) bacteria were purchased from NEB. A simple heat shock protocol was used, including 35 minutes of incubation of the bacteria and plasmid on ice, then a 2 minutes heat shock at 42° C. Then a 5 minutes recovery period on ice and a 1 hour aerated incubation period at 37° C using SOC medium. The culture was concentrated and 100 µL was plated onto a respected antibiotic agar plate. The plate was incubated in a 37° C oven overnight before 4 to 5 colonies were picked for further characterization.

4.11.1.4 Gel electrophoresis

% Agarose	Optimum Resolution for Linear DNA
0.7	800-12,000 bp
1	500-10,000 bp
1.5	200-3,000 bp
2	50-2,000 bp

Table 2: Optimum agarose concentration for different sizes of linear DNA

Gel electrophoresis was utilized to detect digested DNA fragments. Different amounts of agarose (w/v) were added to 100 mL of TAE buffer. Depending on the size of the fragments of interest the percentage of the gel ranged from 0.6% to 2%. Table 2 shows the corresponding percentage of gel to DNA fragment size observed. The mixture was then heated up in the microwave at high heat for 2 minutes. 10 µL of ethidium bromide was added to the mixture (1:10,000) and the mixture swirled to mix. The gel was casted into the casting chamber, bubbles were removed, the comb was inserted. The gel was left to cool down at room temperature for 45 minutes. The comb was carefully removed, and the gel placed into the electrophoresis chamber. DNA was loaded onto the gel and was allowed to run at 120 V

for 45 minutes at room temperature. After the run, the gel was scanned using a Bio-Rad gel DOC XR system.

4.11.1.5 Screening for a correct clone and plasmid preparation

To screen whether the bacteria contained the correct insert, 3-5 bacteria colonies were picked from the transformed population and each inoculated into 5 mL of LB medium containing the appropriate antibiotic (100 mg/mL). The cultures were grown overnight in a 37° C incubator. The next morning a Sigma mini-prep kit was used to isolate plasmid DNA from the bacteria cultures.

	Midi-prep	Maxi-prep	Giga-prep
Culture volume (mL)	100	600	6,000
P1 buffer (mL)	4	10	120
P2 buffer (mL)	4	10	120
P3 buffer (mL)	4	10	120
Incubation time (min)	15	20	30
QTB buffer (mL)	4	10	75
QC buffer (mL)	20	60	600
Isopropanol (mL)	3.5	10.5	70
70% EtOH (mL)	2	5	10
H_2O (µL)	150	500	2,000

Table 3: Different scales preparation of plasmid DNA using Qiagen kit

Overnight bacteria cultures were pelleted separately into a 1.5 mL Eppendorf tube using a benchtop centrifuge. The supernatant was discarded, and the pellets were re-suspended with 200 µL of P1 re-suspension buffer. 200 µL of P2 lysis buffer was added to each tube and the tubes were inverted several times until the mixture turned viscous. 350 µL of P3 neutralization buffer was added to each tube and the tubes were inverted several times until white flocculates appeared. To obtain clean bacteria lysate, the mixture was centrifuged at 13,000 rpm for 10 minutes at room temperature in order to pellet all precipitates. Meanwhile 500 µL of column preparation buffer was added to each column and centrifuged through using a benchtop centrifuge. The flow through was discarded and the bacteria lysate was added to each prepared column. The columns were centrifuged at 13,000 rpm for 1

minute at room temperature and the flow through discarded. 500 µL of wash solution 1 was added to each column and the columns were centrifuged at 13,000 rpm for 1 minute at room temperature and the flow through discarded. 750 µL of wash solution 2 was added to each column. The columns were centrifuged at 13,000 rpm for 1 minute at room temperature and the flow through discarded. The columns were centrifuged at 13,000 rpm for 2 minutes at room temperature to remove all trace of alcohol. The columns were separately placed onto new 1.5 mL Eppendorf tubes and 35 µL of ddH2O was added. The column was incubated for 3 minutes at room temperature and centrifuged at 13,000 rpm for 1 minute at room temperature to elute all the plasmid DNA. The obtained plasmid DNA concentration was measured using a nanodrop and 500 ng of plasmid DNA was used for restriction digest with appropriate enzyme in order to confirm the correct clone.

Higher amounts of plasmid DNA were needed for virus production. Qiagen plasmid Midi, Maxi and Giga kit were used. Generally, midi-prep and maxi-prep were used for small scale virus production and giga-prep was used for large scale virus production. Manufacturer instructions were followed. Table 3 below shows buffers, volumes and incubation times used for each plasmid kit.

4.11.2 Virus Production

Recombinant vector productions were generated by cross-packaging of AAV2-inverted terminal repeat recombinant genomes into AAV6 or AAV9 capsids using the two plasmids transfection protocol described by [133, 134]. High titer vectors were produced using 150 mm cell culture dishes or cell stacks (Corning) with polyethylenimine harvested after 48 hours and purified by filtration and iodixanol gradient as described by [135]. The recombinant adeno-associated viral vectors AAV6 and AAV9 CMV MLC260 FLAG *Rel1*[Rattus] (designated AAV6 RXFP1 or AAV9 RXFP1) and control virus vector AAV6 and AAV9 CMV MLC260 FLAG *Luc*[Firefly] (designated AAV6 LUC or AAV9 LUC) were generated using the described method. Viral titers from both viruses were quantified at the same time using a SYBR-green quantitative real time PCR (qRT-PCR) assay and expressed as viral genomes per milliliter (vg/mL). Figure 11 shows the plasmid used for virus production and *in silico* analysis of RXFP1 protein structure with added FLAG-TAG.

Materials and Methods
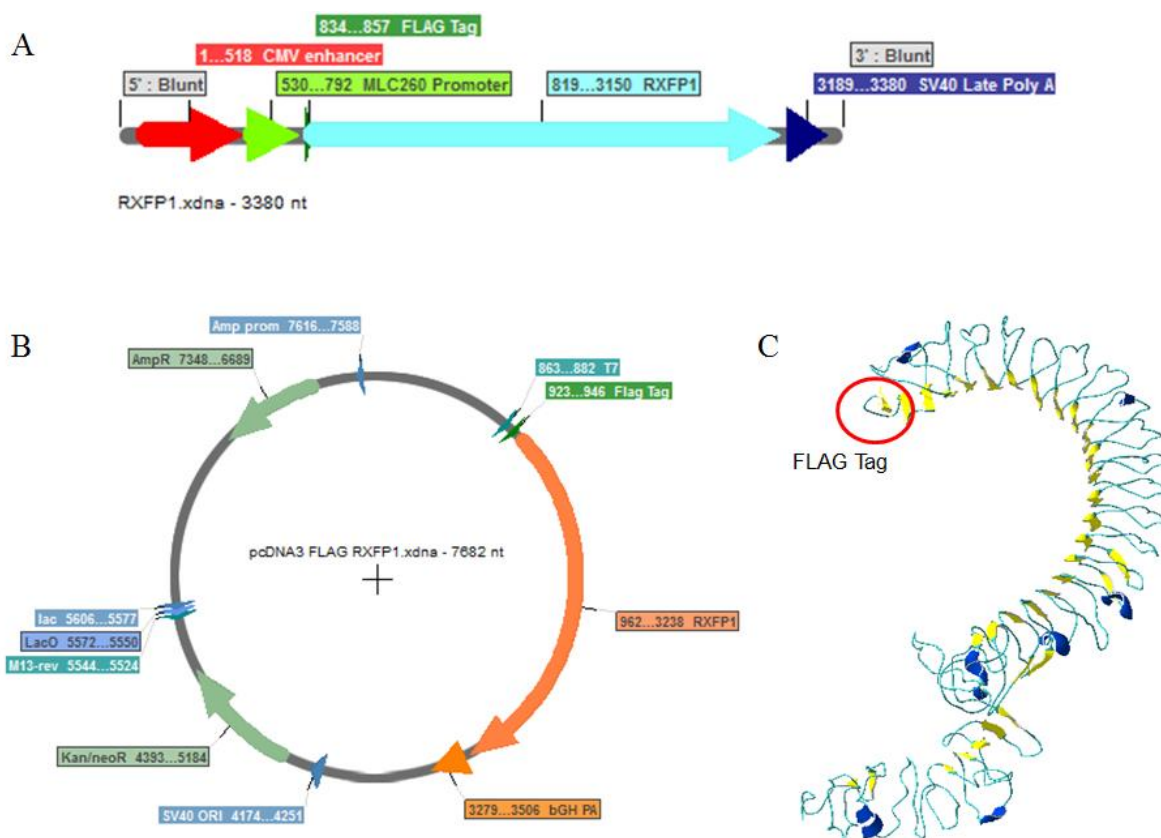
Figure 11: RXFP1 transgene construct.
(A) RXFP1 transgene expression cassette with FLAG-TAG and cardiac specific promoter.
(B) Plasmid map of the RXFP1 construct cloned into pCDNA 3.1 plasmid (Serial cloner).
(C) *In silico* analysis of RXFP1 protein folding with FLAG-TAG modification.

4.11.2.1 Small scale virus (AAV) production

For *in vitro* experiments, small scale productions of AAV serotype 6 were used [136]. HEK 293T cells were seeded in a T175cm^2 cell culture flask with 3 x 10^6 cells in 20 mL of medium. Four flasks were needed to complete one small scale production. 48 hours after seeding, the cells were split into sixteen 150 mm dishes with approximately 8.5 x 10^6 cells per dish. One day after seeding the dishes, the cells were transfected with polyethylenimine (PEI), AAV helper plasmid DNA and the respective AAV genome plasmid DNA. Table 5 below shows the volume of buffer, PEI and the amount of DNA needed for each production. The mixture was mixed in the order shown in Table 5 and incubated at room temperature for 20 minutes before the full medium was added. The medium from all the dishes was removed and 15 mL of the transfection mixture was added to each dish. The cells were incubated for 3 days at 37° C (5% CO$_2$). After the incubation period, the cells were harvested along with the medium. The dishes were washed with PBS and the cells from the medium and wash were pelleted by centrifugation at 2000 rpm for 15 minutes at room temperature. All the pellets

were combined, and the cells were re-suspended in 5 mL of lysis buffer containing protease inhibitor. The cells were lysed by freeze/thaw cycles. Re-suspended cells were frozen in liquid nitrogen for 10 minutes and thawed at 37° C for 10 minutes. The cycle was repeated 4 times. The genomic DNA and other DNA contaminant were digested using Benzonase ® nuclease (50 U per mL lysis buffer) for 1 hour at 37° C. The AAV containing cell lysate was centrifuged for 30 minutes at 4400 rpm to pellet the remaining cell debris. The supernatant was transferred to a new tube and stored in the -20° C until further gradient purification was performed.

4.11.2.2 Large scale virus (AAV) production

Large scale virus production was done using a 10 layered cell stack production unit according to [135, 137]. Only AAV serotype 9 was produced in large scale for the *in vivo* study. Six T175 cm^2 flasks were seeded with $3x10^6$ HEK293T cells each. The cells were incubated at 37° C with 5% CO_2 for 48 hours. Six flasks were split and $2.3x10^8$ cells were re-suspended in 1,040 L of complete medium. One liter of the cell mixture was added to the 10 layered cell stack. The last 40 mL of the cell mixture was split in half and 20 mL was seeded as negative and positive controls accordingly. The cells were incubated at 37° C with 5% CO_2 for 16 hours. The following day, after seeding, transfection was performed using 400 µg of recombinant AAV genome DNA and 1,525 µg of helper plasmid (pDP9rs) mixed with 800 mL serum free medium and 15.5 mL of transfection reagent PEI (Table 4). The DNA mixture was added to a serum free medium and mixed well before PEI was added. The mixture was incubated at room temperature for 20 minutes. 220 mL of full medium was added to the mixture after incubation. The medium from the cell stack was removed and 1.02 liters of the transfection mixture was added to the cell stack. The remaining 20 mL was added to the positive control flask. The cell stack was gently inverted to mix the transfection reagent. The cells were incubated at 37° C with 5% CO_2 for 48 to 60 hours before harvesting

After 72 hours the positive and negative controls were checked under the microscope. At least 40 percent of the cells have to detach in order to harvest the production. If the positive control met the criteria and the negative control showed healthy cells, the production was harvested. The cells were checked again after 12 hours. To harvest the cells, all medium was removed from the cell stack into 500 mL bottle. 300 mL of PBS was used to wash the cell stack. The cells were detached using a solution of 50 mL PBS/EDTA and 50 mL 0.25% trypsin. The cell stack was incubated for 5 minutes at 37° C. After 5 minutes, the cell stack tapped on the bench to facilitate the detachment of the cells. When all cells were detached,

300 mL of old medium was added to stop the reaction. All cells and medium were centrifuged at 4,400 rpm for 5 minutes at 4° C. After centrifugation, the supernatant was transferred to a glass bottle containing 331 g/L ammonium sulfate. The supernatant mixture was incubated overnight at 4° C with constant stirring at 1,000 rpm. The next morning the mixture was centrifuged at 4,400 rpm for 35 minutes at 4° C. The supernatant was removed, and the pellet was resuspended in 20 mL of lysis buffer containing 1x protease inhibitor then stored in - 20° C. The cell pellet was re-suspended by vortexing in 5 mL of lysis buffer containing 1x protease inhibitor and store at - 20° C.

	Small Scale (12 dishes)	Large Scale (10 layers cell stack)
Serum Free Medium (mL)	120	800
Amount of AAV genome plasmid (μg)	150	400
Amount of helper AAV plasmid (μg)	750	1,525
PEI (mL)	2.2	15.5
Full medium with 10% FCS (mL)	60	220
Incubation time (min)	20	20
Amount added to each dish or cell stack (mL)	15	1,000

Table 4: Transfection reagents and volumes used in different scales of viral production

The cells were lysed by freeze/thaw cycles. The cell pellet was frozen in liquid nitrogen for 5 minutes, then thawed in room temperature water for 5 minutes, and further thawed in 37° C warm water for 5 minutes. After all the steps, the cells were vigorously vortexed for 1 minute. The cycle was repeated 4 times in order to effectively lyse the majority of the cells. Contamination from genomic DNA and unpackaged viral DNA was addressed by adding Benzonase® nuclease (50 U per mL lysis buffer) and incubating the mixture at 37° C for 1 hour. The lysate was cleaned by centrifugation at 4,400 rpm for 45 minutes at 4° C. After centrifugation, the clear supernatant containing AAV particles was transferred into a new tube and the pellet was discarded. This step was repeated until no more pellet could form from the supernatant after centrifugation. The clean supernatant was kept at 4° C before purification.

4.11.2.3 Iodixanol density gradient

Iodixanol density gradient was used to purify AAV particles from cell lysate for both small-scale and large-scale viral production (Figure 12) [138].
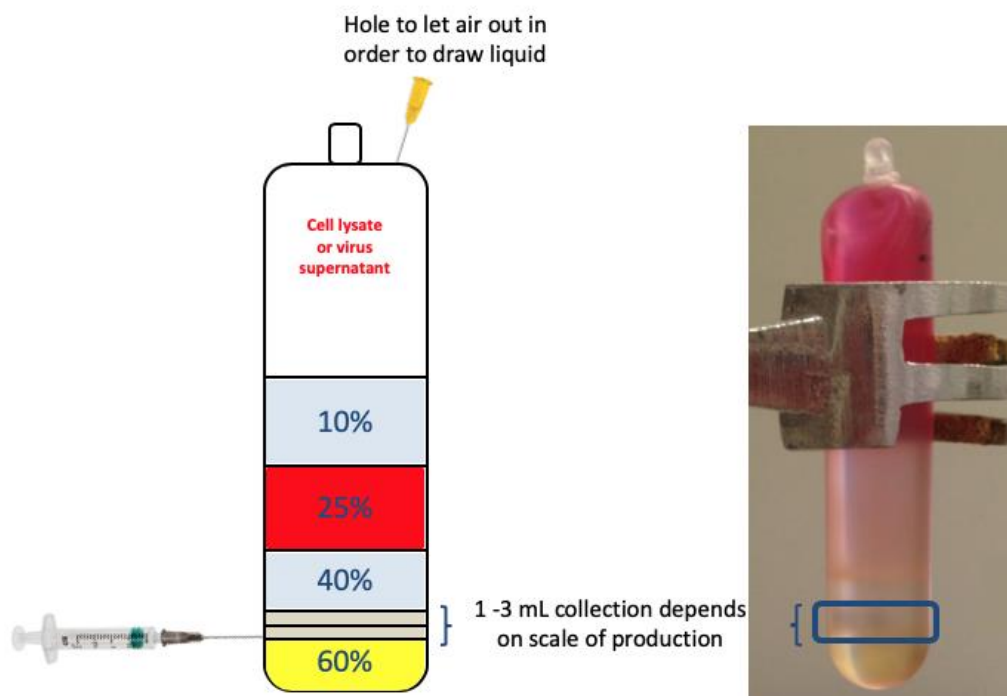
Figure 12: Iodixanol gradient.
Example of how to set up Iodixanol gradient and how to locate virus after centrifugation

The AAV particle was purified from the cell lysate using an iodixanol density gradient. First, AAV containing lysate was filled into an ultra-centrifugation tube using a Pasteur pipette. (15%) iodixanol solution, (25%) iodixanol solution, (40%) iodixanol solution, and (60%) iodixanol solution were added using the underlaying technique. Table 5 below summarizes the loading of both small and large iodixanol gradient.

	Small Gradient (mL)	Large Gradient (mL)
Samples	5	20
(15%) iodixanol solution	2	7
(25%) iodixanol solution	2	5
(40%) iodixanol solution	2	4
(60%) iodixanol solution	2	4

Table 5: Iodixanol density gradient loading for small and large scale AAV production

Materials and Methods

The ultra-centrifugation tubes were heated, sealed and balanced carefully to a margin of error of less than 20 mg between the balanced pair. The samples were centrifuged at 50,000 rpm for 2 hours at 4° C. After centrifugation, the tubes were carefully removed from the rotor and the AAV particles were collected using a syringe with a 21-gauge needle. The AAV particles containing layer (Figure 11) located between the 60% and 40% iodixanol was removed with an approximate volume of 1 mL per small scale gradient and 3 mL per large scale gradient. The collected AAV particles were desalted using a 10 mL Zebra spin desalting column. Manufacture's protocol was followed, in order to exchange iodixanol to PBS. The obtained AAV particles were stored at 4° C for short term storage and -20° C for long term storage. For long term storage, the virus was concentrated before being frozen.

4.11.2.4 Virus titration

AAV vector genomes were quantified using qRT-PCR method against AAV standard kindly provided by AG Müller [135, 139]. AAV vectors were diluted 1:100 in ddH_2O. The diluted samples were mixed with 10 µL TE buffer and 20 µL 2 M NaOH solution. The samples were incubated at 56° C for 30 minutes and neutralized with 960 µL 40 mM HCl solution. AAV vector standard was diluted ranging from 10^3 to 10^9 vg/well. SYBR green supermix was used for the qRT-PCR reaction. All samples including the standard were quantified in triplicate using a 96-well plate. Each standard well contains 10 µL of SYBR green supermix, 0.5 µL of SV40 forward primer (10 pmol/µL), 0.5 µL of SV40 reverse primer (10 pmol/µL), 6 µL of ddH_2O, and 3 µL of standard vector. Each sample well contains 10 µL of SYBR green supermix, 0.5 µL of SV40 forward primer (10 pmol/µL), 0.5 µL of SV40 reverse primer (10 pmol/µL), 6 µL of ddH_2O, and 3 µL of sample. The final volume in each well is 20 µL. A No-Template-Control with water was included in every experiment in order to minimize occurrence of false positive samples. The PCR plate reader was programed as followed (Table 6).

Step	Temperature	Time	Number of Cycles
Denaturation	95° C	1:00	1x
Denaturation	95° C	0:05	40x
Annealing and reading	60° C	0:30	
Melting Curve	65 → 95° C with 0.5° C increment	0:05	60x

Table 6: qRT-PCR program for AAV vectors quantification

The obtained results were analyzed using CFX manage software from Bio-Rad. A standard curve was plotted from the obtained results and the titer was calculated in Microsoft excel using an equation obtained from the best fit line of the standard.

4.11.3 Cell Culture techniques

Aseptic techniques were used to ensure sterile. The HEK293T cell line was kindly provided by AG Most. The cells were grown and preserved in liquid nitrogen at passage 8. HEK cells were generally cultured in a T75 flask or a T175 flask depending on the amount required for the experiment. Primary cells were cultured for a maximum of 7 days in 6-well, 12-well or 96-well plates depending on the experimental set up.

4.11.3.1 Cell line culture techniques

A HEK293 cell line was also used for this study. The cells were cultured in DMEM medium with high glucose supplemented with 10% v/v FCS, 100 U/mL penicillin, AND 100 µg/ streptomycin. This cell line was cultivated in sterile 75 cm^2 or 175 cm^2 culture flasks which were lying horizontally in a humidified incubator containing 37° C and 5% CO_2. The cells were split every two days or when the monolayer reached at least 80 % confluence. To split the cells, the medium was removed, and the cells washed with 10 mL of warm PBS. PBS was removed and 4 mL of 0.25% Trypsin EDTA was added to the bottle for 4 minutes. Then 6 mL of full 10% FCS medium was added to stop the digestion. The cells were pipetted up and down at maximum speed for 7 times. To reseed the bottle, 1 mL containing 3.5 million cells was seeded into a new bottle and 20 mL of full medium was added (Table 8). The cells were discarded after reaching passage 35.

4.11.3.2 Seeding of the cell line

After splitting, HEK293T cells were seeded into multi-well plates for *in vitro* experiments, then reseeded for maintenance of the culture into culture a flask. The Neubauer improved cell counter technique was used to determine the amount of cells in the suspension. First the suspension was diluted 1:10. Then 10 µL was loaded onto the Neubauer chamber. The cells in all four major squares with 16 smaller squares were counted. The average number of cells counted was calculated and the amount of cell per mL could be calculated with the following formula.

(Average cell counted) x (dilution factor of 10) x 10^4 = number of cells per mL

Materials and Methods

Table 7 shows the numbers and volumes of cells seeded in different plates and flasks

	Area per well (cm^2)	Number of cells seeded	Final volume (mL)
6-well plate	10	3×10^5	2
12-well plate	4	1.5×10^5	1
24-well plate	2	7×10^4	0.5
T175 cm^2 flask	175	3×10^6	21
T75 cm^2 flask	75	1.5×10^6	12
T25 cm^2 flask	25	5×10^5	5

Table 7: Volumes and numbers of HEK293T cells seeded in different plates and flasks

4.11.3.3 Transfection of HEK293T cells

Transfection was done on HEK293T cells in order to check the expression level of overexpressed protein and the quality of the plasmid DNA produced. One day after seeding The HEK293T cells, plasmid DNA was transfected into the cell using Polyethylenimine (PEI) transfection reagent. A mixture of 1µg of plasmid DNA, sterile water, 300 mM NaCl and PEI was mixed, incubated for 15 minutes at room temperature, and added to the cells drop-wise. The plate was gently rocked in order to achieve equal distribution of transfection. The cells were incubated for 48 hours at 37° C and 5% CO_2 humidified atmosphere. Table 8 shows the amount of plasmid DNA and mixture volume used for each well.

	6-well plate	12-well plate
Volume of sterile H_2O (µL)	48	25
Volume of 300 mM NaCl (µL)	64	30
Amount of Plasmid DNA (µg)	1 (µg)	1 (µg)
Mixed well		
Volume of PEI (µL)	18	9
Final volume added (µL)	120	90

Table 8: Volumes of DNA and transfection reagent used for HEK293T cells transfection

4.11.3.4 Cryopreservation of cells

To cryopreserve the HEK293T cell line, the cells were resuspended in 8 mL of fresh medium after trypsin exposure. The mixture was centrifuged for 10 minutes at 1,500 rpm. The supernatant was removed, and the cells were re-suspended in 1 mL freezing medium (90% FCS and 10% DMSO). The cell suspension was transferred into cryo-tubes and placed into a freezing box containing DMSO which would lead to more gradual and unified freezing, in order to prevent growing crystal ice. The tubes were frozen in the -80° C for at least 2 days before being thawed for future usage. The frozen cells were removed and stored into liquid nitrogen for further storage.

4.11.3.5 Isolation of neonatal rat cardiomyocytes (NRVCMs)

Primary cultures of neonatal rat ventricular cardiac myocytes (NRVCMs) were prepared from 1-2 days old Wistar rats (Charles River) [140, 141]. The neonatal rats were euthanatized by decapitation and the heart removed and placed in 1x cold ADS solution. The atria and other vessels were removed, and the hearts were transferred into a new 1x cold ADS solution. The ADS solution was removed, and the ventricles were washed with 3 mL of cold ADS before being minced. Tissue fragments were digested in a T75 bottle with 30 mL of a digestion solution containing collagenase and pancreatin for 5 minutes at 37° C. The tissue fragments were allowed to settle on side of the bottle and the solution removed and discarded. Fresh digestion solution was added, and the tissue fragments were digested for 20 minutes at 37° C. After 20 minutes, the tissue fragments were pipetted up and down 5 times at maximum power and the solution removed and filtered through a 40 µm cell strainer into a 50 mL falcon. 10 mL of FCS was added through the cell strainer and the solution was centrifuged at 1,000 rpm for 5 minutes at room temperature. After centrifugation, the supernatant was removed, and 7 mL of FCS was added. The cell solution was placed in a 37° C incubator awaiting further processing. The tissue fragments were digested at least 5 times in order to completely dissolve all the tissue pieces. After the digestion, all cell suspensions were combined, and centrifuged 1,000 rpm for 5 minutes at room temperature. The supernatant was removed, and the cells were resuspended in 12 mL of 1x cold ADS. The fibroblasts and cardiac myocytes were separated using a percoll density gradient.

Materials and Methods

4.11.3.6 Separation of NRVCMs from fibroblasts

To obtain cardiomyocytes with high purity, a two-layer Percoll density gradient was performed [140]. The gradient consisted of 63% red Percoll solution, and a 40.5% clear Percoll solution. 4 mL of red Percoll solution was added into each 15 mL falcon. Then 3 mL of clear Percoll solution was added using the underlaying technique. Lastly, 2 mL of cell solution containing 1x cold ADS was layered at a 45 degrees angle onto of the gradient. The tubes were centrifuged at 2,400 rpm for 30 minutes at 4° C with deceleration speed of 0. The upper stromal cells band including fibroblasts was removed by aspiration. The lower cardiomyocytes band was kept and washed twice with 1x cold ADS before being re-suspended in warm Medium 199 supplemented with 10% v/v FCS, 100 U/mL penicillin, 100 µg/ streptomycin, 2 mM L-glutamine, and 1 mM calcium chloride. The cells were counted manually in a Neubauer chamber and plated accordingly. The NRVCMs were cultured at 37° C and 5% CO_2 humidified atmosphere. After 48 hours fetal calf serum was reduced to 0.5% and cells were cultured for 2-5 days.

4.11.3.7 Cultivation of NRVCMs

	Area per well (cm^2)	Number of cells seeded	Volume per well (mL)
6-well plate	10	2×10^6	2
12-well plate	4	5×10^5	1
96-well plate	0.32	2×10^4	0.1
Glass bottom dish	3.14	2×10^5	2

Table 9: Volumes and numbers of NRVCM cells plated on different types of plate

The NRVCMs were cultured at 37° C and 5% CO_2 humidified atmosphere. The cells were kept in medium M199 (Sigma Aldrich) supplemented with 10% v/v FCS, 100 U/mL penicillin, 100 µg/ streptomycin, 2 mM L-glutamine, and 1 mM calcium chloride. Table 9 shows the number of cells plated for different plate types. Two days after the cells were plated, the medium was removed, and the cells were washed once with warm PBS before starving medium M199 supplemented with 0.5% FCS, 1% penicillin/streptomycin, 1% L-glutamine, 1 mM $CaCl_2$ was added. From this point on, the medium was changed every two days until the cells were harvested. Usually cells were used for a maximum of 7 days before being discarded.

4.11.3.8 Transduction

After confirming the expression of the overexpressed protein in the HEK293T cell and the AAV vector was produced, the NRVCMs were transduced using AAV vectors two days after seeding. AAV6 vectors from small-scale virus productions at the MOI of $1x10^4$ vg/cell were used in transduction experiments. Two days after seeding, the full medium was removed, and the cells were washed with warm PBS to remove as much serum and cell debris as possible. Starving Medium 199, supplemented with 0.5% v/v fetal calf serum, 100 U/mL penicillin, 100 µg/ streptomycin, 2 mM L-glutamine, 1 mM calcium chloride, and the respective amount of AAV6 vectors was added onto the cell. AAV vectors were allowed to transduce the NRVCMs for 48 hours at 37° C and 5% CO_2 before the medium was changed. The medium was changed every two days and the cells were stimulated and harvested five days after transduction.

4.11.4 *In vivo* experimental protocols

All animal procedures and experiments were performed in accordance with the *Guide for the Care and Use of Laboratory Animals* from the National Institutes of Health (NIH) and approved by the local Animal Care and Use Committee of Baden-Württemberg, Germany.

4.11.4.1 Administration of AAV vectors by tail vein injection

Systemic administration of AAV vectors containing the transgene was performed via the tail vein [107]. Before injection, mice were put into a restrainer and their tails were warmed in a 37° C water. When the vein was visible, a total of 100 µL of viral AAV vector was injected intravenously (i.v.) via the tail vein (injection by KEB employees at the animal facility of University of Heidelberg). The vectors were allowed to transduce the targeted cells for four weeks before further experiments were performed on the mice.

4.11.4.2 Alzet® osmotic pumps implantation

To continuously administer relaxin, Alzet® osmotic pumps (Alzet® model 1004) were used. A final volume of 100 µL was filled into each osmotic pump under sterile conditions. The pumps were then implanted subcutaneously (s.c.) into the dorsal side of the mice. To decrease the probability of infection, the mice were shaved at the surgical site under anesthesia before the operation. 5% isoflurane mixed with 0.5 -1.0 L/min 100% O_2 was used to induce anesthesia in the induction chamber. 0.5% of isoflurane mixed with 0.5 -1.0 L/min

100% O_2 was administered via a face mask in order to maintain anesthesia after induction. 1 cm incision was made into the skin of the mice using surgical scissors. Utilizing the blunt edge of the scissors, the skin was separated from the muscle to accommodate the pump. The pump was cleaned with cleaning solution before being implanted subcutaneously into the mice. After implantation, a surgical stapler was used to close the wound. Anti-inflammatory drug, carprofen (5µg/g), was given to the mice via intraperitoneal (i.p.) injection. The mice were checked every day for the next 5 days. The staple was removed on day 5 and the mice were kept for 3 weeks. After 3 weeks the mice were sacrificed, and the organs and plasma collected.

4.11.4.3 Echocardiography

Echocardiography was performed using the Vevo 2100 imaging system from Fujifilm-VisualSonics. First, the mice were shaved on the chest using Veet® hair removal cream. The conscious mice were held in prone position. Warm ultrasound coupling gel (37° C) was placed on the shaved chest area, and the MS400 transducer was positioned to obtain 2D B-mode parasternal long and short axis views and 1D M-mode short axis view. The ejection fraction (EF), fractional area change (FAC), and heart rate (HR) were calculated in the B-mode, both long and short axis, using THE LV trace function. Fractional shortening (FS) and left ventricular internal diameter (LVIDd) were calculated from 6 consecutive heartbeats in the M-mode using the LV trace function. Figure 13 shows representative images of different types of echocardiogram.
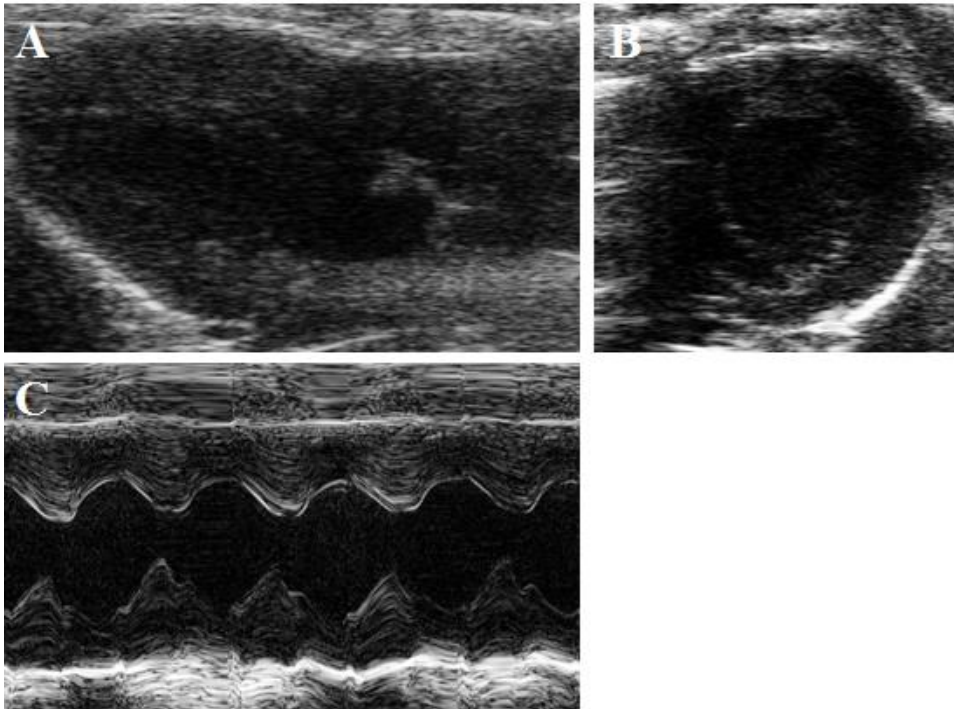
Figure 13: Different mode of echocardiography
Representative echocardiogram from 2D B-mode parasternal **(A)** long axis, **(B)** short axis, and **(C)** M-mode short axis.

4.11.4.4 Pressure-volume loop (PV loop)

Mice were anesthetized using a cocktail containing Xylazine (10 µg/g) and Ketamine (100 µg/g). 75 µL to 100 µL was injected i.p. into each animal depending on the weight of the animal. After 30 minutes, the mice were fixed onto the heating plate in supine position. The body temperature was maintained at 37° C. Mice were catheterized through the left carotid artery with a 1.2 Fr catheter, and pressure volume loops were measured in the left ventricle. Real time data was observed using the ADVantage PV system. All obtained data were recorded using a Scisense 404 – 16 Bit Four Channel Recorder with LabScribe2 software. Parameters such as dP/dtmax and dP/dtmin were calculated.

4.11.4.5 Trans-aortic constriction (TAC) model

A pressure overload heart failure model was generated by TAC surgery [142, 143]. 8 weeks old C57BL/6 mice were shaved from the neckline to mid chest level and echoed one day before the surgery. 75 µL of an anesthetic cocktail of Xylazine (10 µg/g) and Ketamine (100 µg/g) was used to induced anesthesia. The mice were restrained on the heating plate in supine position. The mice were then intubated, and anesthesia was maintained with 0.5% isoflurane mixed with 0.5 -1.0 L/min 100% O_2. A partial thoracotomy to the second rib was

performed under a surgical microscope and the sternum retracted using a chest retractor. Forceps were used to gently separate the thymus and fat tissue from the aortic arch. After the transverse aorta was identified, a small piece of an 8.0 prolene suture was placed between the innominate and left carotid arteries. Two loose knots were tied around the transverse aorta. A small piece of a 26-gauge blunt needle was placed parallel to the transverse aorta. The first knot was quickly tied against the needle, followed by the second and the needle was carefully removed in order to yield a constriction. Next the chest retractor was removed, and the outflow of the ventilator pinched off for 2 seconds to re- inflate the lungs. The rib cage and the skin were closed using a 6.0 prolene suture with an interrupted suture pattern. After the surgery, the mouse was injected with carprofen (5µg/g) s.c. Lastly, anesthesia was turned off, and the mice were extubated when signs of spontaneous breathing had occurred. The mice were placed into prone position and kept on the heating plate to recover for 45 minutes - 1 hour. In the sham control mice, the entire procedure was identical except for the ligation of the aorta. Figure 14 shows the scheme of how TAC operations were performed.
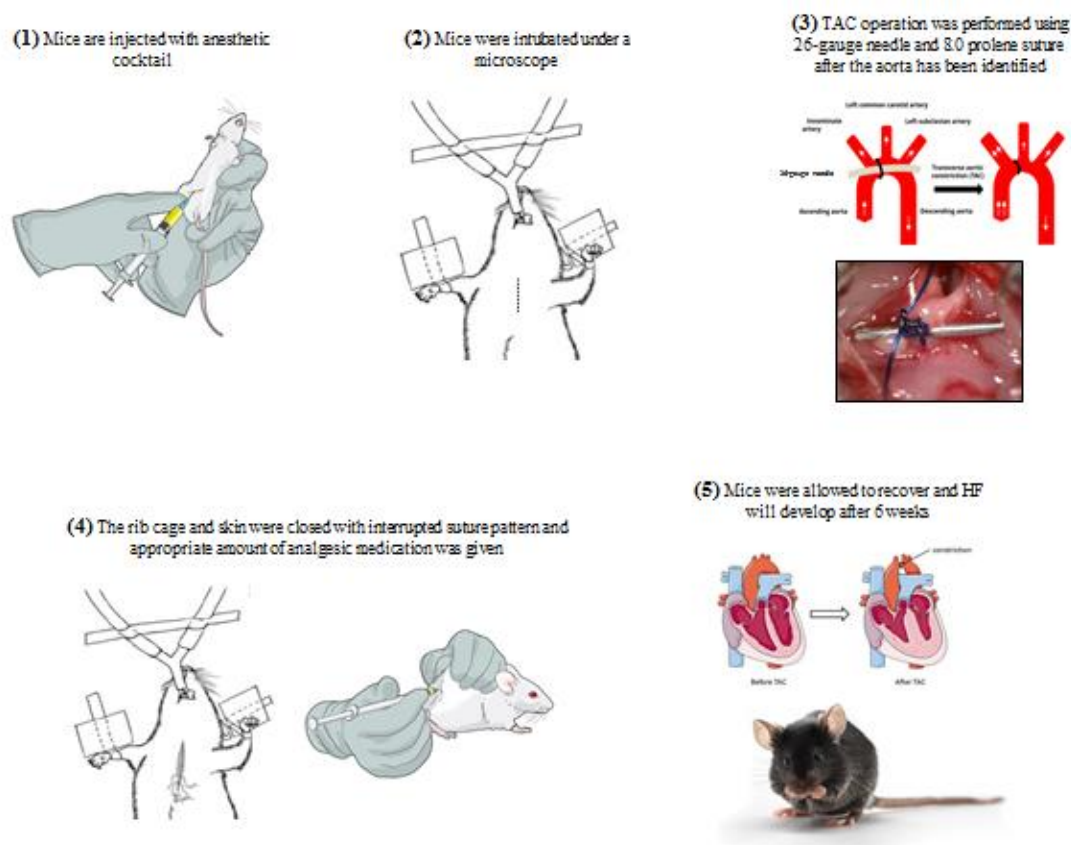
Figure 14: TAC operation scheme
The scheme of TAC operation starting from 1) initial anesthesia, 2) intubation, 3) TAC operation, 4) Suturing and recovery and, 5) post-op follow up and HF development.

4.11.4.6 Sample collection and histology

Before being euthanized, a final blood collection was taken from the mice, and EDTA plasma was collected by centrifuging whole blood at 3,000 x g for 15 minutes at 4° C. At the end of the study all mice were euthanized by cervical dislocation. The chest was opened, and the heart and lungs removed. The heart was washed in cold PBS, weighed and cut into 7 pieces (Figure 15). The lungs were cleaned and weighed. Other organs such as liver, kidney, adrenals, spleen, and skeletal muscle were collected also collected. All tissue pieces were gradually frozen on dry ice and placed in the -80° C freezer for further analysis.

For histology, the second piece of the heart was put into 4% formaldehyde, and kept overnight at 4° C. The next morning the tissues were given to the histology core unit at the University of Heidelberg for further processing and staining.
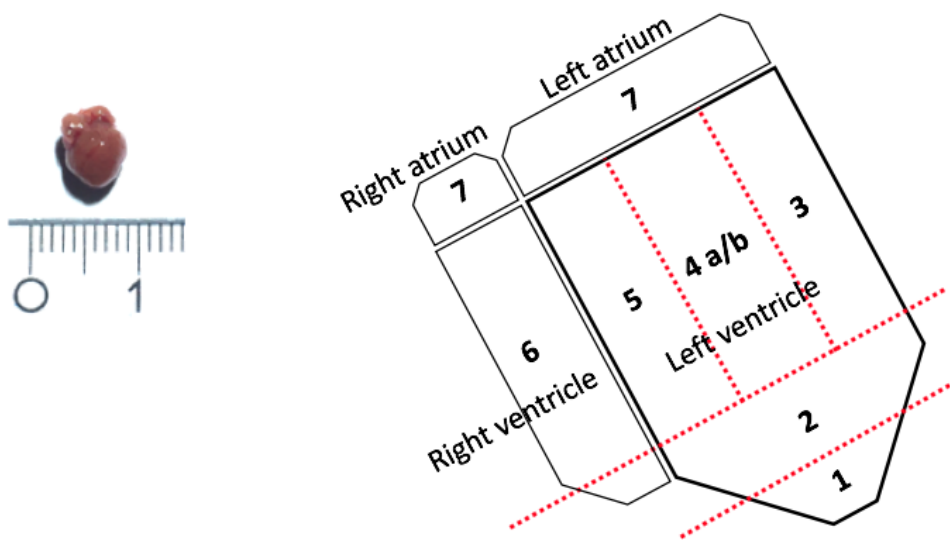
Whole Mouse heart

Figure 15: *In vivo* heart sampling diagram.
The heart was divided into 8 samples according to this diagram. First the atria were removed follow by the right ventricle. Lastly, the left ventricular was divided into 6 pieces. The apex was used for RNA quantification and the lateral wall of the left ventricle was used for protein quantification.

4.11.4.7 Relaxin receptor gene therapy study design

Eight weeks old C57BL/6 mice were echoed and weighed one day before the start of the experiment. The TAC operation was performed on day 1 and the mice were allowed to recover for seven days. At day 7, the second echo was performed on the mice to verify the operating results. Next the mice were randomly assigned into 4 test groups and 2 sham

groups. The virus was injected into the mice via the tail vein on the following day. The virus was allowed to express for 4 weeks. At 3 weeks after TAC, and before osmotic pump implantation, the mice were assessed again by echocardiogram. The osmotic pumps containing relaxin were implanted subcutaneously into the back of the mice. The mice were followed for 4 more weeks before being sacrificed.

4.11.4.8 Relaxin H2 measurement

Circulating levels of recombinant relaxin H2 was measured using a ready to use relaxin H2 Quantikine ELISA kit from R&D Systems (DLR200). The plasma samples were diluted 1:200 as suggested by the manufacturer. The manufacturer's protocol was followed. 50 µL of negative control, positive control, standard, and samples were added to the wells that were pre-coated with RLN H2 capture antibody. After 2 hours of incubation at room temperature, the wells were thoroughly washed 4 times. Conjugated antibody against RLN H2, coupled with horseradish peroxidase, were added into each well and incubated again at room temperature for 2 hours. After 2 hours, the conjugated antibody was discarded, and the wells were thoroughly washed 4 more times. Next, a freshly made substrate solution was added to each well and incubated for 30 minutes at room temperature protected from light. The solution color within the wells gradually turned blue. After 30 minutes, the stop solution was added, and the solution within the wells turned yellow. After the addition of stop solution, the optical density (O.D.) was measured at the wavelength of 540 nm with a correction wavelength at 570 nm within 30 minutes. The detection range of the assay ranged from 7.8 to 500 pg/mL of RLN.

4.11.5 Molecular and biochemical methods
4.11.5.1 RNA isolation

The total RNA was extracted using TRIzol® Reagent from both cells in culture and tissues [141, 144]. For the cell culture experiments, 6-well plates were used. Before harvesting, the medium was removed, and the cells were washed once with warm PBS. Quickly after removing the PBS, 1 mL of TRIzol® Reagent was added to each well. This step needed to be done as quickly as possible to minimize the changes in response to environmental stress occurring within the cells. The TRIzol® solution was pipetted up and down 4 to 5 times and collected into a 1.5 mL Eppendorf tube. After this step, the samples were snap frozen for further analysis, if necessary. Next, 200 µL of chloroform was added to

each of the samples. TRIzol® reagent and chloroform were mixed by vigorous shaking. When the phase separation could be seen, the samples were centrifuged for 15 minutes at 14,000 rpm and 4° C. All steps that followed centrifugation were performed on ice. After centrifugation, 400 µL of the top aqueous phase was transferred into a new tube. Next 400 µL of cold isopropanol and 1.5 µL of polyacryl carrier were added to the mixture. The samples were shaken vigorously again until all the components were mixed thoroughly. RNA was precipitated overnight in a -20° C freezer. After 16-24 hours of precipitation, the RNA was palleted at maximum speed for 15 minutes at 4° C. The supernatant was discarded, and the pallet was washed and centrifuged twice with 75% ethanol for 15 minutes at 14,000 rpm and 4° C. After the centrifugation step, the samples were allowed to air dry at room temperature for 5 to 10 minutes. 20 µL of ddH$_2$O was added to dissolve the RNA pellet. After all the pellets had been dissolved, RNA concentration was measured using a NanoDrop2000.

For tissue samples, approximately 15 mg of tissue was used per sample. The tissues were transferred into bead mill tubes containing 4 ceramic beads and 1 mL of TRIzol® Reagent and homogenized once at 6,000 rpm for 30 seconds. The homogenized solutions were centrifuged for 1 minute and transferred into a normal Eppendorf tube. RNA isolation techniques stated above were followed afterward.

4.11.5.2 Reverse transcription

RNA isolation and reverse transcription were done on the same day. After the RNA concentration measurement, 1 µg of total RNA was diluted with water to make the final volume of 15 µL. Next 4 µL of 5x reverse transcription buffer and 1 µL of reverse transcriptase were added to each reaction to make the final reaction volume of 20 µL. The reactions were performed with the following protocols (Table 10).

Step	Temperature	Time	Number of Cycles
Annealing	25° C	5:00	1x
Reverse transcription	42° C	30:00	1x
Termination	85° C	5:00	1x

Table 10: Reverse transcription program for RNA

After reverse transcription, the resulting cDNA was kept in a -20° C freezer. The cDNA was diluted 1:100 using DEPC treated water. Pending further analysis, the diluted cDNA was also frozen in the -20° C freezer.

4.11.5.3 Quantitative real time PCR (qRT-PCR)

iQ SYBR Green Supermix was used according to the manufacturer's protocol. A final volume of 15 µL per reaction consisted of 7.5 µL iQ SYBR Green Supermix, 1 µL of forward and reverse primers mix (final concentration of 300 nM each), and 6.5 µL diluted cDNA (final concentration of 3.25 ng per reaction) was prepared [137, 141]. The qRT-PCR reaction was performed on a Bio-Rad CFX96 real-time PCR detection system with a protocol described in table 11.

Step	Temperature	Time	Number of Cycles
Denaturation	95° C	3:00	1x
Denaturation	95° C	0:10	40x
Annealing	60° C	0:10	
Elongation and reading	72° C	0:30	
Termination	95° C	0:10	1x
Melting Curve	65 → 95° C with 0.5° C increment	0:05	60x

Table 11: General qRT-PCR protocol

The result of the qRT-PCR reaction was analyzed using CFX manager software. *HPRT1* was used as a reference gene, and relative expression changes were calculated by applying the ΔΔCt method according to Livik and Schmittgen [145].

4.11.5.4 Isolation of proteins

Proteins were isolated using a 1% SDS buffer supplemented with protease inhibitor. After transfection experiments with HEK293T cell or transduction experiments with NRVCMs, the medium was removed from the plate, and the cells were washed once with warm PBS buffer. 100 µL of 1% SDS buffer was added to each well and the cells scratched off with cell scratcher. The lysed cells were sonicated 10 times to fragment the genomic DNA. The protein lysate was centrifuged for 1 minute and put on ice. Protein concentration measurement was performed using Bio-Rad Bradford protein assay. Different concentrations of BSA were used to generate a standard curve. First, in a separate tube, the protein lysate

was diluted 1:10 in 1% SDS buffer. For each reaction, 250 µL of buffer and 5 µL of buffer S were mixed together. The diluted lysate was added to the mixture and 2 mL of buffer B was added. The solution was incubated for 15 minutes away from light. After 15 minutes, the solution turned blue and measurement could be performed on an infrared spectrometry using a 750 nM wavelength. The optical density measurements from standard samples were used to plot a standard curve to generate a linear equation to calculate the amount of protein in each sample. The protein concentration of each sample was adjusted accordingly. For the *in vitro* experiment, 10 µg of protein was loaded per sample per lane, and for the *in vivo* experiment, 20 µg of protein was loaded per sample per lane. After adjusting the concentration, the lysate was frozen in a -20° C freezer for later analysis.

4.11.5.5 Sodium dodecyl sulfate polyacrylamide gel electrophoresis (SDS page)

The 4-20% SDS gels from Novex were purchased and used in all western blot experiments. First, the protein lysate was thawed on ice for half an hour. 5x loading buffer was added, and the lysate was incubated in the heating block at 95° C for 5 minutes. The lysate was centrifuged and loaded into SDS gel. Table 12 shows the amount of lysate that can be loaded onto different SDS gel types. 7 µL of standard ladder (Prestain Protein ladder) was also loaded onto the gel in order to determine the size of the protein of interest. The electrophoresis was performed for 1 hour 45 minutes at 100 V. After the first 20 minutes, the electrophoresis chamber was placed on ice in order to decrease the heat generated from the current.

SDS gel type	Loaded volume (per well)	Maximum volume (per well)
10 lanes gel	35 µL	50 µL
12 lanes gel	30 µL	40 µL
15 lanes gel	25 µL	30 µL

Table 12: Sample volume for each type of SDS gel

4.11.5.6 Western blot

After electrophoresis, the SDS gel was electrophoretically transferred onto a PVDF membrane using the semi-dry blotting method [146, 147]. The blotting was performed in a cassette containing Whatman paper, PVDF membrane, SDS gel, and Whatman paper. The cassette was assembled in a blotting chamber from bottom to top. The membrane was

transferred at 15 V for 50 minutes. The blotted membrane was blocked in 0.2% I-block for 1 hour. The I-block was discarded, and the blot incubated in respective antibodies overnight at 4° C. The next morning, the antibodies were removed, and the membrane washed in TBS-T for 10 minutes 3 times. Then the blot was incubated in the respective secondary antibodies for 1 hour, and the blot was washed in TBS-T for 10 minutes, 3 times again. The signals from the blot were detected using an Odyssey infrared imager (LI-COR) detection system and the Images were processed using an Odyssey imaging software. Last, the blot was deactivated in methanol and allowed to air dry for 1 hour before being frozen in a -20° C freezer for long term storage.

4.11.5.7 cAMP measurement

cAMP measurement was performed using a cAMP Glo™ assay kit from Promega. The manufacture's manual was followed. First, NRVCMs were seeded into a 96-well plate at 20,000 cells per well (100 µL). The cells were transduced and stimulated accordingly. The medium was removed and 20 µL of test compounds in induction buffer (1x PBS supplemented with 500 µM IBMX and 100 µM Ro 20-1724) were added to the cells to stimulate cAMP production. After 15 minutes, 20 µL of lysis buffer was added to all wells. The cells were lysed at room temperature for 15 minutes. 40 µL of Detection buffer (Reaction buffer supplemented with Protein Kinase A) was added to all wells. Then the plate was mixed by shaking for 1 minute and incubated at room temperature for 20 minutes. 80 µL of Kinase Glo® Reagent was added to all wells and the plate was mixed by shaking for 1 minute and incubated at room temperature for 10 minutes. The luminescence was read using a luminometer.

4.11.5.8 Ca^{2+} transient measurement

Intracellular Ca^{2+} transients were measured according to Yu et al. with modifications to fit available apparatus [148, 149]. NRVCMs were transduced with RXFP1 or LUC AAV vectors for 5 days. The medium was changed every two days. On the day of the experiment, the transfected NRVCMs were loaded with 1 µM Fura 2 AM in M199 medium at 37° C for 15 minutes protected from light. After loading, the cells were washed with warm M199 medium for 15 minutes at 37° C protected from light and connected to an electrode system on the table of an inverted fluorescence microscope (IX70 Olympus). The cells were electrically stimulated with 1 Hz bipolar. Using a monochromator, the Fura 2 AM loaded cells were excited at 380 nm. The alternative measurement of the bispectral emission (340 nm/380 nm)

was performed with the fluorescence microscope for a period of 5 minutes and the emission ratio was calculated with the software TILL vision. The data were exported to an online program written by Dr. Martin Bush. The following parameters were analyzed: a) the amplitude of the transient (Δ[340 nm/ 380 nm]) and b) the diastolic Ca^{2+} ([340 nm/ 380 nm]).

4.11.6 Statistical analysis

GraphPad Prism software was used for statistical analysis. Data were expressed as means $\pm$ SEM, unless otherwise indicated. An unpaired two-tailed Student's t test was used when appropriate. A Mann-Whitney U test was used when the data was not normally distributed. To compare means among three or more independent groups exhibiting normal distribution, a one-way analysis of variance (ANOVA) was performed. A Tukey post-hoc test was applied when multiple comparisons were conducted. In case of non-normally distributed data, a Kruskal Wallis test was performed. A Dunn post-hoc test was applied when multiple comparisons were conducted. For all tests, $p < 0.05$ was accepted as statistically significant.

5 Results

RLN and its cognate receptor, RXFP1, both play a vital role in cardiovascular adaptation during pregnancy. RLN naturally exerts its positive inotropic effects in the atria through PKA activation and cAMP accumulation. Increased secretion of RLN from cardiomyocytes during a decompensated HF event suggests that RLN and its receptor RXFP1 could be valuable targets for cardiac gene therapy.

This study aimed to develop a novel regulatable gene therapy treatment for HF. The study was separated into three parts focusing on: 1) establishing a working *in vitro* model for proof of concept, 2) deciphering the mechanism behind the proposed treatment, and 3) testing the proposed treatment in an *in vivo* HF model. The first part of the study aimed to prove the feasibility of introducing functional foreign receptors into a cell, using a transduced primary cell model (NRVCMs). The second part of the study focused on deciphering the pathway responsible for RXFP1 activation, using the *in vitro* model established in part one of the study. Finally, the third part of the study focused on the safety and the efficacy of the gene therapy treatment in the *in vivo* HF model. A TAC operation was used to generate a hypertrophic HF in mice. AAV9 viral capsids containing Rat RXFP1 cDNA with CMV.MLC260 promoter were administered into TAC mice. Chronic administration of RLN was given to the animals using four weeks osmotic subcutaneous pumps. The effect of the treatment was evaluated relative to three control groups: TAC mice receiving control LUC virus with and without relaxin and TAC mice receiving RXFP1 virus without relaxin.

5.1 Determination of RXFP1 expression in the heart

According to the literature, RXFP1 expression in the ventricles is close to absent. This might contribute to the lack of RLN effects seen in the failed clinical trial [123]. To confirm this finding, RNA from different organs and parts of the heart was isolated and quantified. High RXFP1 mRNA expression in the heart could be detected compared to other organs (Figure 16 A). Figure 16 B shows a significant expression of RXFP1 mRNA in the atria compared to the ventricles. Therefore, the results of these experiments confirmed that the lack of RXFP1 expression led the lack of RLN response in the ventricles.
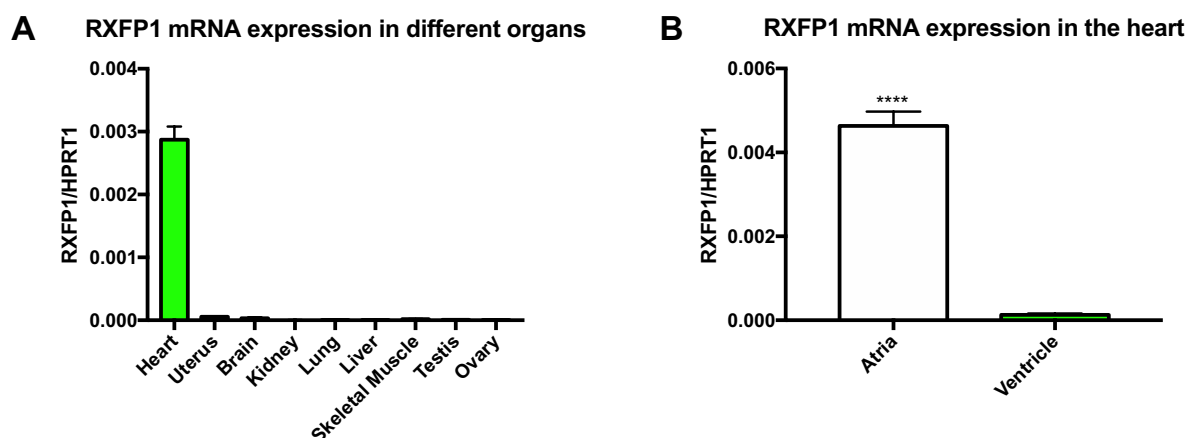
Figure 16: RXFP1 expression profile.
(A) Native RXFP1 mRNA expression in different organs (n=2-4) and **(B)** Native RXFP1 mRNA expression in different parts of the heart (n=10). mRNA was isolated and quantified by qPCR. *HPRT1* was used as a reference gene. *P < 0.05; **P < 0.01; ***P < 0.001. Error bars depict in SEM.

5.2   *In vitro* experiments and proof of concept

Due to the lack of RXFP1 expression in the left ventricle, an overexpression system was needed in order to yield the expression of RXFP1 in the targeted cells. The widely used adeno associated virus (AAV) vector and the cardiac specific MLC promoter were chosen as the systems of choice to deliver the gene of interest.

5.2.1   Generating of AAV containing RXFP1

Modified Rattus norvegicus RXFP1 cDNA sequence was synthesized and cloned into a pcDNA3.1 plasmid containing an N-terminal FLAG-TAG sequence using BamH I and Xho I restriction sites. The cassette was then sub-cloned into a single strand AAV genome plasmid, PSSV9, which contained CMV MLC260 promoter and SV40 poly A signal using Pst I and Xho I restriction sites. *In silico* analysis of the FLAG-TAG RXFP1 was performed and no interaction between the FLAG-TAG and other domains of the receptor was detected. Firefly LUC control virus was cloned using the same method and contained the same N-terminal FLAG-TAG.

Results

5.2.2 *In vitro* **transfection of plasmids into the cell line**
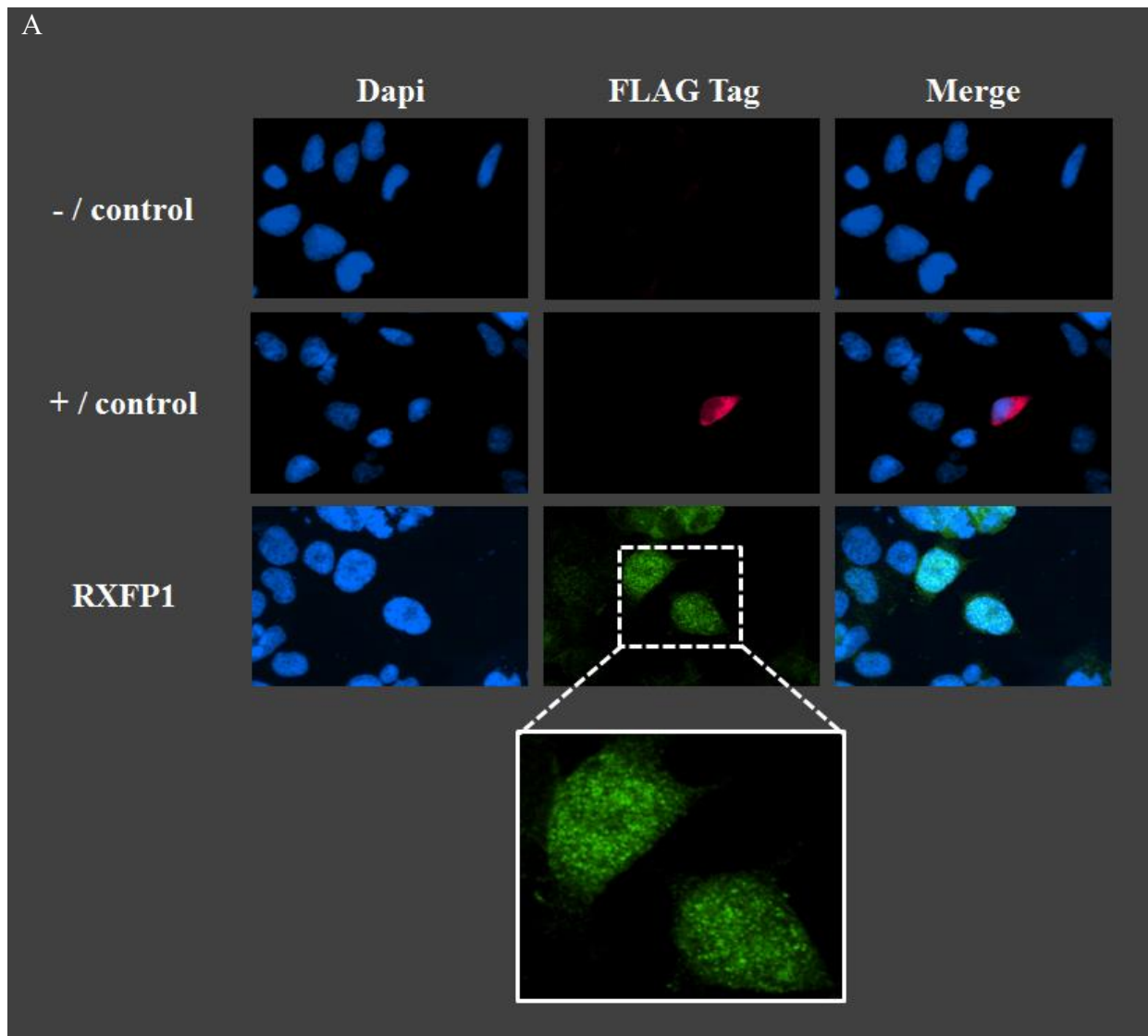
Figure 17: RXFP1 expression in transfected HEK293T Cells.
(A) Immunocytochemistry of RXFP1 transfected HEK293T cells stained with FLAG antibody. None transfected cells and FLAG LUC transfected cells were used as negative and positive control respectively. Positive control cells were stained with red fluorescence secondary antibody and FLAG RXFP1 transfected cells were stained with green fluorescence secondary antibody. **(B)** RXFP1 mRNA expression in transfected HEK293 cells (n=4). HPRT1 was used as a reference gene for qPCR quantification. *P < 0.05; **P < 0.01; ***P < 0.001. Error bars depict in SEM.
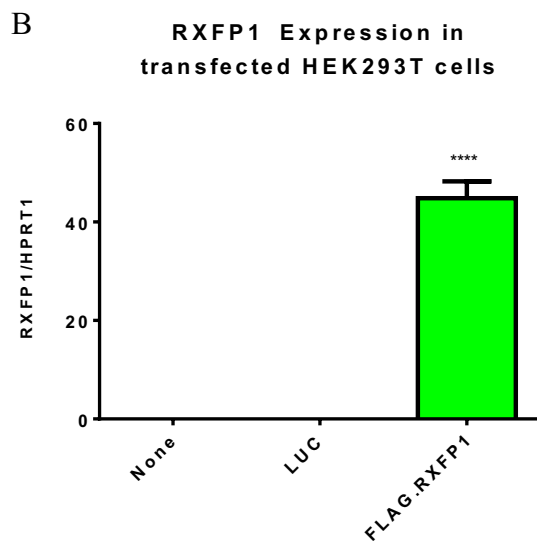
To ensure the expression of RXFP1 from the expression cassette, the plasmid was tested in THE HEK293T cell line. $3x10^5$ HEK293T cells were transfected with 1µg of pCDNA3.1 FLAG RXFP1 plasmid using PEI. After transfection, the cells were allowed to grow for 48 hours before being harvested for mRNA quantification and immunohistochemistry. Figure 17 A shows that RXFP1 protein expression could be detected with immunocytochemistry using FLAG-TAG staining antibody. After transfection HEK293T cells expressed 45-fold more RXFP1 mRNA compared to the negative controls. Therefore, RXFP1 expression from the cassette containing FLAG-TAG was detectable at both transcriptomic and proteomic levels. As a result, AAV virus production began.

5.2.3 *In vitro* **transduction of NRVCMs using AAV6 containing RXFP1 gene**

The FLAG RXFP1 cassette was sub-cloned from the pcDNA3.1 plasmid into a single strand AAV genome plasmid to generate RXFP1 carrying AAVs of serotypes 6 and 9 (AAV6 and AAV9 respectively). Figure 18 A shows the construction of the plasmid. For *in vitro* experiments AAV6 was tested on NRVCMs to ensure sufficient transduction and detection of RXFP1. AAV6 RXFP1 at the MOI of 10,000 vg/cell was used to transduce $2x10^6$ NRVCMs for 5 days. mRNA was isolated, and qPCR was performed. 15-fold more RXFP1 mRNA expression could be seen in the RXFP1 transduced NRVCMs compared to none in the transduced control (Figure 18 B). Interestingly, compared to the native RXFP1 expression in the atria, the RXFP1 transduced NRVCMs showed 10-fold increase in RXFP1 mRNA expression as well (Figure 18 B). Unfortunately, detection at protein levels in NRVCMs was not possible due to unspecific background binding of the FLAG-TAG antibody. Detection of FLAG-TAG using the immunofluorescence technique yielded moderate success with the background signal still visible (Figure 18 C). Thus, artificial RXFP1 expression was able to be induced in NRVCMs using AAV6 RXFP1 viral transduction.
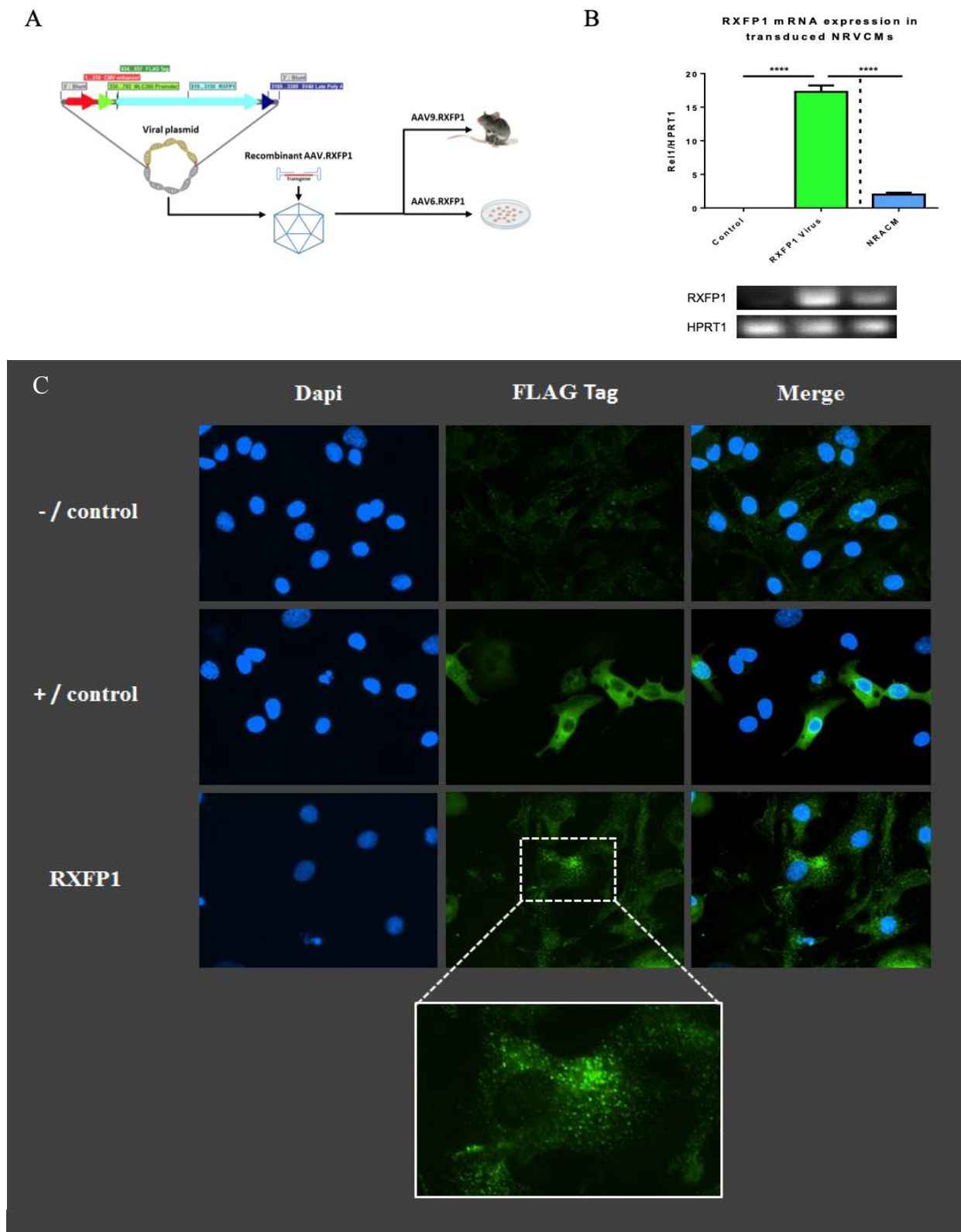
Figure 18: RXFP1 expression in transduced NRVCMs.
(A) Diagram of RXFP1 cassette inserted into AAV viral plasmid. **(B)** RXFP1 mRNA expression in transduced NRVCMs (n=7-10). **(C)** RXFP1 expression in NRVCMs detected using nonpermeabilized immunofluorescence method stained with FLAG antibody. NRVCMs were transduced for 5 days. mRNA was isolated, and qPCR was performed. HPRT1 was used as a reference gene. $*P < 0.05$; $**P < 0.01$; $***P < 0.001$. Error bars depict in SEM.

5.2.4 Evaluating RXFP1 expression using cAMP levels as a readout

Figure 19: cAMP accumulation after RXFP1 activation by RLN.
Amount of cAMP measured in the RXFP1 and LUC transduced NRVCMs. NRVCMs were transduced with RXFP1 virus or LUC virus and treated with RLN. cAMP was measured using cAMP-Glo® kit. RXFP1 transduced NRVCMs treated with NaCl and LUC traduced NRVCMs treated with NaCl or RLN were used as control (n=5-20). *P < 0.05; **P < 0.01; ***P < 0.001. Error bars depict in SEM.

Naturally, ventricular cardiomyocytes do not express RXFP1 at the protein level. Therefore, a successful expression of RXFP1 at the transcriptional level does not necessarily result in functional RXFP1 receptors on the cell membrane. In order to test for the presence of functional receptors on the membrane, 2×10^4 NRVCMs were transduced with AAV6 RXFP1 virus at the MOI of 10,000 vg/cell for 5 days. Subsequently, 100 nM of RLN were used to stimulate the cells for 30 minutes. RXFP1 activation by its ligand is characterized by an increase in cAMP production within the cells. Therefore, cAMP accumulation was measured using a cAMP-Glo® kit. Compared to the control, a 5-fold increase in cAMP accumulation was detected in RXFP1 transduced cells treated with RLN (Figure 19). Thus, AAV mediated delivery of RXFP1results in ectopic expression of functional receptors as characterized by cAMP generation in response to receptor stimulation.

5.2.5 Establishing efficient dosage of AAV6 RXFP1 virus and RLN used for *in vitro* experiments

To establish an efficient viral dosage used for *in vitro* experiments, NRVCMs were transduced with different MOIs of AAV6 RXFP1 virus, ranging from $5x10^3$ to $5x10^4$ vg/cell. After 5 days, the transduced cells were stimulated with 100 nM of RLN for 30 minutes. Then the amount of cAMP was measured and compared to the control. Figure 20 A shows that RXFP1 mRNA expression was increased in all transduced NRVCMs in a dose dependent manner with the highest amount of RXFP1 mRNA in samples treated with $5x10^4$ vg/cell. Figure 20 B shows that viral dosage of $5x10^3$ vg/cell did not alter cAMP production compared to the control treated cells. Other dosages, i.e. $1x10^4$, $2.5x10^4$, and $5x10^4$ vg/cell, did alter cAMP production significantly compared to the control (Figure 20 B). In detail, a 1.5-fold increase in cAMP production was detected in the sample treated with $1x10^4$ vg/cell. Even though no significant increase in cAMP production between this dosage and the other higher dosages was observed, when compared to the control, this dosage of virus did produce a significant increase in RXFP1 mRNA expression and cAMP production. Thus, the viral dosage of $1x10^4$ vg/cell was chosen as it can significantly increase RXFP1 mRNA expression and activation of the RXFP1 dependent signaling.

After establishing an efficient viral dosage for AAV6 RXFP1, we aimed to determine an efficient dosage of RLN stimulation. NRVCMs were transduced with AAV6 RXFP1 at a MOI of $1x10^4$ vg/cell. After 5 days, different dosages of RLN ranging from 1 pM to 100 nM were used to stimulate the cells for 30 minutes. After stimulation, cAMP was measured to detect the strength of RXFP1 activation from RLN stimulation. Figure 20 C shows that an increase in cAMP production can be seen with RLN dosage as low as 10 pM. Although increases in cAMP production could be seen in most test dosages, there was no difference detected between 1nM up to 100 nM RLN (Figure 20 C). However, in order to ascertain the likelihood of RXFP1 activation, the RLN dosage of 100 nM was chosen for further experiments.
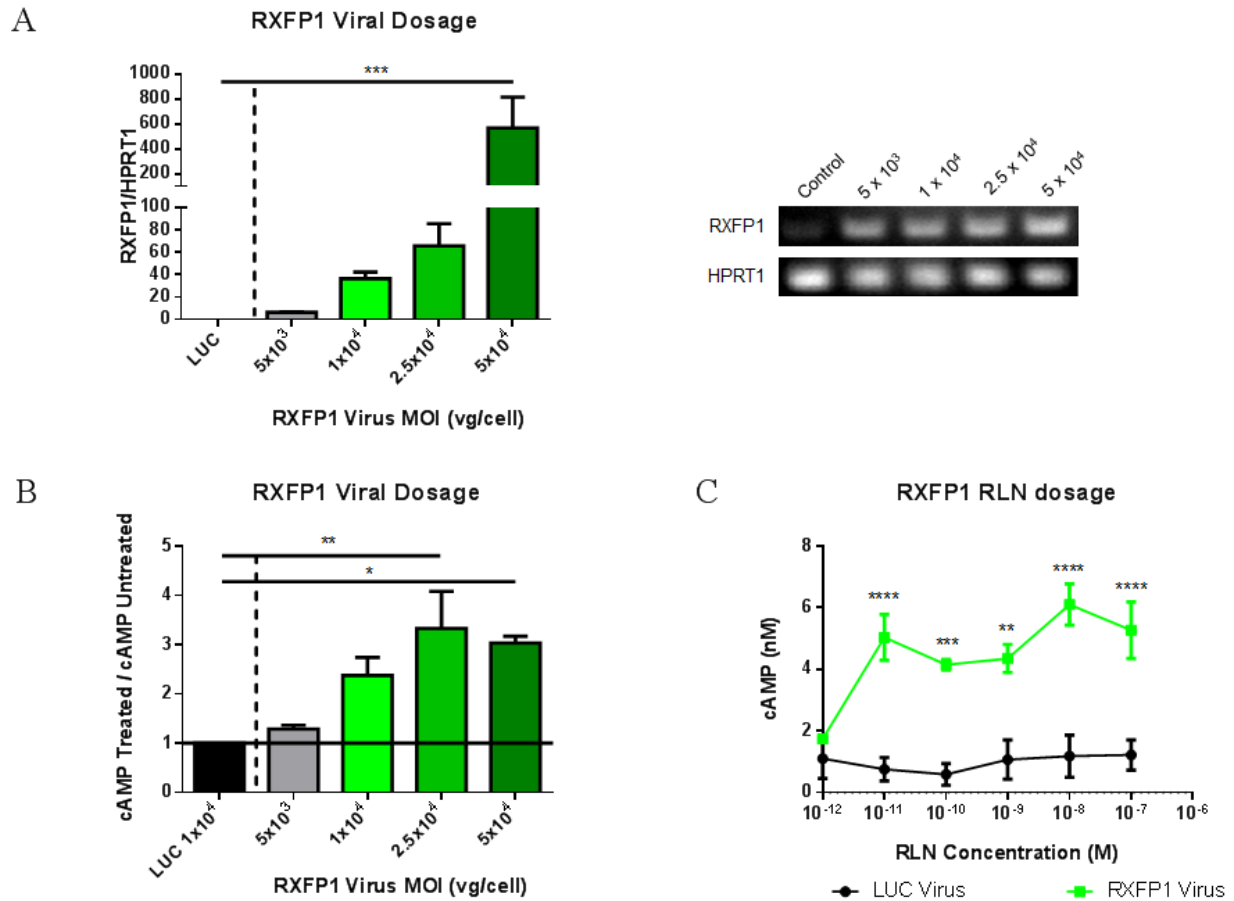
Figure 20: Efficient dosage of RXFP1 virus and RLN in *in vitro* experiments.
(A) RXFP1 mRNA expression in dosage dependent AAV transduction (n=3-4). Different dosages of RXFP1 were used to transduce NRVCMs. RXFP1 mRNA expression was analyzed using HPRT1 as a reference gene. **(B)** cAMP production in viral dose dependent manner (n=3). Different dosages of RXFP1 were used to transduce NRVCMs. 100 nM of RLN was used to stimulate the cells 30 minutes before cAMP production was measured. **(C)** cAMP production in RLN dose dependent manner (n=5). NRVCMs were transduced with RXFP1 virus and treated with different amounts of RLN for 30 minutes. cAMP production was measured. *$P < 0.05$; **$P < 0.01$; ***$P < 0.001$. Error bars depict in SEM.

5.2.6   Downstream signaling of RXFP1 and its potential positive inotropy effects
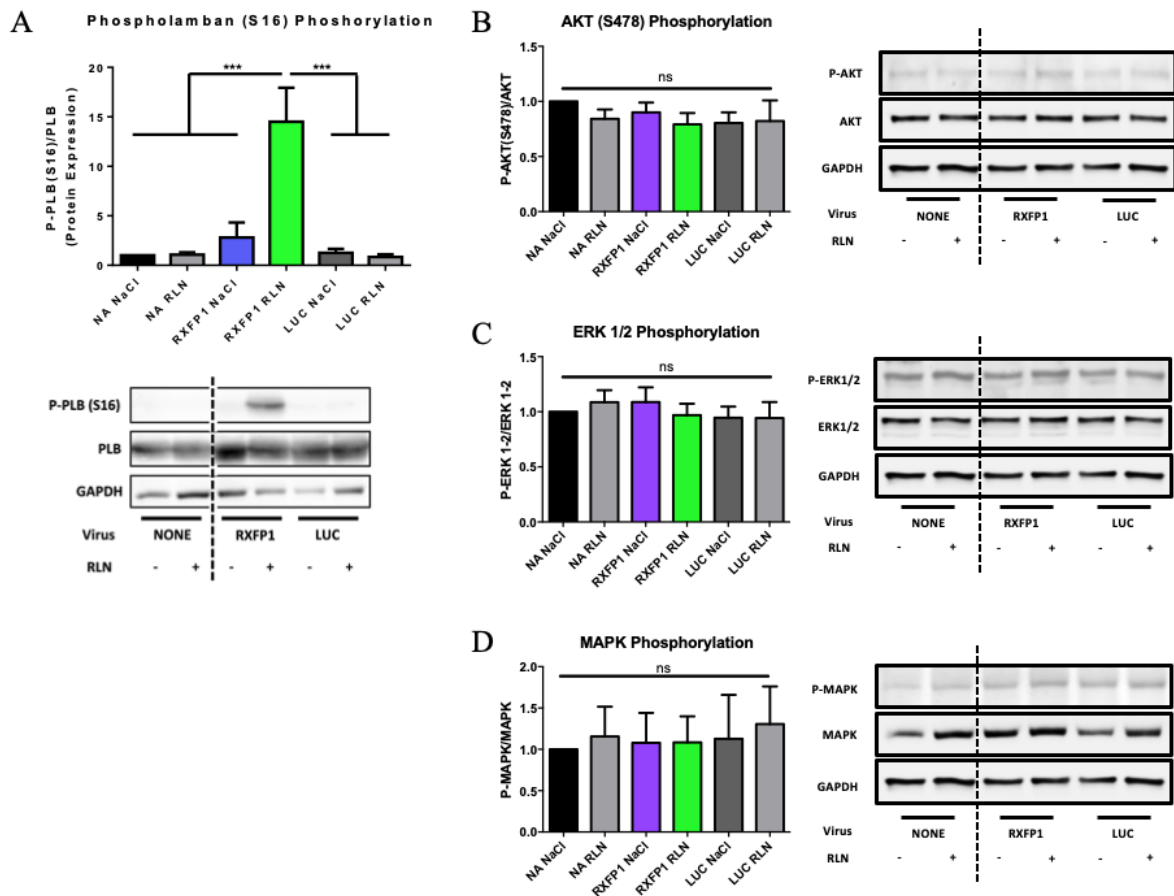
Figure 21: PLB, AKT, ERK1/2 and MAPK phosphorylation in RXFP1 transduced NRVCMs treated with RLN.

(A) P-PLB(S16)/PLB ratio in transduced NRVCMs treated with RLN (n=5), **(B)** P-AKT(S478)/AKT ratio in transduced NRVCMs treated with RLN (n=5), **(C)** P-ERK1-2/ERK1-2 ratio in transduced NRVCMs treated with RLN (n=5), and **(D)** P-MAPK/MAPK ratio in transduced NRVCMs treated with RLN (n=4) NRVCMs were transduced with RXFP1 and stimulated with 100 nM of RLN for 5 hours. Proteins were harvested and immunoblots were performed. GAPDH was used as an internal control for normalization. *P < 0.05; **P < 0.01; ***P < 0.001. Error bars depict in SEM.

After efficient dosages of AAV6 RXFP1 and RLN had been identified, further physiological changes from RXFP1 activation that could potentially lead to a positive inotropic response were investigated. RLN is known to increase the secondary messenger, cAMP, which could lead to physiological changes such as proliferation, differentiation, migration, etc within the cell. One downstream target of cAMP that could lead to positive inotropy is PKA. PKA is known to inactivate PLB by phosphorylation at serine 16 to increase SERCA2a activity, which in turn leads to a positive inotropic response from the cardiomyocytes. Therefore, P-PLB (S16) was used as a biochemical read out for positive inotropy.

Using transduced NRVCMs, 100 nM of RLN was used to stimulate the cells for 5 hours. The amount of P-PLB(S16) was calculated from immunoblots. A significant increase in P-PLB(S16) was detected in RXFP1 treated NRVCMs stimulated with RLN, compared to both viral treated controls and non-viral treated controls, with and without RLN stimulation (Figure 21 A). A 10-fold increase in P-PLB(S16) was consistently detected from all experiments. Interestingly, a trend toward an increase in P-PLB(S16) was also observed in a non-stimulated RXFP1 group. On the other hand, phosphorylation of AKT (S478), ERK1/2, and MAPKs was not increased (Figure 21 B - D). Therefore, P-PLB(S16) was identified as a downstream biochemical effector protein target of RXFP1 activation that could potentially induce positive inotropy in an *in vivo* model.

5.2.7 Induction of RXFP1 by RLN influences intracellular calcium handling

Inactivation of PLB by phosphorylation at serine 16 is known to increase SERCA2a activity, which directly affects intracellular Ca^{2+} handling and positive inotropic effects. Therefore, the changes in intracellular Ca^{2+} current were investigated. The change in Ca^{2+} transients amplitude was used as a readout for an increased contractility that could lead to positive inotropic effects.

Results
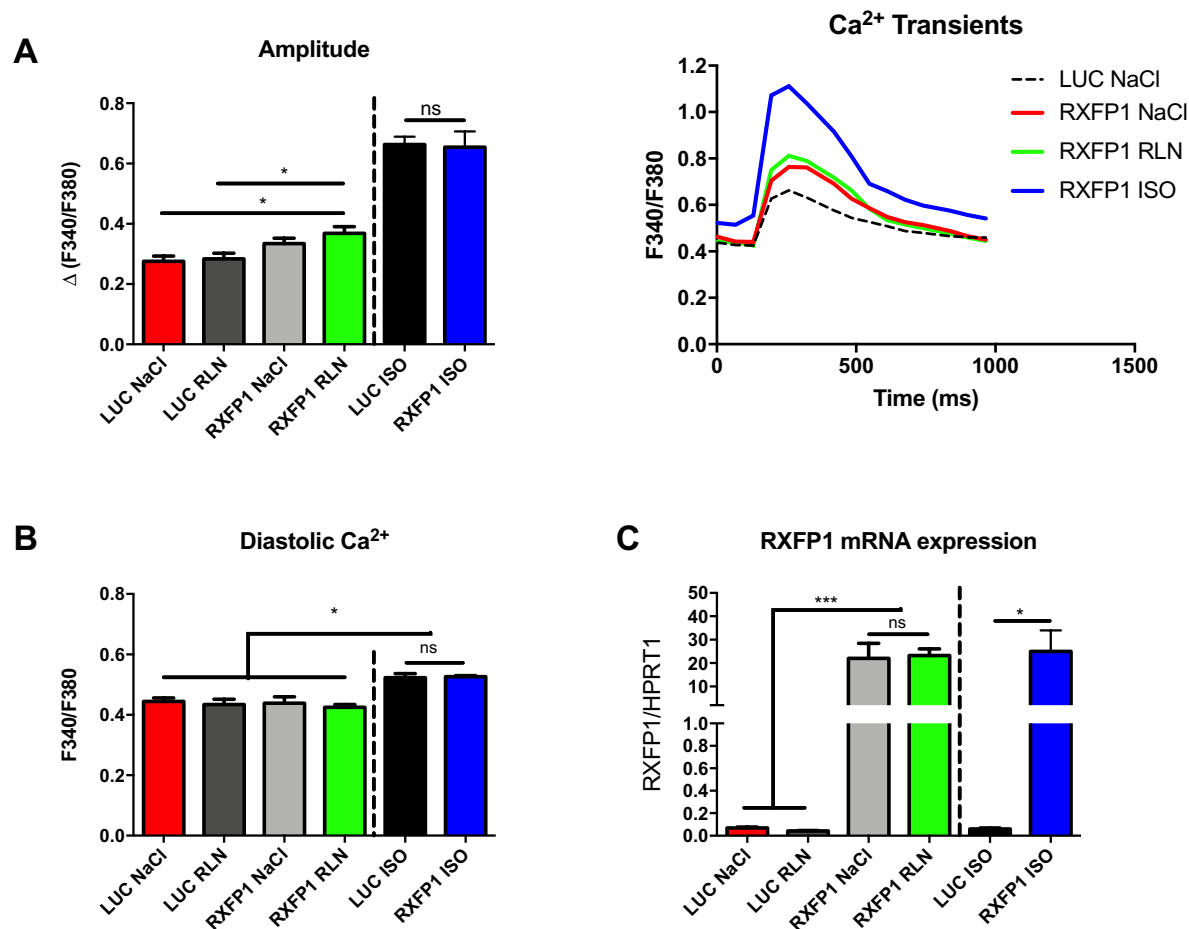
Figure 22: Calcium transients measurement in RXFP1 transduced NRVCMs
(A) Transients amplitude and representative Ca^{2+} transients and (B) Diastolic Ca^{2+} after 5 minutes of NaCl, RLN, and ISO treatments (n=3-8). NRVCMs were transduced with RXFP1 and LUC virus for 5 days. Ca^{2+} transients were measured with 1 Hz electrical stimulation. (C) RXFP1 mRNA expression. RXFP1 mRNA expression was analyzed using HPRT1 as a reference gene. For figure A only the first 4 groups were compared. *P < 0.05; **P < 0.01; ***P < 0.001. Error bars depict in SEM.

Using transduced NRVCMs loaded with 1 µM Fura 2 AM for 15 minutes and stimulated at 1 Hz, 100 nM of RLN was used to stimulate the cells for 5 minutes. 10 nM isoproterenol (ISO) treated NRVCMs were used as positive control. The changes in transients amplitude was measured. Figure 22 A shows a significant increase in amplitude in a group of NRVCMs that received both RXFP1 virus and RLN. Diastolic Ca^{2+} did not change in the analyzed groups except for the positive control (Figure 22 B). RXFP1, measured from isolated mRNA after the experiment, was significantly expressed in all groups of NRVCMs that received RXFP1 virus (Figure 22 C). It was therefore speculated that the significant increase in transients amplitude observed could lead to positive inotropic effects in an *in vivo* model.

5.3 RXFP1 pathway analysis in ventricular cardiomyocytes
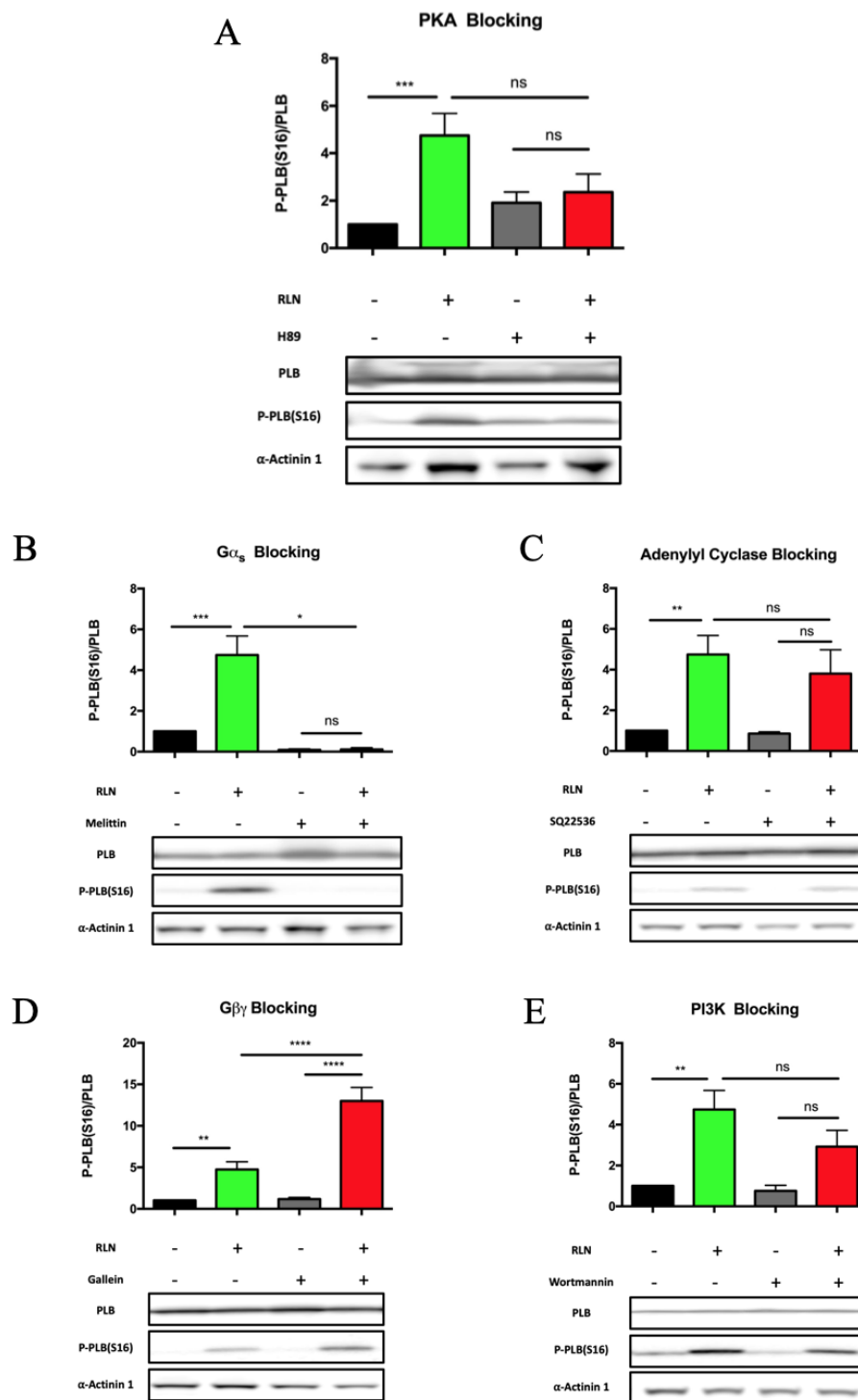
Figure 23: RXFP1-RLN signaling transduction in the presence of different inhibitors. Phosphorylation of PLB at serine 16 after RXFP1 virus treatment and recombinant RLN stimulation in the presence of different inhibitors (n=3-9). (A) H89 (5 µM), (B) melittin (1 µM), (C) SQ22536 (90 µM), (D) gallein (75 µM), and (E) wortmannin (100 nM) respectively were added to transduced NRCVMs for 30 minutes, followed by RLN stimulation for 30 minutes. NRCVMs were harvested and P-PLB(S16)/PLB was quantified by immunoblot. Alpha actinin 1 (α-Actinin 1) immuno-detection was used as an internal control. *P < 0.05; **P < 0.01; ***P < 0.001. Error bars depict in SEM.

<u>Results</u>

Data obtained from the *in vitro* experiments suggested that RXFP1 gene therapy with RLN treatment could improve multiple aspects of cardiac function. To decipher the pathway behind these improvements, a series of blocking experiments were performed using various chemicals that block different classical components of the GPCR signaling pathway. Changes in P-PLB(S16) was used as a readout for RXFP1 signaling induction.

To determine which protein contributes to RXFP1-RLN signaling transduction, different proteins known to transduce classical GPCR signal were blocked. $5x10^5$ NRVCMs were transduced with RXFP1 virus. After five days, PKA, $G\alpha_s$, AC, $G\beta\gamma$, and PI3k were inhibited individually within the cells using H89 (5 µM), melittin (1 µM), SQ22536 (90 µM), gallein (75 µM), and wortmannin (100 nM) respectively for 30 minutes, followed by RLN (100 nM) stimulation for 30 minutes, before being harvested for protein analysis. Immunoblots were performed. PLB and P-PLB(S16) were detected and quantified. α-Actinin 1 was used as an internal loading control.

PKA: Figure 23 A shows that blocking of PKA with H89 markedly reduced downstream signaling of RXFP1 activation by RLN, as a notable decrease in P-PLB(S16) was detected. Thus, PKA could function as an important effector protein downstream of cAMP and up stream of PLB in the RXFP1 signaling pathway.

$G\alpha_s$: $G\alpha_s$ is essential for signaling initiation and signal transduction of RXFP1. $G\alpha_s$ inhibition with melittin diminished RXFP1 activation by RLN, as P-PLB(S16) could not be detected (Figure 23 B). Therefore, blocking $G\alpha_s$ significantly impairs RXFP1 downstream signaling cascade.

AC: AC is a downstream protein that is activated by $G\alpha_s$. Figure 23 C shows, that blocking AC with SQ22536 slightly reduced downstream signaling of RXFP1 upon activation by RLN, resulting in a slight decrease in P-PLB(S16). Thus, AC might play a limited role in transducing the RXFP1 activation signal, by increasing the production of cAMP after RXFP1 was activated by RLN.

Gβγ: Inhibition of Gβγ with Gallein increased P-PLB(S16) after RXFP1 gene therapy and RLN stimulation (Figure 23 D). Thus, like many GPCRs, THE Gβγ protein might function as an inhibitor for the RXFP1 signaling transduction pathway.

PI3K: Blocking of PI3K with wortmannin slightly reduced downstream signaling of RXFP1 activation by RLN. A slight decrease in P-PLB(S16) was detected after wortmannin treatment and RLN stimulation (Figure 23 E). Thus, PI3K potentially has a limited function in RXFP1 signaling pathway.

5.4   RXFP1 signaling vs β-adrenergic signaling

The RXFP1 signaling pathway shares many similarities with the β-adrenergic (β-AR) signaling pathway, as they produce similar effects. Data from *in vitro* and *in vivo* experiments suggest that RXFP1 activation is far less potent in the cells compared to β-AR activation. To evaluate these observations, different aspects of RXFP1and β-AR activation were compared.

5.4.1   Positive inotropy from RXFP1 signaling and β-AR signaling

It is widely accepted that β-AR activation leads to positive inotropy through different mechanisms such as phosphorylation of PLB, cytosolic calcium channels, and the ryanodine receptor (RyR). Likewise, RXFP1 activation potentially induces positive inotropy using a similar mechanism, but the signal strength between the two stimulations can vary. To test the differences in signal strength between RXFP1 activation and β-AR activation, NRVCMs were isolated and transduced with RXFP1 or LUC control viruses. The transduced NRVCMs were treated with RLN (100 nM) or ISO (10 nM) for 30 minutes, before the cells were harvested. Immunoblots were performed to detect PLB and P-PLB(S16). GAPDH was used as an internal loading control. Results from the immunoblot suggested that RXFP1 activation produces less downstream signal compared to β-AR activation (Figure 24). A significant increase in P-PLB(S16) was detected after β-AR activation by ISO stimulation. On the other hand, RXFP1 activation by RLN stimulation only increased P-PLB(S16) to half of that observed in β-AR activation (Figure 24). The signal intensity of the RLN treated group was significantly lower than the ISO treated group (approximately 55% lower). Thus, RLN stimulation only produces moderate downstream inotropic signaling compared to ISO stimulation.
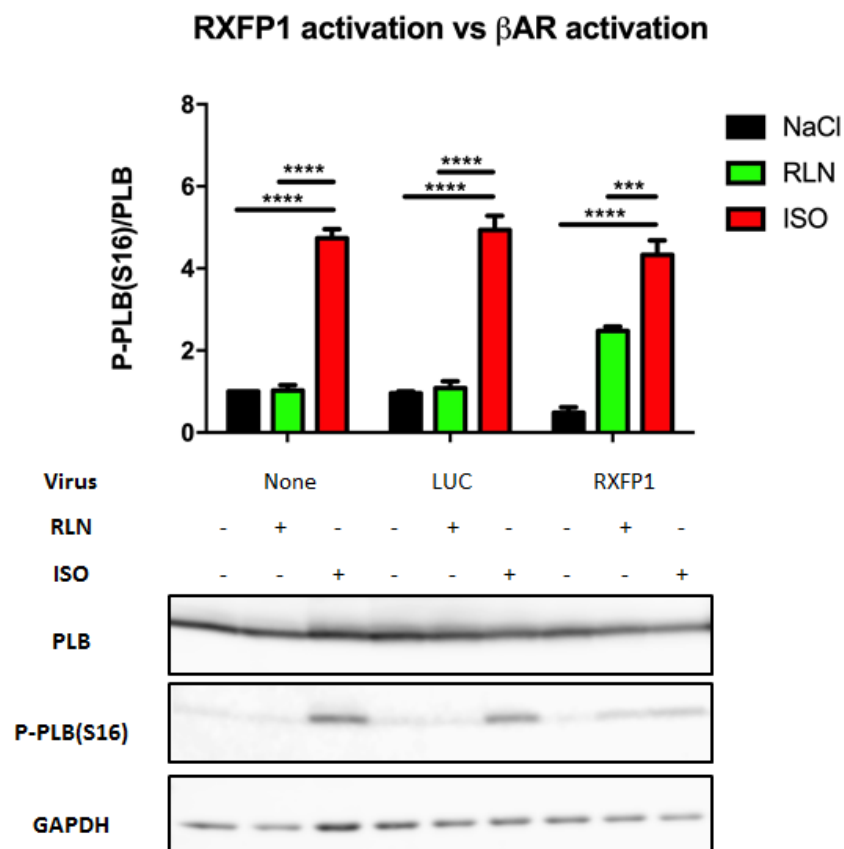
Figure 24: RXFP1 activation and β-adrenergic activation.
Phosphorylation of PLB at serine 16 after RXFP1 viral treatment using various stimulations (n=3). Transduced NRCVMs were stimulated with NaCl, RLN (100 nM), or ISO (10 nM) for 30 minutes. NRCVMs were harvested and P-PLB(S16)/PLB was quantified by immunoblot; GAPDH immuno-detection was used as an internal control. *P < 0.05; **P < 0.01; ***P < 0.001. Error bars depict in SEM.

5.4.2 Effects of RXFP1 activation vs β-AR activation on PLB phosphorylation overtime.

Prolonged activation of RXFP1 and β-AR was examined in order to determine their effects over long term usage. NRVCMs were transduced for 5 days and they were stimulated with either 100 nM of RLN or 10 nM of ISO for 10 minutes, 30 minutes, 1, 3, 6, 12, and 24 hours. The cells were harvested and immunoblots were performed to detect PLB, P-PLB(S16) and P-PLB(T17). GAPDH was used as an internal loading control. Figure 25 shows that RXFP1 activation led to a gradual increase in P-PLB(S16). A significant increase in P-PLB(S16) could be seen after 30 minutes onward, and at least 1 hour was needed in order for the signal to reach its plateau, which it then maintained throughout the experiment (Figure 25). P-PLB(T17) also increased, but at slower rate compared to P-PLB(S16). After 1 hour, an increase in P-PLB(T17) became significant.

A

Phosphorylated PLB (S16)

B

Phosphorylated PLB (T17)
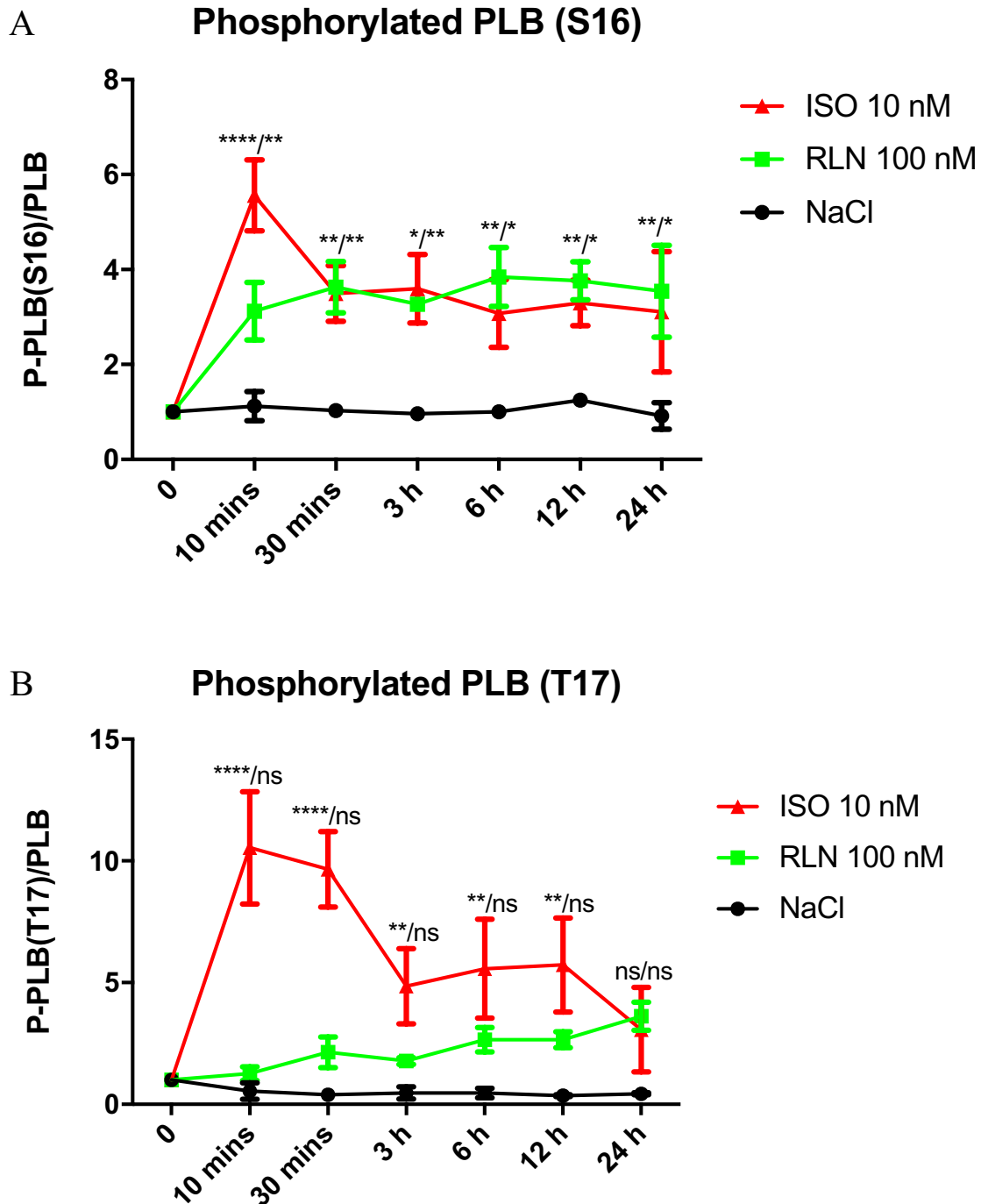
Figure 25: Effects of prolong RXFP1 and β-AR activation.
Phosphorylation of PLB at serine 16 and threonine 17 after prolong activation of RXFP1 and β-AR (n=4). Transduced NRCVMs were stimulated with RLN (100 nM) or ISO (10 nM) for 10 minutes, 30 minutes, 1 hour, 3 hours, 6 hours, 12 hours, and 24 hours. NRCVMs were harvested and P-PLB(S16)/PLB quantified by immunoblot; GAPDH immuno-detection was used as an internal control. *P < 0.05; **P < 0.01; ***P < 0.001; NaCl vs RLN / NaCl vs ISO. Error bars depict in SEM.

On the other hand, β-AR activation led to a sudden increase in both P-PLB(S16) and P-PLB(T17) (Figure 25). ISO stimulation produced a significant increase in P-PLB(S16) and P-PLB(T17) after only 10 minutes of stimulation. After 1 hour, the signal from ISO stimulation decreased and returned to an intermediate baseline, corresponding to the peak signal from RXFP1 activation. Thus, two conclusions could be drawn from these experiments: 1) long term RXFP1 activation is far less potent compared to β-AR activation, and 2) RXPF1 relies on the gradual rise in P-PLB(S16) and P-PLB(T17), which is easier for the cells to cope with

5.4.3   Role of CaMKII in RXFP1 activation comparing to β-AR activation
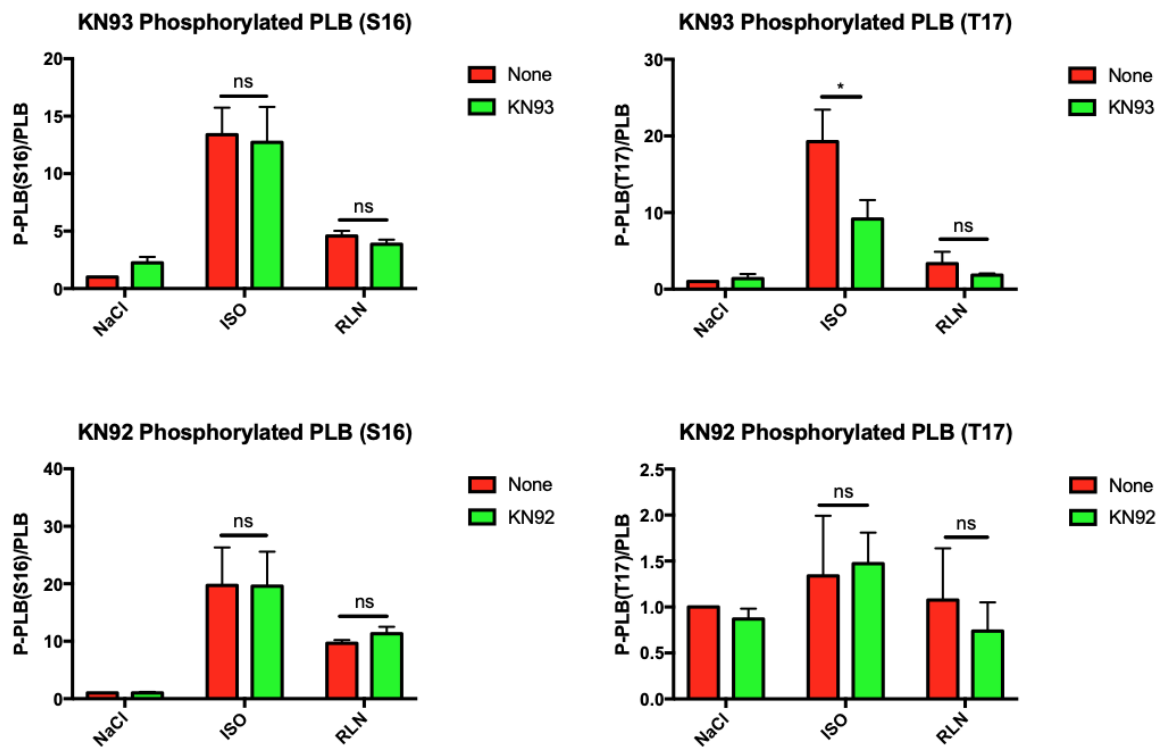
Figure 26: CaMKII activity after RXFP1 activation by RLN.
Phosphorylation of PLB at serine 16 and threonine 17 after RXFP1 and β-AR activation in the presence of CaMKII inhibitor (n=3). Transduced NRCVMs were stimulated with RLN (100 nM) or ISO (10 nM) for 30 minutes after blocking with KN92 and KN93 for 30 minutes. NRCVMs were harvested. P-PLB(S16) and P-PLB(T17) were quantified by immunoblot. Alpha actinin 1 (α-Actinin 1) immuno-detection was used as an internal control. *P < 0.05; **P < 0.01; ***P < 0.001. Error bars depict in SEM.

Since P-PLB(T17) was detected, CaMKII could play some role in RXFP1 activation. To determine whether CaMKII has any influence on signal transduction of RXFP1 by RLN, NRVCMs were transduced with RXFP1 virus and LUC control virus. After five days,

CaMKII was inhibited with KN93 (10 µM) for 30 minutes, followed by RLN (100 nM) stimulation for 30 minutes, before being harvested for protein analysis. Immunoblots were performed. PLB, P-PLB(S16), and P-PLB(T17) were detected and quantified. α-Actinin 1 was used as an internal loading control. RXFP1 activation by RLN showed that blocking of CaMKII using KN 93 did not produce any alteration in P-PLB(S16) and P-PLB(T17) (Figure 26). Figure 26 shows that ISO induced β-AR activation with CaMKII inhibition had no effect on P-PLB(S16) but did significantly decrease P-PLB(T17). Thus, these experiments demonstrate that RXFP1 activation does not influence CaMKII activity compared to β-AR activation.

5.5   RXFP1 activation is independent of β-blocker
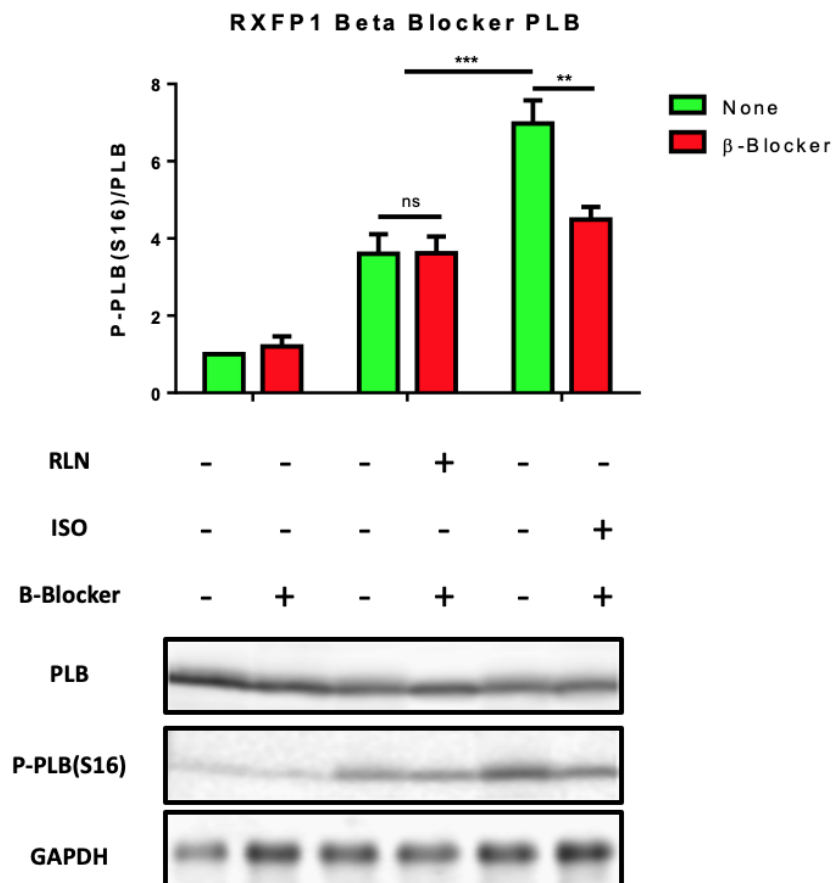
Figure 27: RXFP1 activation in the presence of β-blocker.
Phosphorylation of PLB at serine 16 after RXFP1 and β-AR activation in the presence of β-blocker (n=3). Transduced NRCVMs were stimulated with RLN (100 nM) or ISO (10 nM) for 30 minutes after blocking with β-blocker (propranolol 1 µM) for 30 minutes. NRCVMs were harvested and P-PLB(S16)/PLB was quantified by immunoblot; GAPDH immuno-detection was used as an internal control. *P < 0.05; **P < 0.01; ***P < 0.001. Error bars depict in SEM.

β-blockers such as propranolol, atenolol, metoprolol, and etc. are a class of drug used as a first line treatment for HF. β-blockers block β-AR from being hyperactively activated and delay the progression of HF. The influence of β-blockers on RXFP1 activation was investigated in this experiment. Transduced NRVCMs were treated with β-blockers, propranolol (1µM), for 30 minutes and stimulated with RLN or ISO for 30 minutes. The cells were harvested, and proteins were isolated. Immunoblots were performed. PLB and P-PLB(S16) were detected and quantified. GAPDH was used as an internal loading control. Blocking of β-AR did not influence RXFP1 activation in anyway. A similar amount of P-PLB(S16) was detected with and without the presence of β-blocker (Figure 27). Thus, the RXFP1 and β-AR are different receptors, and blocking of β-AR does not influence RXFP1 activation and its downstream signal transduction.

5.6 Similarity between human and rat RXFP1
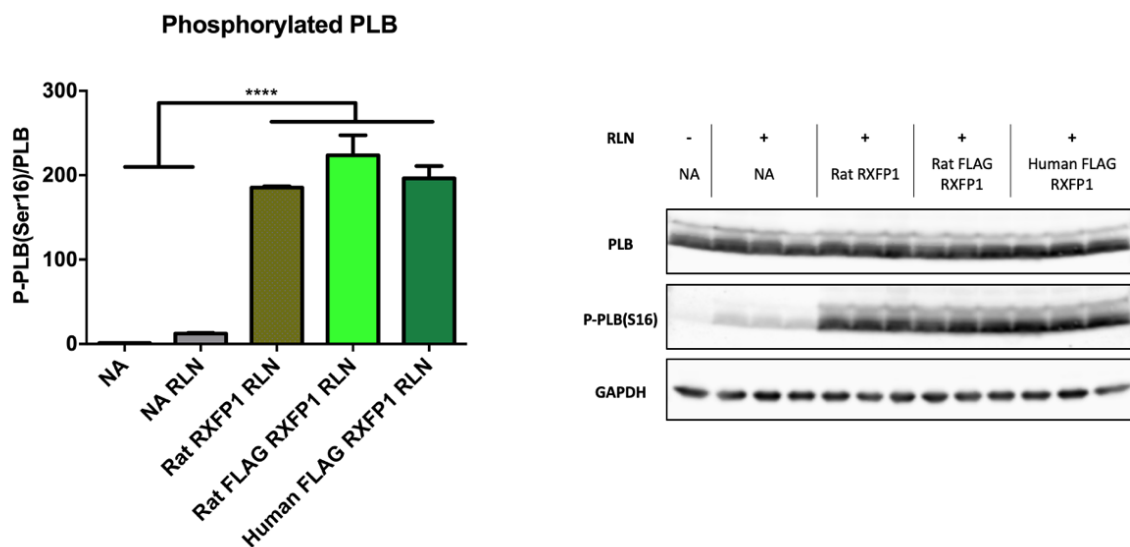
Figure 28: Comparison of RXFP1 between different species.
Activation profile of RXFP1 from different species (n=3). NRCVMs were transduced with RXFP1 from different species for 5 days and stimulated with RLN (100 nM) for 5 hours. The cells were harvested and P-PLB(S16)/PLB was quantified by immunoblot; GAPDH immuno-detection was used as an internal control. *P < 0.05; **P < 0.01; ***P < 0.001. Error bars depict in SEM.

Many previous studies have focused on understanding rat RXFP1 rather than human RXFP1. RXFP1 from both species are highly conserved, but yet different. To evaluate the difference between the two species, DNA and polypeptide chain sequences were compared. 85% similarity in DNA, and 86% similarity in the polypeptide chain were detected,

respectively. Moreover, RXFP1 from both human and rat also exhibit identical response to RLN stimulation. Figure 28 shows that RLN stimulation led to a significant increase in P-PLB(S16) detected in both the rat and human RXFP1 treated group. Thus, both rat and human RXFP1 behave comparably upon RLN stimulation.

5.7 *In vivo* experiments

In vitro detection of a significant increase in P-PLB(S16), after RXFP1 gene therapy with RLN stimulation, suggested that positive inotropy could be achieved in an HF animal model. After phosphorylation, PLB becomes inactive leading to SERCA2a activation followed by an increase in the amount of Ca^{2+} pumped into the SR. As a result, the cardiomyocytes undergo rapid repolarization that could contribute to positive inotropic response.

5.7.1 Virus dose escalation study

To successfully evaluate the proposed RXFP1 gene therapy treatment, an efficient *in vivo* viral transduction dose in a mouse model had to be established.

5.7.1.1 Functional analysis and safety dosage
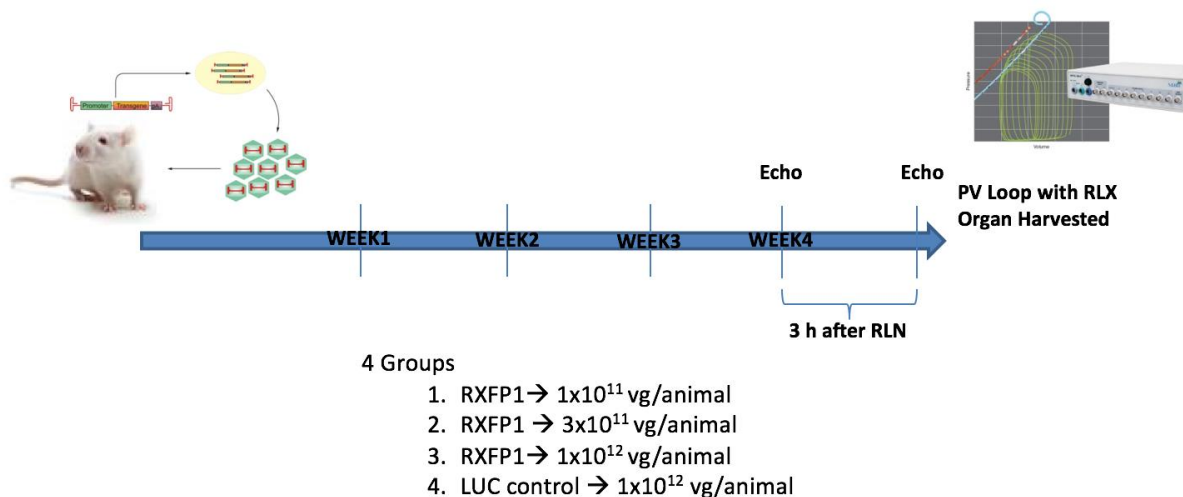
Figure 29: Diagram of viral dose escalation experiments performed *in vivo*.
The diagram shows the time line of the experiments performed in the viral dose escalation study.

Results
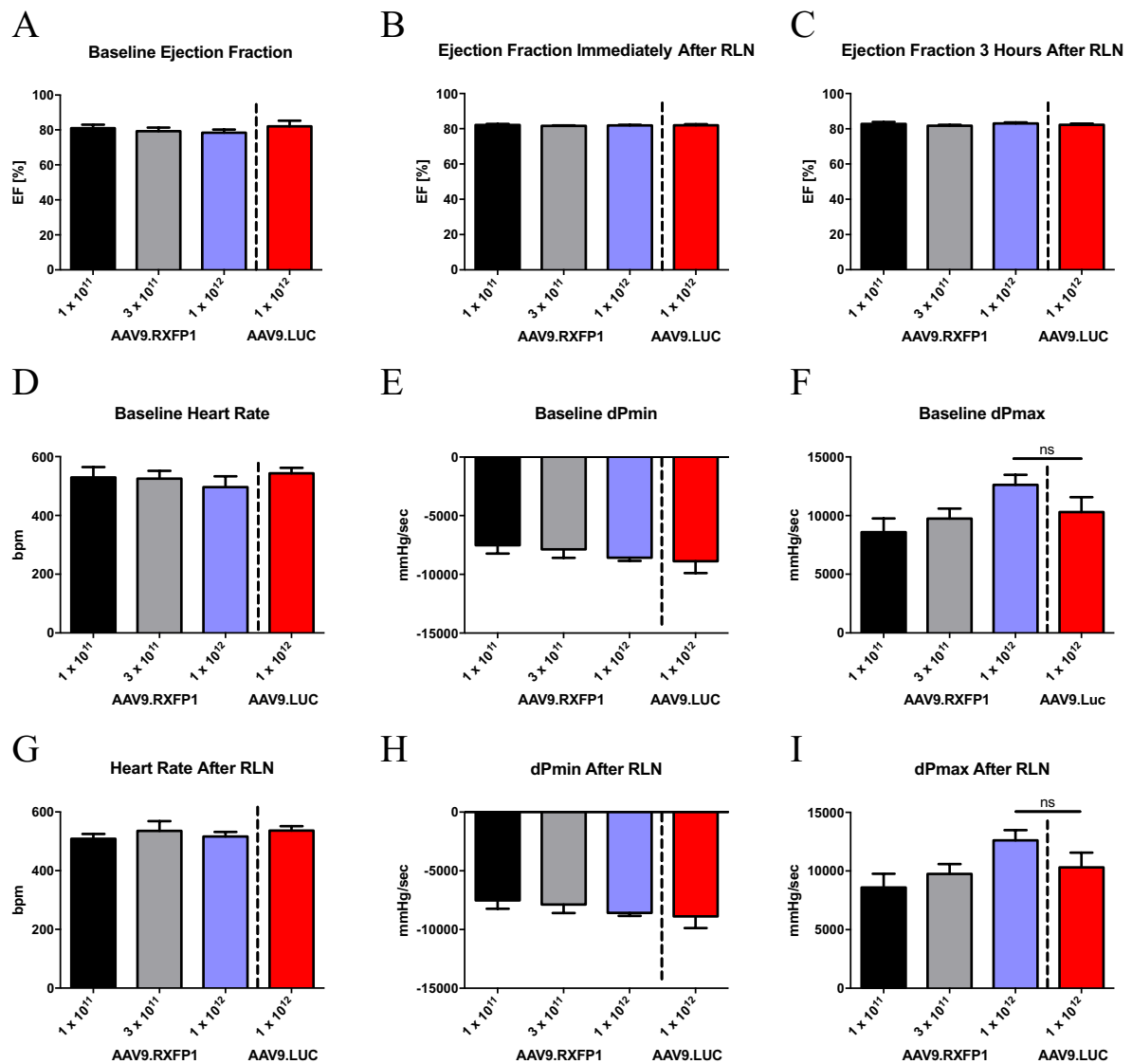
Figure 30: RXFP1 expression with RLN treatment in *in vivo* model.
(**A**) Baseline EF (**B**) Immediately after RLN EF (**C**) 3 hours after RLN EF, mice were administered with different concentrations of RXFP1 virus and allowed to express the transgene for 4 weeks. 1.35 µg/g recombinant RLN was administered intraperitoneally after a baseline echo was performed (n=5). Three echocardiography measurements were performed in order to assess the changes in cardiac function in the treated animals. (**D**) Baseline HR (**E**) baseline dp/dt min (**F**) baseline dp/dt max (**G**) After RLN stimulation HR (**H**) dp/dt min after RLN infusion (**I**) dp/dt max after RLN infusion, mice were given different concentrations of RXFP1 virus and allowed to express the transgene for 4 weeks. 1.35 µg/g recombinant RLN was administered intraperitoneally after baseline PV loop measurement (n=5). Error bars depict in SEM.

To establish the most effective dosage of virus, 8 week old C57BL/6 mice were injected with different dosages of RXFP1 virus, ranging from 1×10^{11} to 3×10^{12} vg/animal. Each dosage group contained four animals. After 4 weeks, an acute dosage of RLN with a concentration of 1.35 µg/g was administered i.p. to each animal. The cardiac function was

measured by echocardiography, immediately after the injection, and three hours after the injection. Finally, the mice were catheterized through the left carotid artery, and left ventricular Pressure/Volume (PV) loop measurements were performed. Figure 29 shows the timeline of the interventions performed on the animals.

The echocardiogram measurements of ejection fraction (EF) from the dose escalation animals showed no difference in any group at any time points (Figure 30 A-D). The EF from all RXFP1/RLN treated animals was similar to the LUC control/RLN treated animals (Figure 30 A-C). The measurements from the echocardiogram suggest that treated animals do not experience any adverse effects from the RXFP1 gene therapy and RLN treatment. On the other hand, figure 30 F and I shows a trend toward an increase in dP/dt max observed before and after RLN treatment in RXFP1 group treated with a viral dose of $1x10^{12}$ vg/animal. The same trend toward a decrease dP/dt min could also be seen as well (Figure 30 E and H). Thus, the cardiac function results suggested that: 1) RXFP1 virus has no adverse effect on cardiac function in an *in vivo* model, and 2) RXFP1 gene therapy with RLN treatment does not enhance cardiac function in healthy animals.

5.7.1.2 Molecular analysis and mRNA expression
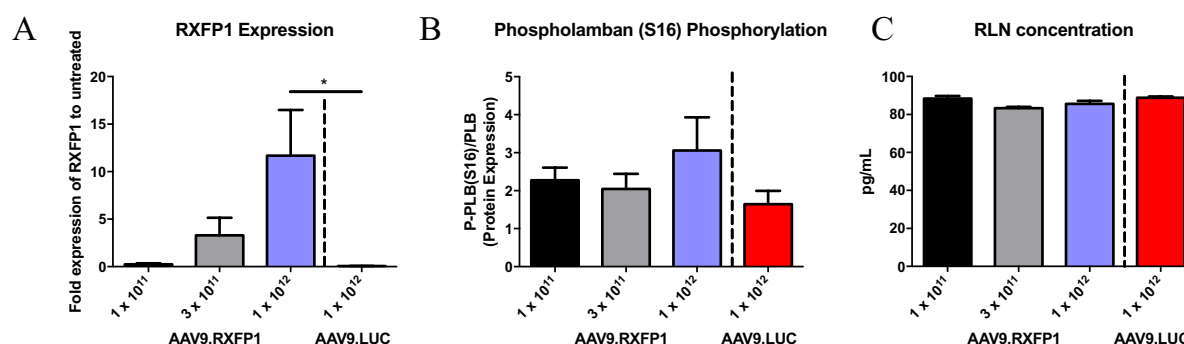
Figure 31: Molecular analysis of RXFP1 expression and RLN treatment in *in vivo* model. **(A)** RXPF1 mRNA expression in treated animals quantified by qPCR using *HPRT1* as a reference gene. **(B)** Post-mortem cardiac P-PLB(S16)/PLB was quantified by immunoblot; glyceraldehyde-3-phosphate dehydrogenase (GAPDH) immuno-detection was used as an internal control (n=5). **(C)** RLN plasma concentration level (n = 5). *P < 0.05; **P < 0.01; ***P < 0.001. Error bars depict in SEM.

Once all the measurements were obtained, the mice organs were harvested for further analysis. qPCR was performed on harvested heart piece number 1. Immunoblots were performed on heart piece number 3 (see Figure 14), and plasma concentration levels of RLN were measured using an RLN ELISA kit. The results for qPCR showed a dose dependent expression pattern of the RXFP1 transgene (Figure 31 A). Significant RXPF1 expression

could be seen in samples treated with at least 1×10^{12} vg/animal, compared to the control. At protein level, a trend toward an increase in P-PLB(S16) could be seen in the groups that received 1×10^{12} vg/animal (Figure 31 B). Figure 31 C shows that similar RLN plasma concentration levels were detected in all animals that were administered RLN. Thus, the molecular evidence suggests that: 1) viral transduction could induce significant expression of RXFP1 in targeted cells, 2) a viral dosage of 1×10^{12} vg/animal with RLN treatment could produce significantly increased RXFP1 mRNA expression within the targeted cells, and 3) similar to *in vitro* model, a trend toward an increased P-PLB(S16) was detected, which could potentially lead to positive inotropic effects.

5.7.2 Molecular effects of the AAV9 RXFP1 viral vector
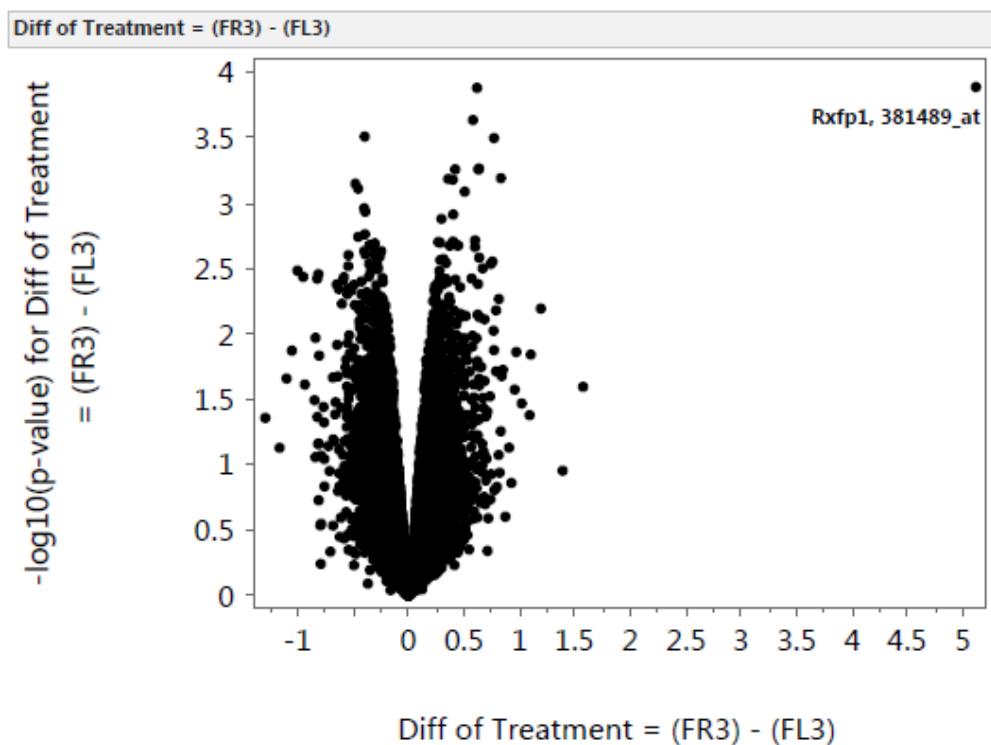
Figure 32: Volcano plot from RXFP1 treated animals.
Volcano plot from RXFP1 treated animals. Microarray was performed on 3 animals with the highest expression of RXFP1 mRNA and 3 animals from LUC control group. The results were plotted in a volcano plot in order to compare the differences in their gene expression profiles.

To evaluate the safety of RXFP1 viral treatment at molecular level, a gene array was performed on 6 animals. Gene expression from 3 animals receiving RXFP1 virus without RLN treatment was compared to gene expression of 3 LUC control animals without RLN treatment. The expression profile was compiled, and a volcano plot was generated. RXFP1

was the only gene significantly up-regulated between the two groups (Figure 32). No alteration in expression pattern could be detected in other genes, as they resembled normal expression ranges. The data from viral dose escalation experiments strongly suggest that RXFP1 gene therapy does not have any off-target effects on normal cardiac function or alters gene expression patterns at the molecular level. The dosage of $1x10^{12}$ vg/animal was chosen for the study because it could significantly increase RXFP1 mRNA expression in the targeted cells.

5.7.3 Relaxin dose escalation
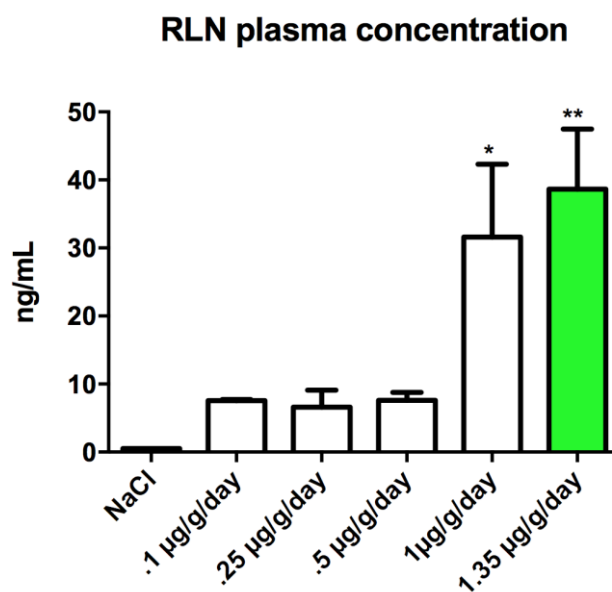
Figure 33: RLN plasma concentrations after chronic RLN administration.
RLN plasma concentration after chronic administration of RLN. Healthy animals were implanted with osmotic pumps containing different concentrations of RLN. After 2 weeks plasma was collected and RLN plasma concentrations were measured. Error bars depict in SEM.

To establish a suitable dosage of RLN, 8 weeks old C57BL/6 were implanted with 4 weeks Alzet® osmotic pumps. Different dosages of RLN were filled into the pumps ranging from 0.35 µg/g/day to 1.35µg/g/day. The pumps were implanted subcutaneously into each animal. After 2 weeks, the amount of circulating RLN was measured using an RLN Elisa kit. The RLN plasma levels of the animals did exhibit a dose dependent pattern (Figure 33). The two lowest dosages of RLN did not lead to a significant increase in RLN plasma concentrations. Figure 33 shows a significant increase in RLN plasma concentration in the group that received an RLN dose of 1.35 µg/g/day. The increase in RLN plasma concentrations observed was in line with previous studies regarding the effects of RLN

(unpublished data). Therefore, an RLN dosage of 1.35µg/g/day was chosen for future animal experiments, because it could reach RLN plasma levels previously shown to induce RXFP1 activation.

5.7.4 Establishment of a TAC-induced hypertrophic cardiomyopathy model
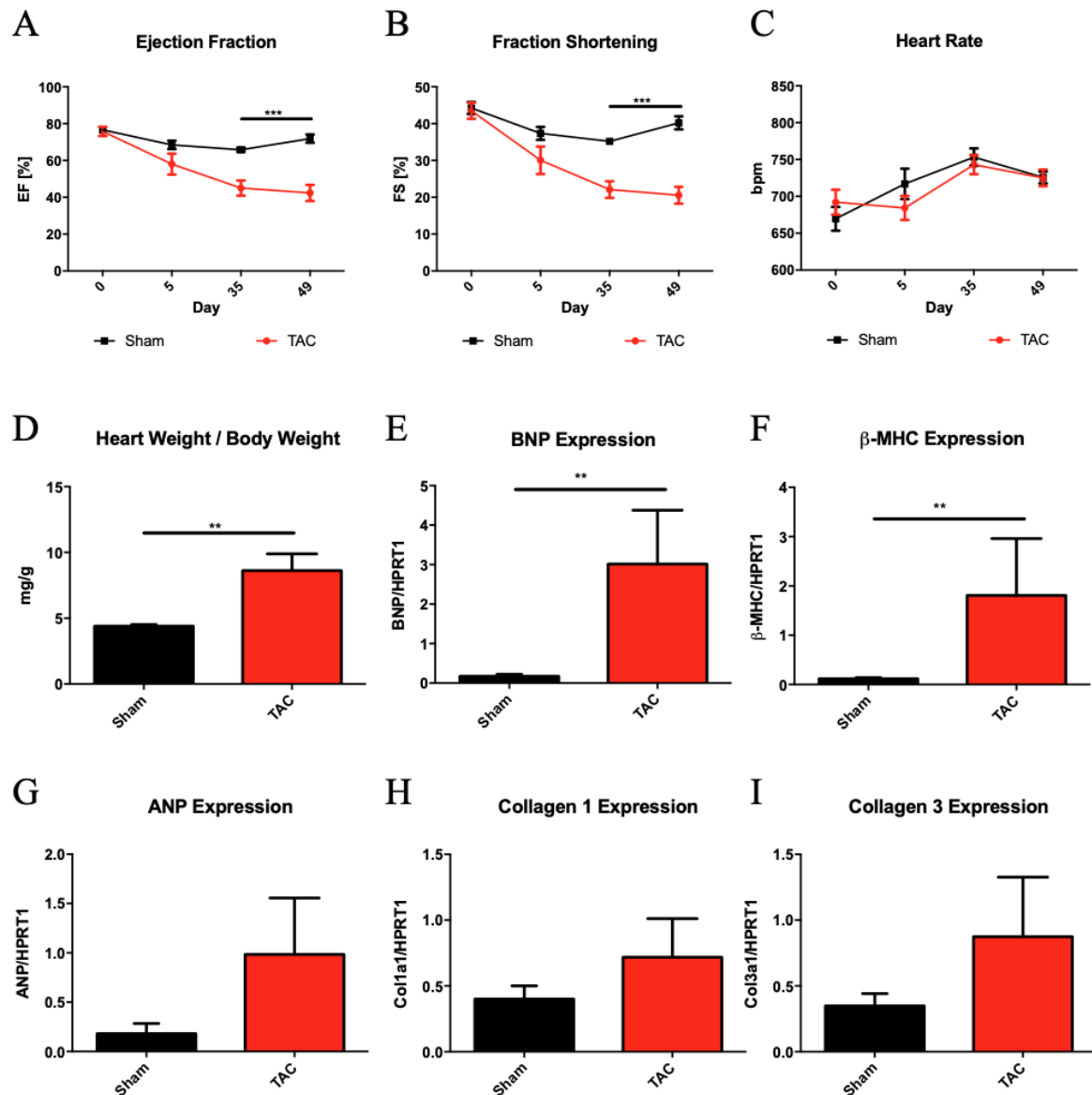
Figure 34: Characterization of TAC-induced HF model.
(A) Ejection Fraction (EF) **(B)** Fraction Shortening (FS) **(C)** Heart rate (HR) of sham and TAC animals over the period of 49 days (n=5-8). **(D)** Heart weight to body weight ratio was compared between sham and TAC animals (n=5-8). Post-mortem pathogenic cardiac remodeling genes expression **(E)** *BNP* **(F)** *β-MHC* **(G)** *ANP* were quantified by qPCR with HPRT1 as a reference gene. Collagen formation genes were also quantified **(H)** *Col1a1* **(I)** *Col3a1* (n=5-8). *$P < 0.05$; **$P < 0.01$; ***$P < 0.001$. Error bars depict in SEM.

To generate a suitable and reproducible hypertrophic cardiomyopathy model, a transverse aortic constriction (TAC) operation was established. TAC operations were performed on 8 week old C57BL/6 mice in order to create a constriction on the aorta leading to an increased pressure in the left ventricle resulting in hypertrophic cardiomyopathy. A blunt 26-gauge needle and 8.0 prolene suture were used to ligate the aorta. Two knots were tied around the transverse aorta using the blunt 26-gauge needle as a guide. After the second knot the needle was promptly removed, and a constriction was created. A similar procedure was performed on the sham animals except the ligation of the aorta. The mice were followed for gradual deterioration in phenotype for 8 weeks after the operation using the echocardiogram. Figure 34 shows a significant decrease in all cardiac output parameters in TAC animals compared to sham animals. Deterioration in cardiac function could be observed from day 5 through completion. Post mortem analysis of heart weight to body weight ratio increased significantly in the 26-gauge TAC group (8.62 ± 2.55 mg/g), compared to the sham group (Figure 34 D). Molecular data also showed an increase in pathological remodeling gene expression in all TAC animals (Figure 34 E - I). Thus, constriction using a 26-gauge needle could produce an HF phenotype with a marked decrease in cardiac function, accompanied by a significant increase in cardiac remodeling genes.

5.7.5 RXFP1 mouse study
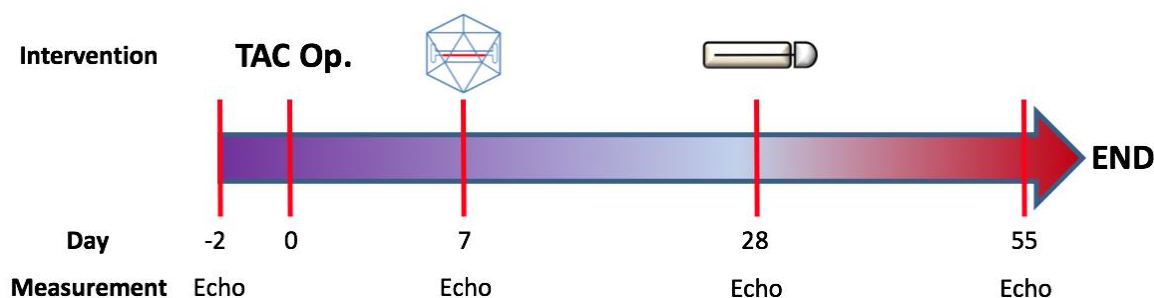
Figure 35: *In vivo* study timeline with all interventions and measurements.
TAC operations were performed on day 0, followed by virus transductions on the 7th day, and pump implantations on the 28th day. Echocardiography was performed at four different time points; two days before the TAC operation, 7 days after the operation, 28 days after the operation and 55 days after the operation.

To prove the beneficial effects of RXFP1 gene therapy with RLN treatment, 8 week old C57BL/6 mice were TAC and sham operated. Figure 35 shows the complete timeline of the experiment. After one week the mice were randomized into groups and viruses were

administered. 3 weeks after viral transduction, the mice were implanted with either saline or RLN pumps. Cardiac functions of the mice were measured by echocardiography at weeks 0, 1, 4, and 8 after the TAC operation (Figures 36). After 8 weeks, blood and tissue samples were collected, and RNA expression and protein expression were analyzed (Figure 37).

5.7.5.1 Functional and pathophysiology analysis

To detect the functional improvement from the RXFP1 gene therapy without bias, the echocardiography measurements were blindly analyzed for all animals.

Functional improvement could be seen in all TAC animals that received RXFP1 gene therapy (Figure 36). Four weeks after the TAC operation, animals treated with RXFP1 gene therapy showed a slight improvement in EF and FS, compared to LUC control treated animals (Figure 36 A - B). Four weeks after pump implantation, a significant improvement in EF and FS were detected in a TAC group that received both RXFP1 gene therapy and RLN treatment. In addition to the functional improvements, a trend toward a decrease in LVIDd and LV mass was also detected (Figure 36 C - D). Post mortem examination of the lung and heart detected no different in HW:BW ratio in all TAC animals. However, a slight but not statistically significant improvement in LW:BW ratio was seen in a TAC group receiving both RXFP1 gene therapy and RLN treatment (Figure 36 E – F). Thus, RXFP1 gene therapy with chronic RLN administration improves cardiac function in a mouse post-TAC HF model.
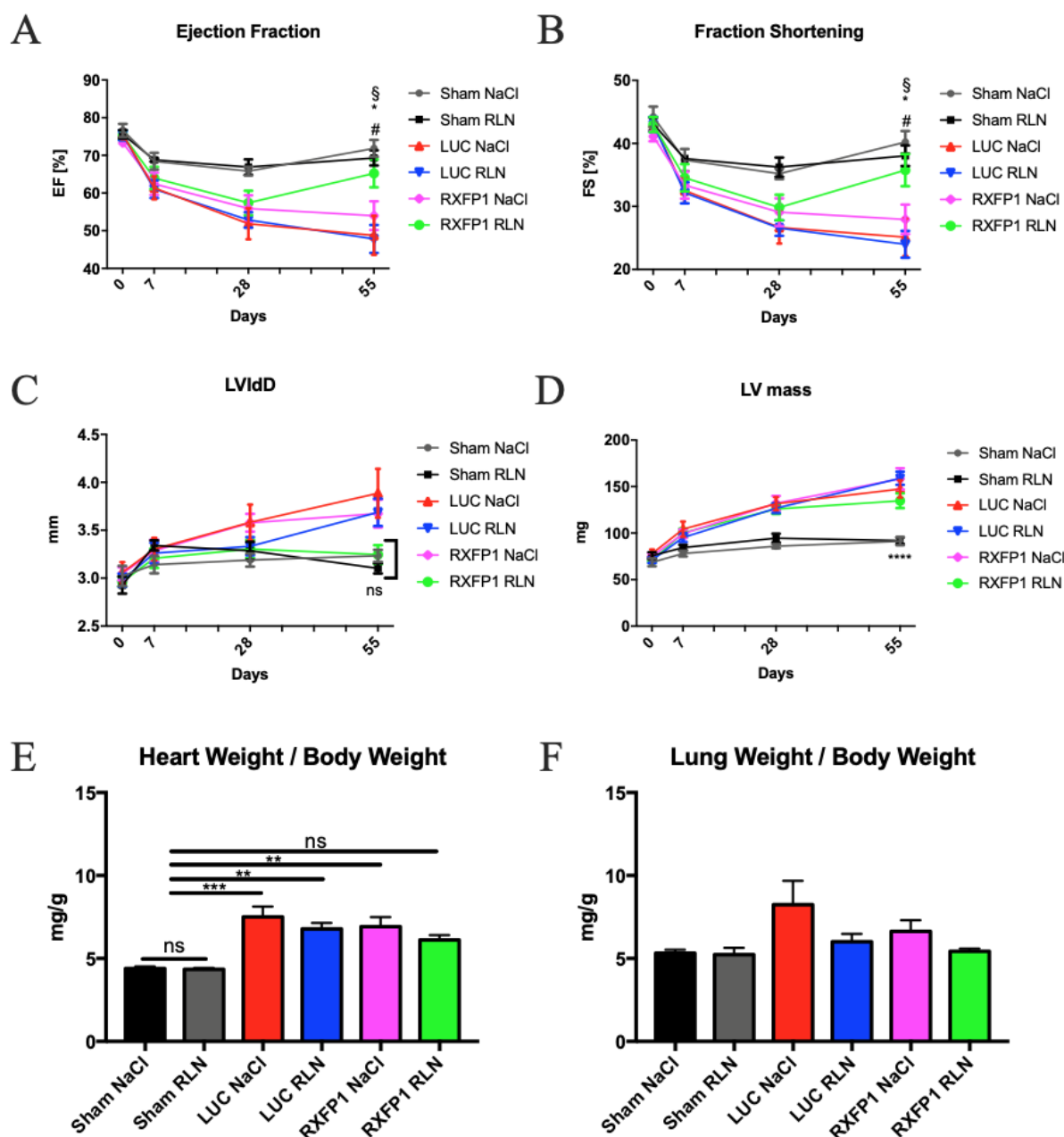
Figure 36: Functional improvements after RXFP1 gene therapy treatment with RLN.
(A) Ejection fraction (EF), **(B)** Fraction shortening (FS), **(C)** Left ventricular internal diameter (LVIDd), **(D)** Left ventricular mass (LV mass) of sham mice treated with and without recombinant RLN treatment and TAC mice treated with and without RXFP1 gene therapy and RLN (Sham + NaCl, Sham + RLN, TAC + LUC + NaCl, TAC + LUC + RLN, TAC + RXFP1 + NaCl and TAC + RXFP1 + RLN, n=8-9 in sham groups and n=14-15 in TAC groups). TAC animals were injected with $1x10^{12}$ vg/animal and implanted with either NaCl pumps or RLN pumps 4 weeks after TAC operation. **(E)** HW/BW, **(F)** LW/BW of tested mice measured post mortem. For **(A)** to **(D)** * FL NaCl vs. FR RLN, # FL RLN vs.FR RLN § FR NaCl vs. FR RLN, for **(E)** and **(F)** *P < 0.05; **P < 0.01; ***P < 0.001. Error bars depict in SEM.

5.7.5.2 Molecular analysis

To evaluate the effectiveness of gene transfer, RXFP1 mRNA expression was measured in all samples by qPCR after the animals were sacrificed. A significant increase in RXFP1 mRNA expression was detected in animals that received RXFP1 gene therapy. Figure 37 A shows that the animals expressed up to 1,500-fold more RXFP1 mRNA in the left ventricle compared to untreated animals and at least 500-fold more than native RXFP1 expression in the atria.

To detect improvement at the gene expression level, qPCR was performed, and expression of HF pathogenic remodeling markers, such as *ANP*, *BNP*, and *β-MHC*, was evaluated. Figure 37 B - D shows a trend toward a decrease in *ANP* and *β-MHC* in animals treated with RXFP1 gene therapy and RLN. This reduction in *ANP* and *β-MHC* expression was accompanied by a significant decrease in *BNP* expression as well (Figure 37 C). Moreover, pro-collagen formation genes such as *Col1a1*, *Col3a1* and *Postn* were also evaluated. A trend toward decreased *Col1a1*, *Col3a1* and *Postn* expression were detected in both RXFP1 gene therapy groups regardless of RLN administration (Figure 37 E - G).

To detect improvement at the protein level, protein expression analysis was performed and P-PLB(S16) was evaluated after the animals were sacrificed. Figure 37 H shows a trend toward increased PLB phosphorylation at serine 16 in the group treated with both RXFP1 gene therapy and RLN. A 5-fold increase in P-PLB(S16) was detected, which is in line with the *in vitro* data obtained from the prior experiments. Thus, the molecular analysis does match the functional analysis from *in vivo* animal experiments.
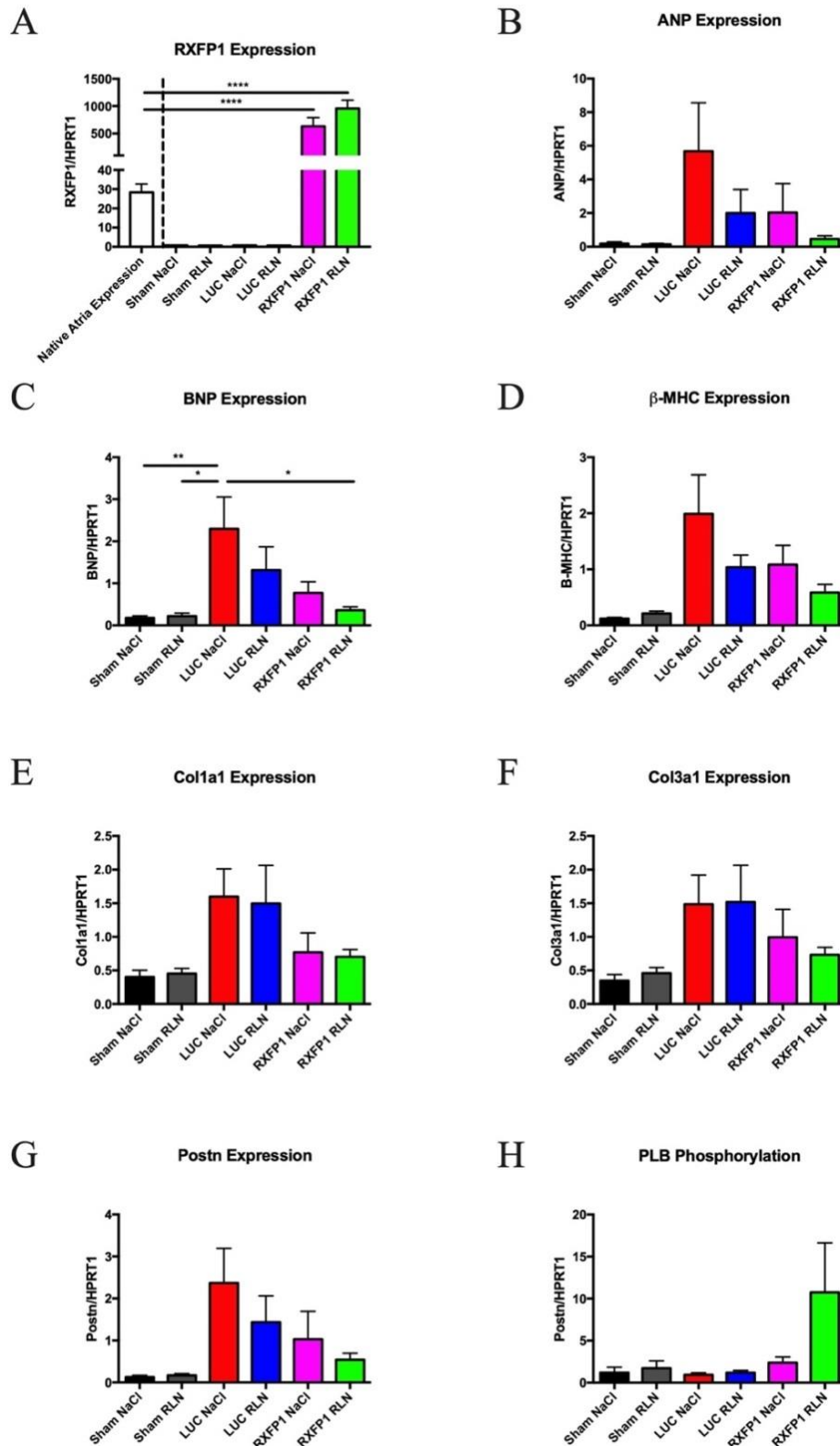
Figure 36: Molecular improvements in TAC animals after RXFP1 and RLN treatment.
(A) RXFP1**, (B)** *ANP,* **(C)** *BNP*, **(D)** *β-MHC*, **(E)** *Col1a1,* **(F)** *Col3a1*, **(G)** *Postn* mRNA expression in the ventricle detected 8 weeks after RXFP1 gene therapy treatment (n=8-15). mRNA expression was quantified using qPCR, with HPRT1 as a reference gene. **(H)** cardiac P-PLB(S16)/PLB quantification by immunoblot; GAPDH immune-detection was used as an internal control (n=8-15). *P < 0.05; **P < 0.01; ***P < 0.00. Error bars depict in SEM.

5.7.6 Relaxin plasma levels

To determine whether circulating levels of RLN were sufficient to induce RXFP1 activation in the treated animals, RLN plasma concentration was measured using an Elisa Kit. All animals that were treated with RLN showed a significant increase in RLN plasma concentration levels, compared to NaCl treated animals (Figure 38). The amount of RLN detected in the *in vivo* experiments was 3-fold lower than the amount or RLN used in the *in vitro* experiments. Nonetheless, this lower amount was still within range to induce RXFP1 activation. Therefore, the obtained results confirm that the improved cardiac functions observed in TAC animals correlate with the beneficial effects of RXFP1 activation from RLN stimulation.
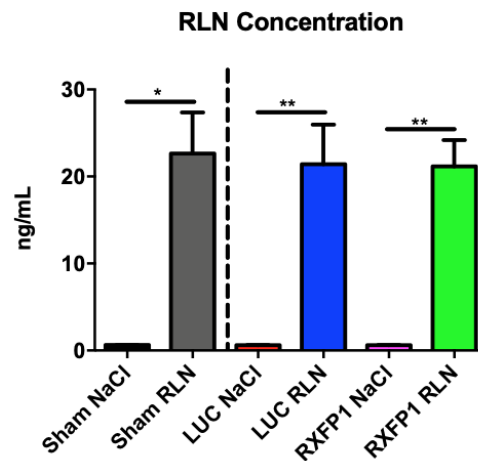
Figure 38: RLN plasma concentrations.
RLN plasma concentrations were determined using an Elisa kit (n=8-15). *P < 0.05; **P < 0.01; ***P < 0.001. Error bars depict in SEM.

6 Discussion

Heart failure is a leading cause of morbidity and mortality in the world [225]. HF is characterized by a dramatic increase in neuroendocrine activity, which raises the amount of circulating catecholamines, renin-angiotensin and mineralocorticoids, leading to long-term detrimental effects. One hallmark of HF is an over activation of the β-AR pathway. This compensation mechanism helps the body cope with the worsening cardiac function but leads to an increase in mortality. On the other hand, over activation of β-ARs will result in their desensitization upon exposure to catecholamines, which will worsen the symptoms of HF and eventually lead to patient decompensation.

Physiologically, RLN is released during pregnancy in order to help the maternal cardiovascular system cope with the stress of pregnancy. However, a recent study by Dschietzig et al. has discovered that RLN is also released upon HF decompensation [46]. In addition, chronic administration of RLN increases global arterial compliance and thereby reduces systemic vascular resistance and ventricular afterload leading to an increase in cardiac output [150]. These changes in the vascular system resulting from RLN secretion help the body recover from the decompensated stage. Other beneficial effects of RLN include angiogenesis, anti-inflammatory, and anti-fibrotic properties [94, 223]. Furthermore, in 2011, Dschietzig et al. discovered that RLN increases the twitch tension of isolated adult atrial cardiomyocytes regardless of HF status [98]. However, no change in ventricular cells was detected.

Taking into consideration the numerous benefits that RLN has on the cardiovascular system, an RLN clinical trial was conducted. The result of a phase I trial concluded that RLN treatment was beneficial for acute HF treatment [151, 152]. However, a larger study cohort failed to meet a defined endpoint, leading to its termination [132]. The failure of RLN treatment was primarily attributed to the lack of RXFP1 expression in the left ventricle, which is essential for the beneficial effects of RLN [55, 81]. Likewise, endogenous secretion of RLN during HF can increase the likelihood of beneficial effects being observed after RXFP1 gene therapy [131].

Therefore, the aim of this study was to investigate whether the ectopic expression of RXFP1 combined with RLN treatment can be developed into a gene therapy treatment for HF in an *in vivo* HF model. Although overexpression of RXFP1 in the heart has been investigated [153], coupling the overexpressed receptor to its ligand, RLN, has never been

studied before. This study would represent the first attempt at developing a gene therapeutic approach for the treatment of HF that is controllable by an exogenous RLN application.

6.1 Effects of RXFP1 overexpression in an *in vitro* model

6.1.1 Validation of RXFP1 expression

In order to study RXFP1's intracellular function, an effective overexpression and detection system was needed. To aid RXFP1 detection at the protein level, a FLAG-TAG was added to the RXFP1 construct used in this study. *In silico* analysis had demonstrated minimal structural interaction between the FLAG-TAG and RXFP1 that could interfere with protein folding and ligand binding sites. Native RXFP1 expression was detected in NRACMs, but not NRVCMs. Previous studies of an adult murine heart showed similar results. The same expression pattern was also seen in human hearts [154, 155]. Native RXFP1 expression in other organs was observed to be much lower compared to the expression in the atria of the heart. Mouse RXFP1 expression is only detectable in the heart and brain, which is different from human RXFP1 expression that could be detected in many organs. Protein expression database (Protein Atlas) also suggests that RXFP1 is only expressed at a very low level in most organs, which could be impossible to detect by qPCR. Using an AAV viral system, NRVCMs were transduced with an RXFP1 carrying virus, which resulted in overexpression of RXFP1 at mRNA level. Compared to the native expression of RXFP1 in the atria, viral overexpression significantly increased the amount of RXFP1 mRNA by 10-fold. Moreover, the amount of RXFP1 mRNA observed in the overexpression experiments was also much higher compared to native RXFP1 expression in all organs that are known to express it. Although RXFP1 was tagged with a specific epitope, detection at the protein level was still a challenge. Immunofluorescence images did not lead to a clear conclusion regarding the expression of RXFP1, due to unspecific interactions between the FLAG-TAG antibody and other membrane proteins. Furthermore, interference from post-translational modifications could lead to a lack of interaction between the FLAG-TAG antibody and the targeted epitope, resulting in a decrease in signal strength and an increase in background noise [156]. Finally, RXFP1 expression on transduced cardiomyocytes was detected with moderate success using an optimized immunofluorescence stain without permeabilization. This method still produced some background noises, but cardiomyocytes with high RXFP1 expression could still be distinguished. It is known, that GPCRs, such as β-adrenergic receptor, are challenging to detect at the protein level due to their high molecular weight and post-translational

modifications [157]. Hence, this limitation in protein detection is acceptable for this type of study, because it is considered to be a characteristic of the family of GPCR proteins.

6.1.2   Safety of RXFP1 overexpression and positive inotropic potential from RXFP1-RLN signaling

In addition to developing a method to overexpress RXFP1 in targeted cells, the receptor function was also assessed. Upon recombinant RLN stimulation in NRVCMs, an increase in cAMP production was observed in a dose dependent manner. A viral MOI as low as 5,000 vg/cells could induce a cAMP response in the transduced cells. Increasing dosages of virus led to further increase in cAMP production, until a decline was detected at a viral MOI of 50,000 vg/cells. This decline was attributed to stress from unfolded protein production [158]. Proteins produced in the cell need to undergo post translational processing in the ER before being transported to the correct compartment [158, 159]. Delicate cellular mechanisms for monitoring ER environment are essential for cells to effectively produce and secrete mature proteins [160]. Accumulation of unfolded proteins from overproduction leads to a disruption in this monitoring mechanism, which could result in ER stress induced cell death. This mechanism could explain why at high viral MOI, there is less cAMP production within the transduced cells.

On the other hand, when different dosages of RLN were used for stimulation, an increase in cAMP production was detected, with a dosage as low as 10 pM. Normally a ligand concentration threshold has to be met in order to activate the receptor [47]. However, at very low RLN concentrations (sub pM through pM range), RXFP1 utilizes a preassembled signalosome to scaffold to AC2 via AKAP79 and thereby induces cAMP accumulation [47, 161]. The cAMP produced is tightly regulated by the activity of PKA-activated PDE4D3 scaffolded to the receptor C-terminus by β-arrestin 2 [47]. A higher dosage of RLN (nM range) further increases cAMP production through the classical RXFP1-RLN signaling pathway, utilizing $G\alpha_s$, PI3K and AC5 [68, 76, 78, 162]. The production of cAMP reached its plateau at the RLN concentration of 10 nM.

Classical downstream signaling proteins in the RXFP1-RLN signaling pathway affected by an increase in cAMP production are: MAPKs [163], ERK1/2 [164, 165], and AKT [165-167]. However, none of these proteins were affected in the transduced ventricular cardiomyocytes in our study, since no difference in MAPKs, ERK1/2 and AKT phosphorylation was observed in NRVCMs receiving both RXFP1 virus and RLN

stimulation. On the other hand, when transduced NRVCMs were stimulated with RLN, an increase in P-PLB(S16) was detected. Many previous studies have linked phosphorylation of phospholamban to SERCA2a activation, leading to an increase in SR calcium uptake, resulting in positive inotropy [168-171]. Furthermore, a significant increase in Ca^{2+} transients amplitude was detected in NRVCMs treated with RXFP1 gene therapy and recombinant RLN stimulation. The observed higher amount of intracellular Ca^{2+} could be the result of prolonged action potential (AP), which increases the amount of Ca^{2+} entering the cell through both L-type and T-type Ca^{2+} channels [57, 62, 172]. Interestingly, the observed increase in cAMP, P-PLB(S16) and Ca^{2+} transient amplitude could explain what Dschietzig et al. observed when RLN stimulation resulted in an increase in twitch tension in atrial cardiomyocytes [98]. Thus, the increase in Ca^{2+} from prolonged AP coupled with a higher activity of SERCA2a through phospholamban phosphorylation could link molecular changes to stronger contractility observed in an *in vivo* model seen later [173].

In summary, these experiments prove that viral transduction could lead to a significant increase in RXFP1 expression on the targeted cells. Furthermore, the expressed receptors are fully functional and signal through the classical RXPF1-RLN pathway utilizing cAMP. Increase in cAMP activates PKA, which phosphorylates phospholamban at serine 16 and subsequently increases the activity of SERCA2a. On the other hand, RXFP1 stimulation by RLN also increases the Ca^{2+} influx through prolonged AP. Thus, this chain of events suggests potential positive inotropic effects that could be derived from RXFP-RLN signaling pathway in the transduced ventricular cardiomyocytes.

6.2 Evaluation of RXFP1 gene therapy treatment *in vivo*

6.2.1 Establishing effective dosage of RXFP1 and RLN *in vivo*

A major milestone in the advancement of gene therapy was the development of tissue specific viral capsids that were reliable and precise enough to deliver a onetime gene alteration treatment to a targeted cell type. Attempting to develop a regulatable gene therapy treatment by combining a receptor and its agonist has never been done before and therefore presented many challenges.

As a first step in this study, we aimed to determine the effective dosage of RXFP1 virus in healthy animals. Different dosages of RXFP1 virus in the range of 3×10^{11} to 1×10^{12} vg/animal were given to healthy animals by systemic injection through the tail vein. Systemic injection, as opposed to other routes of administration, such as direct injection, has a lower

risk and a higher translational potential in terms of treatment [174, 175]. Significant increase in RXFP1 mRNA expression was detected in the left ventricle at the 1×10^{12} vg/animal dose. In line with previous studies, viral genome concentration of 1×10^{12} lead to a significant increase in the expression of the gene of interest in the host animals [176-178]. Compared to native RXFP1 expression in the un-transduced atrial cells, a10-fold increase was detected in the transduced ventricles. Therefore, it can be assumed that 1×10^{12} vg/animal is an optimal concentration of virus that could lead to the required RXFP1 expression needed for RLN signal transduction.

Many studies have detected high variation in RLN plasma concentration levels when RLN was administered intraperitoneally or subcutaneously, due to different absorption rates between animals. Alongside i.p. and s.c. routes, intravenous (i.v.) administration of RLN might lead to a higher level of RLN presented systemically; however, rapid metabolization of the peptide by the body would result in quick excretion without maintaining an effective plasma concentration [179, 180]. Hence, implantation of osmotic pumps remains the only effective method for a chronic administration of RLN. Different dosages of recombinant RLN were administered to healthy animals via osmotic pumps for 28 days. Stable plasma concentration levels were reached after 14 days. In our study, recombinant RLN dosage of 1.35 µg/g/day led to RLN plasma concentration levels of 38.66 ± 12.27 ng/mL. This concentration is 3-fold less than what was used in the *in vitro* experiments, but it was still calculated to be ~30 nM of RLN, which is capable of inducing RXFP1 activity. *In vitro* experiments showed that significant induction of RXFP1 activity occurred when RLN concentration is in excess of 10 pM. In addition, this evidence suggests that the amount of RLN could be adjusted to induce RXFP1 activity that is suitable for individual needs. Considering the higher metabolism of rodents, the effective dosage of RLN established here was expected to be higher than the 30 µg/kg/day dosage, which is effective in humans [46]. Even higher dosages were not tested due to technical limitations as this was the highest concentration of commercially available RLN. On the other hand, lower concentrations of RLN were tested but no used, since lower concentrations: 1) could not produce effective plasma concentration and 2) could introduce unnecessary error from dilution. Thus, RLN dosage of 1.35 µg/g/day was determined as most likely to produce measurable effects from RXFP1 activation that are beneficial for cardiac function.

6.2.2 Effects of RXFP1 overexpression and RLN treatment in healthy animal

In this study, AAV mediated overexpression of RXFP1 in healthy animals did not produce any observable side effects during a one-month evaluation period. The treated animals did not exhibit any pathological phenotype neither physically nor molecularly. Furthermore, a microarray mRNA expression analysis detected similar mRNA expression profiles between RXFP1-transduced and LUC control transduced animals, with a significant increase in RXFP1 mRNA expression being the only significant difference detected. As such, expression of RXFP1 in healthy animals does not affect any functional or molecular parameters.

The effects of RXFP1 activation by RLN depend largely on the cell type being stimulated. So far, these effects have been well studied in cells that naturally express RXFP1 or cell lines generated specifically for the study of RXFP1 activation [49]. Nonetheless, all these models have never addressed artificial *in vitro* and *in vivo* RXFP1 expression and activation in a cell type that does not express it naturally. In our study, animals with ectopic ventricular RXFP1 expression were functionally assessed before and after recombinant RLN treatment. The results showed no functional change in HR, EF and FS before or after RLN administration. Additional evaluation using a more sensitive PV loop measurement detected a slight trend toward a rise in myocardial contractility (dP/dt max) in animals receiving the highest dosage of RXFP1 gene therapy regardless of RLN stimulation when compared to the LUC control animal. This trend could be interpreted as an effect of RXFP1 overexpression alone rather than the combined effect of RXFP1 with RLN induction.

Many studies demonstrated that *in vitro* activation of RXFP1 in the atria cardiomyocytes lead to positive inotropic and chronotropic responses [55, 181, 182], but these effects might not be detectable in healthy animals. It is important to note that RXFP1 was expressed in healthy animals, which might have blunted the beneficial effects of the concurrent RLN treatment, as the maximum cardiac function is already reached in these animals. On the other hand, it could be theorized that the downstream components of RXPF1 might not be readily available in heathy tissues which could lead to a lack of response as well. This component could be $G\alpha_i$, which is known to be upregulated in HF [26]. In addition, it is also well known that $G\alpha_i$ is essential for second surge of cAMP and PKA activation in the RXFP1-RLN signaling pathway, which could lead to an increase in PLB phosphorylation and calcium influx [78-80, 183]. In summary, these experiments suggest that: 1) RXFP1 gene therapy with RLN treatment does not have detrimental effects in an animal model, 2) RXFP1 expression does not lead to any increased in cardiac output in

healthy animals, 3) significant increase in RXFP1 mRNA expression could be achieved with viral dosage of $1x10^{12}$ vg/animal.

6.2.3 Generation of a relevant HF model

Several mouse models exist for the study of HF [184]. These models start with various types of cardiac remodeling through the introduction of different kinds of stress. A common end point of all cardiac remodeling is HF [11, 185]. In this study, HF was a result of TAC surgery, which causes pressure overload in the left ventricle due to the constriction of the aorta [142, 143]. This pressure overload leads to cardiac hypertrophy similar to what is observed in patients with chronic hypertension and aortic stenosis[186, 187]. Eventually the systolic pumping function of the heart will start to fail as a result of left ventricular hypertrophy leading to HF. Previous studies using this model have shown that HF develops anywhere from 6 to 8 weeks after TAC depending on the response to the strain of mouse used [188, 189].

Assessment of cardiac function and post mortem analysis of molecular alterations in *ANP*, *BNP*, *β-MHC*, *Col1a1*, *Col3a1*, and *Postn,* all hallmarks of HF, were used to ensure that the generated phenotype resembles what has been described in THE literature [190, 191]. Significant decrease in cardiac function such as EF and FS accompanied by significant upregulation of *ANP*, *BNP*, *β-MHC*, *Col1a1*, *Col3a1*, and *Postn* were indeed detected in the TAC animals in this study, 8 weeks after TAC. In line with previous studies, the HF phenotype was accompanied by significant up-regulation of pathological cardiac remodeling genes [190, 192, 193]. Moreover, up-regulation in collagen formation genes led to a significant increase in heart-weight to body-weight ratio, observed in all TAC animals evaluated. In summary, the TAC operation used in this study was able to generate a HF phenotype that have been described before by numerus reports.

6.3 Potentially controllable gene therapy rescues HF in the TAC model

6.3.1 Expression of RXFP1 alone is moderately beneficial for HF

Many studies have described the beneficial effects of RXFP1 activation by RLN in different cell types such as fibroblasts, endothelia, and atrial cells both *in vitro* and *in vivo* [55, 194-196]. However, none has described the beneficial effects of RXFP1 expression alone. In this study, the beneficial effects of RXFP1 expression in the ventricular cardiomyocytes was confirmed. RXFP1 expression slightly improved cardiac function in the

TAC animals. However, these increases in EF and FS did not lead to an overall functional improvement in HF. Similar improvement can be seen at the molecular level, as a decrease in *ANP*, *BNP*, *β-MHC*, *Col1a1*, *Col3a1*, and *Postn* expression was detected. These improvements might be the result of RXFP1 activation by endogenous RLN. Previous studies have discovered that male reproductive organs secrete a small amount of RLN which can enter circulation and lead to activation of RXFP1 [197-199]. Moreover, Dschietzig et al. have discovered that RLN is also secreted by the cardiomyocytes themselves during HF. It is therefore tempting to speculate that the moderately beneficial effects from LV-specific RXFP1 expression are (at least in part) due to the activity of endogenous RLN. Even though only a small amount of RLN is produced, it might be still enough to induce RXFP1 activation and improve the contractility of the heart.

6.3.2 RXFP1 gene therapy with RLN treatment rescues HF

The beneficial effects of RXFP1 gene therapy combined with RLN treatment were validated in an experimental HF model, to confirm the potential inotropic property shown earlier in NRVCMs. Thus far, RLN has been shown to only induce positive inotropy in the atria, but not in the ventricle, due to lack of ventricular RXFP1 expression [55, 62, 81]. Consequently, we chose to use a cardiac targeted system (cardiotropic AAV-based viral vector and cardiac enriched promoter) to enrich RXFP1 expression specifically in the heart. With RXFP1 gene therapy, RXFP1 is readily available in the ventricle to interact with RLN. First, RXFP1 activation by RLN induced positive inotropy, as significant increase in EF and FS were detected after RLN treatment, compared to that of the control animals. These improvements in cardiac function were accompanied by a rise in PLB phosphorylation at Serine 16. Increase in cardiac contractility has been linked to inactivation of PLB through phosphorylation [200, 201]. PLB binds to and inhibits SERCA2a. Phosporylation of PLB results in the release of SERCA2a binding and thereupon its disinhibition. SERCA2 activation in turn leads to more efficient Ca^{2+} sequestration to SR and a lusitropic effect, or higher muscle relaxation, which could explain the observed improvement in cardiac function [224]. In addition to improvement in contractility, a trend towards a decrease in heart-weight to body-weight and lung-weight to body-weight were detected as well. These trends suggest that the treated animals experienced less hypertrophy and less apoptosis, resulting in a milder form of HF compared to the control treated animals.

Several underlying mechanisms have been proposed to explain the cardioprotective effects of RLN. Samuel et al. demonstrated that RLN has anti-fibrotic and anti-hypertrophic properties, which are mediated by cardiac fibroblasts [154, 202]. Lekgabe et al. further demonstrated that long-term administration of RLN lowers collagen content in the left ventricle, reverses cardiac fibrosis, and ameliorates left ventricular dysfunction [203]. Furthermore, Moore et al. proposed that RLN might exert its anti-hypertrophic property by changing the secretion profile of cardiac fibroblasts to suppress hypertrophy in cardiomyocytes [204]. Xu et al. and Chan et al. demonstrated that effects of RLN on the vascular system could protect against hypertension-induced cardiac dysfunction and reverse hypertension-associated fibrosis [205, 206]. Additionally, Nistri et al. theorized that RLN could induce maturation of myocardial progenitor cells through expression of cardiac specific structural genes at both mRNA and protein level [60]. All in all, the cardioprotective effects on both cardiomyocytes and vascular cell could result in an improved cardiac cell survival, which in turn leads to the preserved cardiac function observed in this experiment.

The molecular data were in line with what was observed phenotypically and functionally. First, several hypertrophic markers were analyzed. Classically *BNP* mRNA expression correlated to the severity of HF[207]. Since the phenotype of heart failure is less severe after RXFP1 gene therapy and RLN treatment, a significant decrease in *BNP* was detected. Furthermore, a trend toward a decrease in *ANP* and *β-MHC* was also observed in this treatment group which is in agreement with the phenotype seen. Second, a molecular signature of collagen depositions was evaluated, as this is a very important mechanism in cardiac remodeling and a hallmark of HF development [208]. Its attenuation will result in an improvement in the HF phenotype. Indeed, expression of collagen production related genes, such as *Col1a1, Col3a1, and Postn,* was blunted in RXFP1 gene therapy groups regardless of RLN treatment. Thus, cardiac remodeling could be attenuated in our mouse model by RXFP1 gene therapy. Moreover, HF could be rescued by a combined treatment of RXFP1 gene therapy and RLN stimulation.

Apart from the RXFP1-RLN effects in the ventricle, other pleotropic effects of RLN could have also led to an improvement in the HF phenotype. RLN is also known for its vasodilative and angiogenic properties [195, 209]. Increase in RLN concentration could have activated the NO/cGMP pathway in vascular smooth muscle and coronary artery endothelium, leading to an increased production of NO, and ultimately resulting in vasodilatory responses [57, 209, 210]. Long-term exposure to RLN could have induced

production of VEGF and b-FGF in endometrial cells leading to angiogenesis at injured sites and promote healing [211, 212]. These pleotropic effects of RLN could have also contributed to the improved HF phenotype observed in RXFP1 treated animals. These potential effects go beyond the scope of this thesis and should be evaluated in future studies.

In conclusion, the proposed treatment is based on the interaction of two components that need each other to effectively treat HF. Viral gene transfer of RXFP1 leads to stable expression of the receptor (approximately 500 folds more than native RXFP1 expression in the atria), which was shown to be safe. The second arm of the treatment, RLN, is a peptide, whose administration can be spatiotemporally controlled. Different amounts of RLN could control the beneficial effects of RXFP1-RLN interaction, as demonstrated in this study. Based on this observation, the effects of the combined treatment could be tightly controlled and fine-tuned by adjusting the dose of exogenous RLN. Thus, this study demonstrates for the first time a potentially controllable gene therapy treatment utilizing a membrane protein and its ligand.

6.4 Elucidation of RXFP1-RLN signaling pathway in ventricular cardiomyocytes

As described before, RXPF1 activation by RLN induces an increased production of second messengers such as cAMP, cGMP and NO within the cell [213]. As a result, mRNA expression and protein phosphorylation patterns are altered depending on the cell type being stimulated. RLN has been extensively studied in endothelial cells and fibroblasts, as the current widely believed hypothesis, is that RLN has mainly vasodilatory, anti-fibrotic and angiogenic properties [57, 195, 202, 210-212, 214]. On the other hand, the inotropic effects of RLN discovered in atrial cardiomyocytes by Dschietzig et al. never gained momentum for further investigation.

In this study, the inotropic pathway of RXFP1 activation by RLN was elucidated *in vitro*. Different signaling proteins of the RXFP1-RLN signaling pathway were inhibited in RXFP1 transduced NRVCMs before RLN stimulation. Change in P-PLB(S16) levels was used as an endpoint in this study in order to assess which protein played an important role in the signaling pathway.

Gα_s: When the Gα_s subunit of the heterotrimeric g-protein was inhibited, RXFP1 activation by RLN could not produce any detectable P-PLB(S16), compared to control cells, where P-PLB(S16) was abundant. Gα_s is the component that initiates a signaling cascades in many GPCRs [215]. However, some GPCRs might signal through other subunits of heterotrimeric

G-protein [78, 216]. Many studies, including this one, have shown that RLN signals through $G\alpha_s$ in order to increase cAMP production, which leads to further responses from the cell [68, 88]. When compared to strong inotropic agents, such as ISO, RXFP1 activation produces a noticeably lower cAMP and P-PLB signal. However, this could be attributed to a loose coupling between RXFP1 and $G\alpha_s$ subunit [77]. To conclude, the $G\alpha_s$ subunit of the heterotrimeric G-protein is essential for RXFP1-RLN signaling pathway, and it is needed for all downstream signaling.

AC: When AC was inhibited, RXFP1 activation from RLN stimulation resulted in a moderate reduction in P-PLB(S16) signal (20% lower than the original signal). As described before, in different cell types other than cardiomyocytes, $G\alpha_s$ stimulates AC in order to increase cAMP production after RXFP1 activation. This increase in secondary messenger production leads to alterations in gene expression and protein phosphorylation. However, in this study, RLN seems to signal through other specific ACs presented in cardiomyocytes. Current understanding of RXFP1 signaling specifies various isoforms of AC as being responsible for cAMP production, depending on the type of cell being stimulated [217, 218]. However, most of these studies were done in fibroblast or endothelia which have different AC expression profiles than cardiomyocytes. There are two primary isoforms of AC in cardiomyocytes, AC5 and AC6 [219-221]. AC5 is primarily expressed in adult cardiomyocytes and AC6 is primarily expressed in neonatal cardiomyocytes [222]. Other isoforms of AC are also present in the heart, but in much lower quantities [223, 224]. This difference in expression profile can explain why the expected decrease in P-PLB(S16) was dampened. In addition, the AC inhibitor displays different affinities toward different isoforms of AC [219], resulting in an insufficient blockage of the relevant isoforms. In this experiment, increasing the amount of inhibitor to block the dominant isoforms was not possible, without having a detrimental effect on the cells. Thus, the moderate inhibition of P-PLB(S16) could be attributed to the insufficient inhibition of the AC isoform (e.g. AC5 and AC6), through which RLN induces cAMP production and positive inotropic response.

PKA: In this study, inhibition of PKA led to a substantial decrease in P-PLB(S16) levels. PKA is a signaling protein downstream of cAMP [225]. Activation of PKA by cAMP lead to phosphorylation of many proteins and ion channels [225, 226]. PKA is known to directly phosphorylate PLB at serine 16, thus disinhibiting/activating SERCA2a activity [200, 227]. SERCA2a is a Ca^{2+}-ATPase, which transports Ca^{2+} from the cytosol into the lumen of the SR [228]. As the activity of SERCA2a increases, the amount of Ca^{2+} pumped into the SR also

increases, resulting in myocardial relaxation and better calcium handling in the cardiomyocytes [229]. Improved calcium cycling contributes to a tightly spatiotemporally-regulated elevated level of intracellular Ca^{2+} ($[Ca^{2+}]_i$) and stronger contractions of cardiac muscle without increased resting $[Ca^{2+}]_i$, which leads to diastolic dysfunction and HF [230].

PI3K: In this study, inhibition of PI3K with wortmannin resulted in a marked decrease in cAMP production and P-PLB(S16). PI3K was described to be important for maintaining cAMP production after RLN stimulation [77]. Activation of RXFP1 triggers the activation of PI3K, independent of the $G\alpha_s$ activation. Activation of PI3K leads to PIP3 production, which activates PKC ζ, resulting in activation of AC for further production of cAMP [77, 217, 218]. This fact would explain how RXPF1-RLN signaling maintains the amount of cAMP needed for downstream signaling activation.

Gβγ: Inhibition of $G_{\beta\gamma}$ led to an increase in P-PLB(S16) signal. Kern et al. have described that RXFP1 is not easily deactivated and may behave differently than other GPCRs [231]. However, the results from the $G\beta_\gamma$ inhibition could not confirm these finding. Gβγ functions by recruiting different GRKs to the membrane in order to phosphorylate GPCRs, thereby resulting in a desensitization of the receptor [232, 233]. Furthermore, Gβγ also plays a role in the inhibition of PI3K, which could further decrease GPCRs signal [184, 234, 235]. Thus, it is reasonable to assume that RXPF1 might not behave like other GPRCs, when being stimulated for a prolonged period of time.

Lastly, it should be noted that the RXFP1-RLN pathway was studied in healthy cardiomyocytes. It would be interesting to further investigate the RXFP-RLN pathway in failing cardiomyocytes. The molecular alterations in these cells could lead to a better understanding of the RXFP1-RLN signaling pathway.

6.5 Difference between RXFP1 and β-adrenergic signaling

In this study, RLN is assumed to be a positive inotropic agent when coupled to its artificially expressed RXPF1 receptor in the heart. Other positive inotropic agents, such as isoproterenol, couple to the naturally expressed β-adrenergic receptor (β-AR) in the heart to produce positive inotropy [236]. Comparing the signaling pathways of both inotropic agents, similarity between RLN and ISO can be observed many areas. For example, RLN and ISO both signal through $G\alpha_s$ and utilize cAMP as a second messenger to activate PKA, which leads to an increase in phosphorylation of PLB at Serine 16. However, the strength with which RLN and ISO activate the signaling cascade is different.

Activation of β-AR by isoproterenol stimulates the production of cAMP by AC and thereby activates PKA. PKA phosphorylates L-type calcium channels, PLB and RyR2, which contributes to the increase of intracellular Ca^{2+} transient, resulting in increased cellular contractility [237]. Phosphorylated L-type calcium channels increase the amount of Ca^{2+} influx into the cell, and phosphorylated RyR2 increases the amount of Ca^{2+} released from the SR [168, 170, 229, 238, 239]. Compared to an unstimulated myocardium, this increased amount of Ca^{2+} leads to an increase in muscle contraction during the cardiac excitation-contraction coupling period [237]. During relaxation, phosphorylated PLB increases the SERCA2a Ca^{2+} reuptake rate into the SR, leading to better Ca^{2+} cycling and removal of Ca^{2+} from the cytosol [238-240].

In this study, activation of β-AR by ISO strongly and abruptly induced phosphorylation of PLB at both serine 16 and threonine 17, leading to an enhanced Ca^{2+} cycling within the cell. A significant decrease in P-PLB(T17) was detected by a series of blocking experiments, after CaMKII activity was chemically blocked in ISO treated cells. In normal excitation-contraction coupling, PLB phosphorylation at serine 16 is required before threonine 17 can be phosphorylated [170]. ISO induces a strong influx of Ca^{2+} into the cytosol from both outside of the cell, through L-type calcium channels, and within the cell, from the SR through RyR2 [237, 238]. Single site PLB phosphorylation is not sufficient to induce SERCA2a activity required for efficient Ca^{2+} reuptake into the SR. As a result, SR Ca^{2+} reuptake rate is slower than required, excess cytosolic Ca^{2+} quickly binds to calmodulin to induce the activation of CaMKII, which phosphorylates PLB at threonine 17 and thereby further increases the activity of SR SERCA2a Ca^{2+} reuptake rate [241]. This chain of phosphorylation events happens extremely quickly after β-AR stimulation by ISO and persisted for hours as PLB phosphorylation status did not return to baseline even 24 hours afterward. As a consequence, CaMKII activation from excess cytosolic Ca^{2+} and a prolonged phosphorylation of RyR2 and P-PLB(T17) is a hallmark of Ca^{2+} mishandling, which could eventually lead to pathological cardiac remodeling and mitochondria dysfunction [242, 243]. Hence, CaMKII does play a crucial role in β-adrenergic activation compared to RXFP1 activation.

In contrast, activation of RXFP1 by RLN induces phosphorylation of PLB at both serine 16 and threonine 17 in a more gradual and sequential fashion. Moreover, when CaMKII activity was chemically blocked, P-PLB(T17) was unaffected both before and after RXFP1 activation by RLN. In addition, Piedras-Rentería et al. discovered that, apart from

increased cAMP accumulation, RLN also increases Ca^{2+} influx through prolonged AP, which increases Ca^{2+} current through L-type and T-type calcium channels [62]. Gradually, an excess influx of Ca^{2+}, which cannot be transferred into the SR by SERCA2a, will bind to calmodulin and activate CaMKII, resulting in phosphorylation of PLB at threonine 17 [170]. Similar but yet different from β-AR signaling, RXFP1 time curve and CaMKII blocking experiments presented in this study show that RXFP1-RLN signaling also generated PLB phosphorylation at both serine 16 and threonine 17 in the myocardium, but at a much more reduced strength. Throughout the experiment, phospholamban phosphorylation at threonine 17 has never reached a significant level compared to none treated cell. As a result, CaMKII activation is much lower in RXFP1 samples treated with RLN and the pathway could be conceded as a natural coping mechanism within the cells as previous studies revealed that P-PLB(S16) is required for P-PLB(T17) sine qua non and a slight CaMKII activation is therefore considered as beneficial [236, 244, 245].

Lastly, this study confirms that RXFP1 activation is independent of β-adrenergic activation, since blocking of the β-adrenergic receptor did not alleviate the downstream signaling of RXFP1 stimulation by RLN. In line with previous finding, RXFP1 activation by relaxin acts independently of β-adrenergic activation [62]. Thus, this evidence strongly suggests that RXFP1 has its own independent signaling pathway and – unlike classical β-adrenergic receptor – it is not detrimental to the cells, as it only increases Ca^{2+} influx to the level that the cell can physically cope with.

6.6 Similarity between rat, human and mouse RXFP1 signaling

Many studies have described the similarity between human and rat RXFP1 receptors [37, 246]. In this study, the similarity of the receptors was confirmed, as both seem to potentially induce positive inotropy when stimulated with recombinant RLN. Human and rat RXFP1 are quite similar, sharing approximately 89% similarity in both mRNA and amino acid sequence [68, 247-249]. Both also share sequence homology at all ligand biding domains [37, 246], suggesting to a belief that both sequences would behave the same way when overexpressed and stimulated with recombinant RLN. This assumption was confirmed as a combination of human RXFP1 overexpression and RLN stimulation led to an increased phosphorylation of PLB at serine 16 at a level similar to what was seen with rat RXFP1 activation. In addition, the use of human RXFP1 for future gene therapy treatment might be more desirable than rat RXFP1 because of a reduced risk for immunological reaction. In

conclusion, the human RXFP1 receptor warrants further investigation into its therapeutic potential as well.

6.7 Conclusion and outlook

While the results presented in this study are far from providing a complete understanding of the beneficial effects of RXFPI gene therapy and activation by RLN in both *in vivo* and *in vitro*, they do extend our knowledge of the ectopic expression of RXFP1 and its subsequent signaling cascade upon RLN stimulation:

A combined treatment consisting of ectopic expression of RXFP1 through RXFP1 gene therapy and chronic RLN stimulation is capable of rescuing a HF phenotype in an *in vivo* HF model.

With regard to its mechanism, this study clearly demonstrates that ectopically expressed RXFP1 in the left ventricular myocardium has some moderate cardioprotective properties, which can blunt the effects of TAC surgery, leading to a reduced pathological cardiac molecular remodeling. By combining RXFP1 gene therapy with exogenous recombinant RLN administration, these cardioprotective effects are multiplied and a further positive inotropic response in the left ventricle is induced. This study also indicates that RXFP1 expressed in the ventricle, signals through a $G\alpha_s$ subunit of the heterotrimeric G-protein and PI3K, in order to increase cAMP production, PKA activation, and phosphorylation of PLB at serine 16. Lastly, due to similar positive inotropic effects observed, both β-adrenergic activation and RXFP1 activation were examined. The results indicate that induction of RXFP1 leads to mild activation of the downstream signaling pathways compared to the induction through β-adrenergic receptor. This mild and gradual activation might play a key role in preventing RXFP1 from becoming detrimental.

Still, some questions from this study remain unanswered:

- Will human RXFP1 exhibit similar behavior compared to rat RXFP1?
- Will prolonged stimulation of RXFP1 lead to its desensitization?
- Does RXFP1 remain active after on and off treatment of RLN?
- What are the long-term consequences of RXFP1 activation by RLN?

Answering these questions will help us to understand RXFP1-RLN signaling transduction in cardiomyocytes further and could lead to the development of a more efficient treatment option for HF. Nonetheless, these questions will be addressed in future studies.

7 References

1. Moran, A.E., et al., *The global burden of ischemic heart disease in 1990 and 2010: the Global Burden of Disease 2010 study.* Circulation, 2014. **129**(14): p. 1493-501.
2. Bui, A.L., T.B. Horwich, and G.C. Fonarow, *Epidemiology and risk profile of heart failure.* Nat Rev Cardiol, 2011. **8**(1): p. 30-41.
3. Störk, S., et al., *Epidemiology of heart failure in Germany: a retrospective database study.* Clinical research in cardiology : official journal of the German Cardiac Society, 2017. **106**(11): p. 913-922.
4. Coronel, R., J.R. de Groot, and J.J. van Lieshout, *Defining heart failure.* Cardiovasc Res, 2001. **50**(3): p. 419-22.
5. McMurray, J.J., et al., *ESC Guidelines for the diagnosis and treatment of acute and chronic heart failure 2012: The Task Force for the Diagnosis and Treatment of Acute and Chronic Heart Failure 2012 of the European Society of Cardiology. Developed in collaboration with the Heart Failure Association (HFA) of the ESC.* Eur Heart J, 2012. **33**(14): p. 1787-847.
6. Ponikowski, P., et al., *2016 ESC Guidelines for the diagnosis and treatment of acute and chronic heart failure: The Task Force for the diagnosis and treatment of acute and chronic heart failure of the European Society of Cardiology (ESC)Developed with the special contribution of the Heart Failure Association (HFA) of the ESC.* Eur Heart J, 2016. **37**(27): p. 2129-2200.
7. Mann Douglas, L. and R. Bristow Michael, *Mechanisms and Models in Heart Failure.* Circulation, 2005. **111**(21): p. 2837-2849.
8. Pazos-Lopez, P., et al., *The causes, consequences, and treatment of left or right heart failure.* Vasc Health Risk Manag, 2011. **7**: p. 237-54.
9. Mosterd, A. and A.W. Hoes, *Clinical epidemiology of heart failure.* Heart, 2007. **93**(9): p. 1137-46.
10. Dickstein, K., et al., *ESC guidelines for the diagnosis and treatment of acute and chronic heart failure 2008: the Task Force for the diagnosis and treatment of acute and chronic heart failure 2008 of the European Society of Cardiology. Developed in collaboration with the Heart Failure Association of the ESC (HFA) and endorsed by the European Society of Intensive Care Medicine (ESICM).* Eur J Heart Fail, 2008. **10**(10): p. 933-89.
11. Hunt, S.A., et al., *2009 Focused update incorporated into the ACC/AHA 2005 Guidelines for the Diagnosis and Management of Heart Failure in Adults A Report of the American College of Cardiology Foundation/American Heart Association Task Force on Practice Guidelines Developed in Collaboration With the International Society for Heart and Lung Transplantation.* J Am Coll Cardiol, 2009. **53**(15): p. e1-e90.
12. Jessup, M., et al., *2009 focused update: ACCF/AHA Guidelines for the Diagnosis and Management of Heart Failure in Adults: a report of the American College of Cardiology Foundation/American Heart Association Task Force on Practice Guidelines: developed in collaboration with the International Society for Heart and Lung Transplantation.* Circulation, 2009. **119**(14): p. 1977-2016.
13. Sharma, K. and D.A. Kass, *Heart failure with preserved ejection fraction: mechanisms, clinical features, and therapies.* Circ Res, 2014. **115**(1): p. 79-96.
14. Andersson, C. and R.S. Vasan, *Epidemiology of heart failure with preserved ejection fraction.* Heart Fail Clin, 2014. **10**(3): p. 377-88.

15.   Schirone, L., et al., *A Review of the Molecular Mechanisms Underlying the Development and Progression of Cardiac Remodeling.* Oxid Med Cell Longev, 2017. **2017**: p. 3920195.

16.   McMurray, J.J. and M.A. Pfeffer, *Heart failure.* Lancet, 2005. **365**(9474): p. 1877-89.

17.   Triposkiadis, F., et al., *The sympathetic nervous system in heart failure physiology, pathophysiology, and clinical implications.* J Am Coll Cardiol, 2009. **54**(19): p. 1747-62.

18.   Mann, D.L. and M.R. Bristow, *Mechanisms and models in heart failure: the biomechanical model and beyond.* Circulation, 2005. **111**(21): p. 2837-49.

19.   Hasking, G.J., et al., *Norepinephrine spillover to plasma in patients with congestive heart failure: evidence of increased overall and cardiorenal sympathetic nervous activity.* Circulation, 1986. **73**(4): p. 615-21.

20.   Wallukat, G., *The beta-adrenergic receptors.* Herz, 2002. **27**(7): p. 683-90.

21.   Pierce, K.L. and R.J. Lefkowitz, *Classical and new roles of beta-arrestins in the regulation of G-protein-coupled receptors.* Nat Rev Neurosci, 2001. **2**(10): p. 727-33.

22.   Steinfath, M., et al., *Regional distribution of beta 1- and beta 2-adrenoceptors in the failing and nonfailing human heart.* Eur J Clin Pharmacol, 1992. **42**(6): p. 607-11.

23.   Port, J.D. and M.R. Bristow, *Altered beta-adrenergic receptor gene regulation and signaling in chronic heart failure.* J Mol Cell Cardiol, 2001. **33**(5): p. 887-905.

24.   Bristow, M.R., et al., *Beta 1- and beta 2-adrenergic-receptor subpopulations in nonfailing and failing human ventricular myocardium: coupling of both receptor subtypes to muscle contraction and selective beta 1-receptor down-regulation in heart failure.* Circ Res, 1986. **59**(3): p. 297-309.

25.   Wallukat, G., et al., *Functional and structural characterization of anti-beta1-adrenoceptor autoantibodies of spontaneously hypertensive rats.* Mol Cell Biochem, 2003. **251**(1-2): p. 67-75.

26.   Eschenhagen, T., et al., *Increased messenger RNA level of the inhibitory G protein alpha subunit Gi alpha-2 in human end-stage heart failure.* Circ Res, 1992. **70**(4): p. 688-96.

27.   Ishikawa, Y., et al., *Downregulation of adenylylcyclase types V and VI mRNA levels in pacing-induced heart failure in dogs.* The Journal of Clinical Investigation, 1994. **93**(5): p. 2224-2229.

28.   Volpe, M., et al., *Transition from asymptomatic left ventricular dysfunction to congestive heart failure.* J Card Fail, 1995. **1**(5): p. 409-19.

29.   Peterson, R.C. and M.E. Dunlap, *Angiotensin II receptor blockers in the treatment of heart failure.* Congest Heart Fail, 2002. **8**(5): p. 246-50; 256.

30.   Berliner, D. and J. Bauersachs, *Current Drug Therapy in Chronic Heart Failure: the New Guidelines of the European Society of Cardiology (ESC).* Korean circulation journal, 2017. **47**(5): p. 543-554.

31.   Yancy, C.W., et al., *2013 ACCF/AHA guideline for the management of heart failure: a report of the American College of Cardiology Foundation/American Heart Association Task Force on Practice Guidelines.* J Am Coll Cardiol, 2013. **62**(16): p. e147-239.

32.   Moss, A.J., et al., *Improved survival with an implanted defibrillator in patients with coronary disease at high risk for ventricular arrhythmia. Multicenter Automatic Defibrillator Implantation Trial Investigators.* N Engl J Med, 1996. **335**(26): p. 1933-40.

33.   Bergethon Kristin, E., et al., *Trends in 30-Day Readmission Rates for Patients Hospitalized With Heart Failure.* Circulation: Heart Failure, 2016. **9**(6): p. e002594.

References

34.   Neumann, T., et al., *Heart failure: the commonest reason for hospital admission in Germany: medical and economic perspectives.* Deutsches Arzteblatt international, 2009. **106**(16): p. 269-275.

35.   Hossain, M.A., et al., *A single-chain derivative of the relaxin hormone is a functionally selective agonist of the G protein-coupled receptor, RXFP1.* Chem Sci, 2016. **7**(6): p. 3805-3819.

36.   van der Westhuizen, E.T., et al., *Relaxin family peptide receptors--from orphans to therapeutic targets.* Drug Discov Today, 2008. **13**(15-16): p. 640-51.

37.   Bathgate, R.A., et al., *Relaxin family peptides and their receptors.* Physiol Rev, 2013. **93**(1): p. 405-80.

38.   Conrad, K.P., *Maternal vasodilation in pregnancy: the emerging role of relaxin.* Am J Physiol Regul Integr Comp Physiol, 2011. **301**(2): p. R267-75.

39.   MacLennan, A.H., *The role of the hormone relaxin in human reproduction and pelvic girdle relaxation.* Scand J Rheumatol Suppl, 1991. **88**: p. 7-15.

40.   Chan, L.J., et al., *The relaxin peptide family--structure, function and clinical applications.* Protein Pept Lett, 2011. **18**(3): p. 220-9.

41.   Schwabe, C. and J.K. McDonald, *Relaxin: a disulfide homolog of insulin.* Science, 1977. **197**(4306): p. 914-5.

42.   Crawford, R.J., et al., *Two human relaxin genes are on chromosome 9.* The EMBO journal, 1984. **3**(10): p. 2341-2345.

43.   Hossain, M.A. and J.D. Wade, *Synthetic relaxins.* Curr Opin Chem Biol, 2014. **22**: p. 47-55.

44.   Teichman, S.L., et al., *Relaxin, a pleiotropic vasodilator for the treatment of heart failure.* Heart failure reviews, 2009. **14**(4): p. 321-329.

45.   Parry, L.J. and L.A. Vodstrcil, *Relaxin physiology in the female reproductive tract during pregnancy.* Adv Exp Med Biol, 2007. **612**: p. 34-48.

46.   Dschietzig, T., et al., *The pregnancy hormone relaxin is a player in human heart failure.* FASEB J, 2001. **15**(12): p. 2187-95.

47.   Halls, M.L., et al., *International Union of Basic and Clinical Pharmacology. XCV. Recent advances in the understanding of the pharmacology and biological roles of relaxin family peptide receptors 1-4, the receptors for relaxin family peptides.* Pharmacol Rev, 2015. **67**(2): p. 389-440.

48.   Bathgate, R.A., et al., *Relaxin: new peptides, receptors and novel actions.* Trends Endocrinol Metab, 2003. **14**(5): p. 207-13.

49.   Sarwar, M., et al., *The actions of relaxin on the human cardiovascular system.* Br J Pharmacol, 2017. **174**(10): p. 933-949.

50.   Samuel, C.S., *Relaxin: antifibrotic properties and effects in models of disease.* Clinical medicine & research, 2005. **3**(4): p. 241-249.

51.   Park, J.-I., et al., *Regulation of Receptor Signaling by Relaxin A Chain Motifs: DERIVATION OF PAN-SPECIFIC AND LGR7-SPECIFIC HUMAN RELAXIN ANALOGS.* Journal of Biological Chemistry, 2008. **283**(46): p. 32099-32109.

52.   BÜLlesbach, E.E. and C. Schwabe, *On the receptor binding site of relaxins.* International Journal of Peptide and Protein Research, 1988. **32**(5): p. 361-367.

53.   Büllesbach, E.E. and C. Schwabe, *Synthesis and conformational analysis of the insulin-like 4 gene product.* The Journal of Peptide Research, 2001. **57**(1): p. 77-83.

54.   Büllesbach, E.E. and C. Schwabe, *The Relaxin Receptor-binding Site Geometry Suggests a Novel Gripping Mode of Interaction.* Journal of Biological Chemistry, 2000. **275**(45): p. 35276-35280.

55. Dschietzig, T., et al., *The positive inotropic effect of relaxin-2 in human atrial myocardium is preserved in end-stage heart failure: role of G(i)-phosphoinositide-3 kinase signaling.* J Card Fail, 2011. **17**(2): p. 158-66.

56. Du, X.J., et al., *Cardiovascular effects of relaxin: from basic science to clinical therapy.* Nat Rev Cardiol, 2010. **7**(1): p. 48-58.

57. Bani, D., et al., *Relaxin protects against myocardial injury caused by ischemia and reperfusion in rat heart.* Am J Pathol, 1998. **152**(5): p. 1367-76.

58. Debrah Dan, O., et al., *Relaxin Increases Cardiac Output and Reduces Systemic Arterial Load in Hypertensive Rats.* Hypertension, 2005. **46**(4): p. 745-750.

59. Boccalini, G., et al., *Relaxin protects cardiac muscle cells from hypoxia/reoxygenation injury: involvement of the Notch-1 pathway.* FASEB J, 2015. **29**(1): p. 239-49.

60. Nistri, S., et al., *Relaxin promotes growth and maturation of mouse neonatal cardiomyocytes in vitro: clues for cardiac regeneration.* Journal of cellular and molecular medicine, 2012. **16**(3): p. 507-519.

61. Samuel, C.S., et al., *'Relaxin' the stiffened heart and arteries: the therapeutic potential for relaxin in the treatment of cardiovascular disease.* Pharmacol Ther, 2006. **112**(2): p. 529-52.

62. Piedras-Renteria, E.S., O.D. Sherwood, and P.M. Best, *Effects of relaxin on rat atrial myocytes. II. Increased calcium influx derived from action potential prolongation.* Am J Physiol, 1997. **272**(4 Pt 2): p. H1798-803.

63. Pintalhao, M., et al., *Relaxin serum levels in acute heart failure are associated with pulmonary hypertension and right heart overload.* Eur J Heart Fail, 2017. **19**(2): p. 218-225.

64. Kupari, M., et al., *Is the pregnancy hormone relaxin an important player in human heart failure?* Eur J Heart Fail, 2005. **7**(2): p. 195-8.

65. Xie, J., et al., *H2 relaxin expression and its effect on clinical outcomes in patients with chronic heart failure.* International journal of clinical and experimental medicine, 2015. **8**(3): p. 4420-4424.

66. Allen, L.A., et al., *Decision making in advanced heart failure: a scientific statement from the American Heart Association.* Circulation, 2012. **125**(15): p. 1928-1952.

67. Bathgate, R.A., et al., *International Union of Pharmacology LVII: Recommendations for the Nomenclature of Receptors for Relaxin Family Peptides.* Pharmacological Reviews, 2006. **58**(1): p. 7.

68. Hsu, S.Y., et al., *Activation of orphan receptors by the hormone relaxin.* Science, 2002. **295**(5555): p. 671-4.

69. Hopkins, E.J., et al., *The NMR solution structure of the relaxin (RXFP1) receptor lipoprotein receptor class A module and identification of key residues in the N-terminal region of the module that mediate receptor activation.* J Biol Chem, 2007. **282**(6): p. 4172-84.

70. Büllesbach, E.E. and C. Schwabe, *The Trap-like Relaxin-binding Site of the Leucine-rich G-protein-coupled Receptor 7.* Journal of Biological Chemistry, 2005. **280**(14): p. 14051-14056.

71. Scott, D.J., K.J. Rosengren, and R.A.D. Bathgate, *The different ligand-binding modes of relaxin family peptide receptors RXFP1 and RXFP2.* Molecular endocrinology (Baltimore, Md.), 2012. **26**(11): p. 1896-1906.

72. Hartley, B.J., et al., *Resolving the unconventional mechanisms underlying RXFP1 and RXFP2 receptor function.* Ann N Y Acad Sci, 2009. **1160**: p. 67-73.

73. Scott, D.J., G.W. Tregear, and R.A. Bathgate, *Modeling the primary hormone-binding site of RXFP1 and RXFP2.* Ann N Y Acad Sci, 2009. **1160**: p. 74-7.

References

74.   Hu, X., et al., *Structural Insights into the Activation of Human Relaxin Family Peptide Receptor 1 by Small-Molecule Agonists.* Biochemistry, 2016. **55**(12): p. 1772-1783.

75.   Halls, M.L., et al., *Relaxin family peptide receptor (RXFP1) coupling to G(alpha)i3 involves the C-terminal Arg752 and localization within membrane Raft Microdomains.* Mol Pharmacol, 2009. **75**(2): p. 415-28.

76.   Halls, M.L., R.A. Bathgate, and R.J. Summers, *Relaxin family peptide receptors RXFP1 and RXFP2 modulate cAMP signaling by distinct mechanisms.* Mol Pharmacol, 2006. **70**(1): p. 214-26.

77.   Kompa, A.R., C.S. Samuel, and R.J. Summers, *Inotropic responses to human gene 2 (B29) relaxin in a rat model of myocardial infarction (MI): effect of pertussis toxin.* Br J Pharmacol, 2002. **137**(5): p. 710-8.

78.   Dessauer, C.W. and B.T. Nguyen, *Relaxin stimulates multiple signaling pathways: activation of cAMP, PI3K, and PKCzeta in THP-1 cells.* Ann N Y Acad Sci, 2005. **1041**: p. 272-9.

79.   Nguyen, B.T., et al., *Phosphoinositide 3-kinase activity is required for biphasic stimulation of cyclic adenosine 3',5'-monophosphate by relaxin.* Mol Endocrinol, 2003. **17**(6): p. 1075-84.

80.   Xiao, J., et al., *Discovery, optimization, and characterization of a novel series of dopamine D2 versus D3 receptor selective antagonists*, in *Probe Reports from the NIH Molecular Libraries Program.* 2010: Bethesda (MD).

81.   Osheroff, P.L., M.J. Cronin, and J.A. Lofgren, *Relaxin binding in the rat heart atrium.* Proc Natl Acad Sci U S A, 1992. **89**(6): p. 2384-8.

82.   Xiang, Y. and B.K. Kobilka, *Myocyte Adrenoceptor Signaling Pathways.* Science, 2003. **300**(5625): p. 1530.

83.   Métrich, M., et al., *Epac Mediates β-Adrenergic Receptor–Induced Cardiomyocyte Hypertrophy.* Circulation Research, 2008. **102**(8): p. 959-965.

84.   Najafi, A., et al., *β-adrenergic receptor signalling and its functional consequences in the diseased heart.* European Journal of Clinical Investigation, 2016. **46**(4): p. 362-374.

85.   Xiao, R.-P., *β-Adrenergic Signaling in the Heart: Dual Coupling of the β<sub>2</sub>-Adrenergic Receptor to G<sub>s</sub> and G<sub>i</sub> Proteins.* Science's STKE, 2001. **2001**(104): p. re15.

86.   Sikkel, M.B., et al., *SERCA2a gene therapy in heart failure: an anti-arrhythmic positive inotrope.* British journal of pharmacology, 2014. **171**(1): p. 38-54.

87.   de Lucia, C., A. Eguchi, and W.J. Koch, *New Insights in Cardiac β-Adrenergic Signaling During Heart Failure and Aging.* Frontiers in pharmacology, 2018. **9**: p. 904-904.

88.   Halls, M.L., R.A.D. Bathgate, and R.J. Summers, *Relaxin Family Peptide Receptors RXFP1 and RXFP2 Modulate cAMP Signaling by Distinct Mechanisms.* Molecular Pharmacology, 2006. **70**(1): p. 214.

89.   Callander, G.E., W.G. Thomas, and R.A. Bathgate, *Prolonged RXFP1 and RXFP2 signaling can be explained by poor internalization and a lack of beta-arrestin recruitment.* Am J Physiol Cell Physiol, 2009. **296**(5): p. C1058-66.

90.   Atchison, R.W., B.C. Casto, and W.M. Hammon, *Adenovirus-Associated Defective Virus Particles.* Science, 1965. **149**(3685): p. 754-6.

91.   Hoggan, M.D., N.R. Blacklow, and W.P. Rowe, *Studies of small DNA viruses found in various adenovirus preparations: physical, biological, and immunological characteristics.* Proc Natl Acad Sci U S A, 1966. **55**(6): p. 1467-74.

92.   Buller, R.M., et al., *Herpes simplex virus types 1 and 2 completely help adenovirus-associated virus replication.* J Virol, 1981. **40**(1): p. 241-7.

93.   McPherson, R.A., L.J. Rosenthal, and J.A. Rose, *Human cytomegalovirus completely helps adeno-associated virus replication.* Virology, 1985. **147**(1): p. 217-22.

94.   Schlehofer, J.R., M. Ehrbar, and H. zur Hausen, *Vaccinia virus, herpes simplex virus, and carcinogens induce DNA amplification in a human cell line and support replication of a helpervirus dependent parvovirus.* Virology, 1986. **152**(1): p. 110-7.

95.   Meyers, C., et al., *Altered biology of adeno-associated virus type 2 and human papillomavirus during dual infection of natural host tissue.* Virology, 2001. **287**(1): p. 30-9.

96.   Chiorini, J.A., et al., *Cloning and characterization of adeno-associated virus type 5.* J Virol, 1999. **73**(2): p. 1309-19.

97.   Gao, G., et al., *Clades of Adeno-associated viruses are widely disseminated in human tissues.* J Virol, 2004. **78**(12): p. 6381-8.

98.   Muramatsu, S., et al., *Nucleotide sequencing and generation of an infectious clone of adeno-associated virus 3.* Virology, 1996. **221**(1): p. 208-17.

99.   Srivastava, A., E.W. Lusby, and K.I. Berns, *Nucleotide sequence and organization of the adeno-associated virus 2 genome.* J Virol, 1983. **45**(2): p. 555-64.

100.   Rutledge, E.A., C.L. Halbert, and D.W. Russell, *Infectious clones and vectors derived from adeno-associated virus (AAV) serotypes other than AAV type 2.* J Virol, 1998. **72**(1): p. 309-19.

101.   Xiao, W., et al., *Gene therapy vectors based on adeno-associated virus type 1.* J Virol, 1999. **73**(5): p. 3994-4003.

102.   Gao, G.P., et al., *Novel adeno-associated viruses from rhesus monkeys as vectors for human gene therapy.* Proc Natl Acad Sci U S A, 2002. **99**(18): p. 11854-9.

103.   Chiorini, J.A., et al., *Cloning of adeno-associated virus type 4 (AAV4) and generation of recombinant AAV4 particles.* J Virol, 1997. **71**(9): p. 6823-33.

104.   Mori, S., et al., *Two novel adeno-associated viruses from cynomolgus monkey: pseudotyping characterization of capsid protein.* Virology, 2004. **330**(2): p. 375-83.

105.   Schmidt, M., et al., *Adeno-associated virus type 12 (AAV12): a novel AAV serotype with sialic acid- and heparan sulfate proteoglycan-independent transduction activity.* J Virol, 2008. **82**(3): p. 1399-406.

106.   Forsayeth, J.R. and K.S. Bankiewicz, *AAV9: over the fence and into the woods.* Mol Ther, 2011. **19**(6): p. 1006-7.

107.   Zincarelli, C., et al., *Analysis of AAV serotypes 1-9 mediated gene expression and tropism in mice after systemic injection.* Mol Ther, 2008. **16**(6): p. 1073-80.

108.   Zincarelli, C., et al., *Analysis of AAV Serotypes 1–9 Mediated Gene Expression and Tropism in Mice After Systemic Injection.* Molecular Therapy, 2008. **16**(6): p. 1073-1080.

109.   Zinn, E. and L.H. Vandenberghe, *Adeno-associated virus: fit to serve.* Current opinion in virology, 2014. **8**: p. 90-97.

110.   Clark, K.R., T.J. Sferra, and P.R. Johnson, *Recombinant Adeno-Associated Viral Vectors Mediate Long-Term Transgene Expression in Muscle.* Human Gene Therapy, 1997. **8**(6): p. 659-669.

111.   Louis Jeune, V., et al., *Pre-existing anti-adeno-associated virus antibodies as a challenge in AAV gene therapy.* Human gene therapy methods, 2013. **24**(2): p. 59-67.

112.   Qiao, C., et al., *K137R mutation on adeno-associated viral capsids had minimal effect on enhancing gene delivery in vivo.* Human gene therapy methods, 2014. **25**(1): p. 33-39.

References

113. Koo, T., et al., *Triple Trans-Splicing Adeno-Associated Virus Vectors Capable of Transferring the Coding Sequence for Full-Length Dystrophin Protein into Dystrophic Mice.* Human Gene Therapy, 2013. **25**(2): p. 98-108.

114. Mitchell, A.M., et al., *AAV's anatomy: roadmap for optimizing vectors for translational success.* Current gene therapy, 2010. **10**(5): p. 319-340.

115. Grieger, J.C. and R.J. Samulski, *Adeno-associated virus vectorology, manufacturing, and clinical applications.* Methods Enzymol, 2012. **507**: p. 229-54.

116. Chamberlain, K., J.M. Riyad, and T. Weber, *Cardiac gene therapy with adeno-associated virus-based vectors.* Current opinion in cardiology, 2017: p. 10.1097/HCO.0000000000000386.

117. Jaski, B.E., et al., *Calcium upregulation by percutaneous administration of gene therapy in cardiac disease (CUPID Trial), a first-in-human phase 1/2 clinical trial.* Journal of cardiac failure, 2009. **15**(3): p. 171-181.

118. Wu, Z., et al., *Alpha2,3 and alpha2,6 N-linked sialic acids facilitate efficient binding and transduction by adeno-associated virus types 1 and 6.* J Virol, 2006. **80**(18): p. 9093-103.

119. Akache, B., et al., *The 37/67-kilodalton laminin receptor is a receptor for adeno-associated virus serotypes 8, 2, 3, and 9.* J Virol, 2006. **80**(19): p. 9831-6.

120. Duan, D., et al., *Dynamin is required for recombinant adeno-associated virus type 2 infection.* J Virol, 1999. **73**(12): p. 10371-6.

121. Sanlioglu, S., et al., *Endocytosis and nuclear trafficking of adeno-associated virus type 2 are controlled by rac1 and phosphatidylinositol-3 kinase activation.* J Virol, 2000. **74**(19): p. 9184-96.

122. Nonnenmacher, M. and T. Weber, *Adeno-associated virus 2 infection requires endocytosis through the CLIC/GEEC pathway.* Cell Host Microbe, 2011. **10**(6): p. 563-76.

123. Akache, B., et al., *A two-hybrid screen identifies cathepsins B and L as uncoating factors for adeno-associated virus 2 and 8.* Mol Ther, 2007. **15**(2): p. 330-9.

124. Bartlett, J.S., R. Wilcher, and R.J. Samulski, *Infectious entry pathway of adeno-associated virus and adeno-associated virus vectors.* J Virol, 2000. **74**(6): p. 2777-85.

125. Xiao, W., et al., *Adenovirus-facilitated nuclear translocation of adeno-associated virus type 2.* J Virol, 2002. **76**(22): p. 11505-17.

126. Schnepp, B.C., et al., *Characterization of adeno-associated virus genomes isolated from human tissues.* J Virol, 2005. **79**(23): p. 14793-803.

127. Chandler, R.J. and C.P. Venditti, *Gene Therapy for Metabolic Diseases.* Transl Sci Rare Dis, 2016. **1**(1): p. 73-89.

128. Katus, H.A., R. Bekeredjian, and O.J. Müller, *Targeting the heart with gene therapy-optimized gene delivery methods.* Cardiovascular Research, 2007. **73**(3): p. 453-462.

129. Franz, W.M., et al., *Analysis of tissue-specific gene delivery by recombinant adenoviruses containing cardiac-specific promoters.* Cardiovasc Res, 1997. **35**(3): p. 560-6.

130. Aikawa, R., G.S. Huggins, and R.O. Snyder, *Cardiomyocyte-specific gene expression following recombinant adeno-associated viral vector transduction.* J Biol Chem, 2002. **277**(21): p. 18979-85.

131. Muller, O.J., et al., *Improved cardiac gene transfer by transcriptional and transductional targeting of adeno-associated viral vectors.* Cardiovasc Res, 2006. **70**(1): p. 70-8.

132. Teerlink, J.R., et al., *Serelaxin in addition to standard therapy in acute heart failure: rationale and design of the RELAX-AHF-2 study.* Eur J Heart Fail, 2017. **19**(6): p. 800-809.

120

133.	Grimm, D., M.A. Kay, and J.A. Kleinschmidt, *Helper virus-free, optically controllable, and two-plasmid-based production of adeno-associated virus vectors of serotypes 1 to 6.* Mol Ther, 2003. **7**(6): p. 839-50.

134.	Grimm, D., et al., *Novel Tools for Production and Purification of Recombinant Adenoassociated Virus Vectors.* Human Gene Therapy, 1998. **9**(18): p. 2745-2760.

135.	Jungmann, A., et al., *Protocol for efficient generation and characterization of adeno-associated viral (AAV) vectors.* Hum Gene Ther Methods, 2017.

136.	McClure, C., et al., *Production and titering of recombinant adeno-associated viral vectors.* Journal of visualized experiments : JoVE, 2011(57): p. e3348-e3348.

137.	Pleger, S.T., et al., *Cardiac AAV9-S100A1 gene therapy rescues post-ischemic heart failure in a preclinical large animal model.* Science translational medicine, 2011. **3**(92): p. 92ra64-92ra64.

138.	Zolotukhin, S., et al., *Recombinant adeno-associated virus purification using novel methods improves infectious titer and yield.* Gene Therapy, 1999. **6**: p. 973.

139.	Jungmann, A., et al., *Rapid and highly efficient inducible cardiac gene knockout in adult mice using AAV-mediated expression of Cre recombinase.* Cardiovascular Research, 2014. **104**(1): p. 15-23.

140.	Golden, H.B., et al., *Isolation of Cardiac Myocytes and Fibroblasts from Neonatal Rat Pups*, in *Cardiovascular Development: Methods and Protocols*, X. Peng and M. Antonyak, Editors. 2012, Humana Press: Totowa, NJ. p. 205-214.

141.	Schlegel, P., et al., *G protein-coupled receptor kinase 2 promotes cardiac hypertrophy.* PLoS One, 2017. **12**(7): p. e0182110.

142.	deAlmeida, A.C., R.J. van Oort, and X.H. Wehrens, *Transverse aortic constriction in mice.* J Vis Exp, 2010(38).

143.	Rockman, H.A., et al., *Segregation of atrial-specific and inducible expression of an atrial natriuretic factor transgene in an in vivo murine model of cardiac hypertrophy.* Proceedings of the National Academy of Sciences of the United States of America, 1991. **88**(18): p. 8277-8281.

144.	Rio, D.C., et al., *Purification of RNA using TRIzol (TRI reagent).* Cold Spring Harb Protoc, 2010. **2010**(6): p. pdb prot5439.

145.	Livak, K.J. and T.D. Schmittgen, *Analysis of relative gene expression data using real-time quantitative PCR and the 2(-Delta Delta C(T)) Method.* Methods, 2001. **25**(4): p. 402-8.

146.	Towbin, H., T. Staehelin, and J. Gordon, *Electrophoretic transfer of proteins from polyacrylamide gels to nitrocellulose sheets: procedure and some applications.* Proceedings of the National Academy of Sciences of the United States of America, 1979. **76**(9): p. 4350-4354.

147.	Mahmood, T. and P.-C. Yang, *Western blot: technique, theory, and trouble shooting.* North American journal of medical sciences, 2012. **4**(9): p. 429-434.

148.	Yu, J., et al., *Differential Activation of Cultured Neonatal Cardiomyocytes by Plasmalemmal Versus Intracellular G Protein-coupled Receptor 55.* Journal of Biological Chemistry, 2013. **288**(31): p. 22481-22492.

149.	Grynkiewicz, G., M. Poenie, and R.Y. Tsien, *A new generation of Ca2+ indicators with greatly improved fluorescence properties.* Journal of Biological Chemistry, 1985. **260**(6): p. 3440-3450.

150.	Debrah, D.O., et al., *Relaxin increases cardiac output and reduces systemic arterial load in hypertensive rats.* Hypertension, 2005. **46**(4): p. 745-50.

151.	Teerlink, J.R., et al., *Serelaxin, recombinant human relaxin-2, for treatment of acute heart failure (RELAX-AHF): a randomised, placebo-controlled trial.* Lancet, 2013. **381**(9860): p. 29-39.

References

152. Teerlink, J.R., et al., *Relaxin for the treatment of patients with acute heart failure (Pre-RELAX-AHF): a multicentre, randomised, placebo-controlled, parallel-group, dose-finding phase IIb study.* Lancet, 2009. **373**(9673): p. 1429-39.

153. Devarakonda, T.V., et al., *Targeted Gene Therapy with RXFP1 Attenuates Myocardial Infarction and Preserves Left Ventricular Function in Mice.* The FASEB Journal, 2018. **32**(1_supplement): p. 580.14-580.14.

154. Samuel, C.S., et al., *Relaxin Modulates Cardiac Fibroblast Proliferation, Differentiation, and Collagen Production and Reverses Cardiac Fibrosis in Vivo.* Endocrinology, 2004. **145**(9): p. 4125-4133.

155. Scott, D.J., et al., *Characterization of the Mouse and Rat Relaxin Receptors.* Annals of the New York Academy of Sciences, 2006. **1041**(1): p. 8-12.

156. Zordan, R.E., et al., *Avoiding the ends: internal epitope tagging of proteins using transposon Tn7.* Genetics, 2015. **200**(1): p. 47-58.

157. Elliott, S., et al., *Progress in detecting cell-surface protein receptors: the erythropoietin receptor example.* Annals of hematology, 2014. **93**(2): p. 181-192.

158. Walter, P. and D. Ron, *The Unfolded Protein Response: From Stress Pathway to Homeostatic Regulation.* Science, 2011. **334**(6059): p. 1081.

159. Bravo, R., et al., *Endoplasmic reticulum and the unfolded protein response: dynamics and metabolic integration.* International review of cell and molecular biology, 2013. **301**: p. 215-290.

160. Schröder, M. and R.J. Kaufman, *ER stress and the unfolded protein response.* Mutation Research/Fundamental and Molecular Mechanisms of Mutagenesis, 2005. **569**(1): p. 29-63.

161. Halls, M.L. and D.M. Cooper, *Sub-picomolar relaxin signalling by a pre-assembled RXFP1, AKAP79, AC2, beta-arrestin 2, PDE4D3 complex.* EMBO J, 2010. **29**(16): p. 2772-87.

162. Hsu, S.Y., et al., *The Three Subfamilies of Leucine-Rich Repeat-Containing G Protein-Coupled Receptors (LGR): Identification of LGR6 and LGR7 and the Signaling Mechanism for LGR7.* Molecular Endocrinology, 2000. **14**(8): p. 1257-1271.

163. Dschietzig, T., et al., *Relaxin, a pregnancy hormone, is a functional endothelin-1 antagonist: attenuation of endothelin-1-mediated vasoconstriction by stimulation of endothelin type-B receptor expression via ERK-1/2 and nuclear factor-kappaB.* Circ Res, 2003. **92**(1): p. 32-40.

164. Sarwar, M., et al., *Serelaxin-mediated signal transduction in human vascular cells: bell-shaped concentration-response curves reflect differential coupling to G proteins.* Br J Pharmacol, 2015. **172**(4): p. 1005-19.

165. Zhang, Q., et al., *Relaxin activates the MAP kinase pathway in human endometrial stromal cells.* J Cell Biochem, 2002. **85**(3): p. 536-44.

166. Ahmad, N., et al., *Relaxin induces matrix-metalloproteinases-9 and -13 via RXFP1: induction of MMP-9 involves the PI3K, ERK, Akt and PKC-ζ pathways.* Molecular and cellular endocrinology, 2012. **363**(1-2): p. 46-61.

167. Dschietzig, T., et al., *RXFP1-inactive relaxin activates human glucocorticoid receptor: Further investigations into the relaxin–GR pathway.* Regulatory Peptides, 2009. **154**(1): p. 77-84.

168. Haghighi, K., P. Bidwell, and E.G. Kranias, *Phospholamban interactome in cardiac contractility and survival: A new vision of an old friend.* J Mol Cell Cardiol, 2014. **77**: p. 160-7.

169. Kaikkonen, L., et al., *p38alpha regulates SERCA2a function.* J Mol Cell Cardiol, 2014. **67**: p. 86-93.

170. Kranias, E.G. and R.J. Hajjar, *Modulation of cardiac contractility by the phospholamban/SERCA2a regulatome.* Circ Res, 2012. **110**(12): p. 1646-60.

171. Smeazzetto, S., et al., *Structure-function relation of phospholamban: modulation of channel activity as a potential regulator of SERCA activity.* PloS one, 2013. **8**(1): p. e52744-e52744.

172. Piedras-Renteria, E.S., O.D. Sherwood, and P.M. Best, *Effects of relaxin on rat atrial myocytes. I. Inhibition of I(to) via PKA-dependent phosphorylation.* American Journal of Physiology-Heart and Circulatory Physiology, 1997. **272**(4): p. H1791-H1797.

173. Bouchard, R.A., R.B. Clark, and W.R. Giles, *Effects of action potential duration on excitation-contraction coupling in rat ventricular myocytes. Action potential voltage-clamp measurements.* Circ Res, 1995. **76**(5): p. 790-801.

174. Duan, D., *Systemic delivery of adeno-associated viral vectors.* Current opinion in virology, 2016. **21**: p. 16-25.

175. Hodges, B.L., et al., *Local Delivery of a Viral Vector Mitigates Neutralization by Antiviral Antibodies and Results in Efficient Transduction of Rabbit Liver.* Molecular Therapy, 2005. **12**(6): p. 1043-1051.

176. Chan, K.Y., et al., *Engineered AAVs for efficient noninvasive gene delivery to the central and peripheral nervous systems.* Nature neuroscience, 2017. **20**(8): p. 1172-1179.

177. Gruntman, A.M., et al., *Gene transfer in skeletal and cardiac muscle using recombinant adeno-associated virus.* Current protocols in microbiology, 2013. **Chapter 14**: p. Unit-14D.3.

178. Wang, L., et al., *Systemic protein delivery by muscle-gene transfer is limited by a local immune response.* Blood, 2005. **105**(11): p. 4226-4234.

179. Ismay, G., *RELAXIN: ITS EFFECTS IN A CASE OF ACROSCLEROSIS.* British Journal of Dermatology, 1958. **70**(5): p. 171-175.

180. Samuel, C.S., et al., *Drugs of the future: the hormone relaxin.* Cellular and Molecular Life Sciences, 2007. **64**(12): p. 1539.

181. Han, X., Y. Habuchi, and W.R. Giles, *Relaxin increases heart rate by modulating calcium current in cardiac pacemaker cells.* Circ Res, 1994. **74**(3): p. 537-41.

182. Thomas, G.R. and R. Vandlen, *The purely chronotropic effects of relaxin in the rat isolated heart.* Journal of Pharmacy and Pharmacology, 1993. **45**(10): p. 927-928.

183. Xiao, J., et al., *Discovery, optimization, and biological activity of the first potent and selective small-molecule agonist series of human relaxin receptor 1 (RXFP1)*, in *Probe Reports from the NIH Molecular Libraries Program*. 2010: Bethesda (MD).

184. Houser Steven, R., et al., *Animal Models of Heart Failure.* Circulation Research, 2012. **111**(1): p. 131-150.

185. Zannad, F., et al., *Heart failure as an endpoint in heart failure and non-heart failure cardiovascular clinical trials: the need for a consensus definition.* European Heart Journal, 2008. **29**(3): p. 413-421.

186. Martins, J.B., W. Kim, and M.L. Marcus, *Chronic hypertension and left ventricular hypertrophy facilitate induction of sustained ventricular tachycardia in dogs 3 hours after left circumflex coronary artery occlusion.* Journal of the American College of Cardiology, 1989. **14**(5): p. 1365-1373.

187. Koyanagi, S., C. Eastham, and M.L. Marcus, *Effects of chronic hypertension and left ventricular hypertrophy on the incidence of sudden cardiac death after coronary artery occlusion in conscious dogs.* Circulation, 1982. **65**(6): p. 1192-7.

188. Barrick, C.J., et al., *Cardiac response to pressure overload in 129S1/SvImJ and C57BL/6J mice: temporal- and background-dependent development of concentric left*

References

    ventricular hypertrophy. American Journal of Physiology-Heart and Circulatory Physiology, 2007. **292**(5): p. H2119-H2130.

189. Garcia-Menendez, L., et al., *Substrain specific response to cardiac pressure overload in C57BL/6 mice.* American journal of physiology. Heart and circulatory physiology, 2013. **305**(3): p. H397-H402.

190. Wang, D., et al., *Effects of Pressure Overload on Extracellular Matrix Expression in the Heart of the Atrial Natriuretic Peptide–Null Mouse.* Hypertension, 2003. **42**(1): p. 88-95.

191. Songstad, N.T., et al., *Effect of Transverse Aortic Constriction on Cardiac Structure, Function and Gene Expression in Pregnant Rats.* PLOS ONE, 2014. **9**(2): p. e89559.

192. Xia, Y., et al., *Characterization of the inflammatory and fibrotic response in a mouse model of cardiac pressure overload.* Histochemistry and cell biology, 2009. **131**(4): p. 471-481.

193. Zhao, M., et al., *Microarray analysis of gene expression after transverse aortic constriction in mice.* Physiological Genomics, 2004. **19**(1): p. 93-105.

194. Baccari, M.C., et al., *Reversal by relaxin of altered ileal spontaneous contractions in dystrophic (mdx) mice through a nitric oxide-mediated mechanism.* Am J Physiol Regul Integr Comp Physiol, 2007. **293**(2): p. R662-8.

195. Dschietzig, T., et al., *Relaxin improves TNF-alpha-induced endothelial dysfunction: the role of glucocorticoid receptor and phosphatidylinositol 3-kinase signalling.* Cardiovasc Res, 2012. **95**(1): p. 97-107.

196. Mookerjee, I., et al., *Relaxin inhibits renal myofibroblast differentiation via RXFP1, the nitric oxide pathway, and Smad2.* FASEB J, 2009. **23**(4): p. 1219-29.

197. Agoulnik, A.I., *Relaxin and Related Peptides in Male Reproduction*, in *Relaxin and Related Peptides*, A.I. Agoulnik, Editor. 2007, Springer New York: New York, NY. p. 49-64.

198. Ivell, R., et al., *Relaxin family peptides in the male reproductive system—a critical appraisal.* MHR: Basic science of reproductive medicine, 2011. **17**(2): p. 71-84.

199. Weiss, G., *Relaxin in the male.* Biol Reprod, 1989. **40**(2): p. 197-200.

200. Chu, G., et al., *A Single Site (Ser16) Phosphorylation in Phospholamban Is Sufficient in Mediating Its Maximal Cardiac Responses to β-Agonists.* Journal of Biological Chemistry, 2000. **275**(49): p. 38938-38943.

201. Shuai, X.-x., et al., *Relaxin-2 improves diastolic function of pressure-overloaded rats via phospholamban by activating Akt.* International Journal of Cardiology, 2016. **218**: p. 305-311.

202. Samuel, C.S., et al., *Relaxin remodels fibrotic healing following myocardial infarction.* Lab Invest, 2011. **91**(5): p. 675-90.

203. Lekgabe Edna, D., et al., *Relaxin Reverses Cardiac and Renal Fibrosis in Spontaneously Hypertensive Rats.* Hypertension, 2005. **46**(2): p. 412-418.

204. Moore, X.L., et al., *Relaxin antagonizes hypertrophy and apoptosis in neonatal rat cardiomyocytes.* Endocrinology, 2007. **148**(4): p. 1582-9.

205. Chan, S.-L., J.G. Sweet, and M.J. Cipolla, *Treatment for cerebral small vessel disease: effect of relaxin on the function and structure of cerebral parenchymal arterioles during hypertension.* FASEB journal : official publication of the Federation of American Societies for Experimental Biology, 2013. **27**(10): p. 3917-3927.

206. Xu, Q., et al., *Relaxin Therapy Reverses Large Artery Remodeling and Improves Arterial Compliance in Senescent Spontaneously Hypertensive Rats.* Hypertension, 2010. **55**(5): p. 1260-1266.

207. Sakurai, S., et al., *Brain natriuretic peptide facilitates severity classification of stable chronic heart failure with left ventricular dysfunction.* Heart (British Cardiac Society), 2003. **89**(6): p. 661-662.

208. Fan, D., et al., *Cardiac fibroblasts, fibrosis and extracellular matrix remodeling in heart disease.* Fibrogenesis & tissue repair, 2012. **5**(1): p. 15-15.

209. McGuane, J.T., et al., *Angiogenic growth factors are new and essential players in the sustained relaxin vasodilatory pathway in rodents and humans.* Hypertension, 2011. **57**(6): p. 1151-60.

210. Bani-Sacchi, T., et al., *Relaxin-induced increased coronary flow through stimulation of nitric oxide production.* Br J Pharmacol, 1995. **116**(1): p. 1589-94.

211. Unemori, E.N., et al., *Relaxin stimulates expression of vascular endothelial growth factor in normal human endometrial cells in vitro and is associated with menometrorrhagia in women.* Hum Reprod, 1999. **14**(3): p. 800-6.

212. Unemori, E.N., et al., *Relaxin induces vascular endothelial growth factor expression and angiogenesis selectively at wound sites.* Wound Repair Regen, 2000. **8**(5): p. 361-70.

213. Halls, M.L., et al., *International Union of Basic and Clinical Pharmacology. XCV. Recent Advances in the Understanding of the Pharmacology and Biological Roles of Relaxin Family Peptide Receptors 1–4, the Receptors for Relaxin Family Peptides.* Pharmacological Reviews, 2015. **67**(2): p. 389.

214. Perna, A.M., et al., *Novel drug development opportunity for relaxin in acute myocardial infarction: evidences from a swine model.* FASEB J, 2005. **19**(11): p. 1525-7.

215. Tuteja, N., *Signaling through G protein coupled receptors.* Plant signaling & behavior, 2009. **4**(10): p. 942-947.

216. Horinouchi, T., et al., *Endothelin Receptor Signaling: New Insight Into Its Regulatory Mechanisms.* Journal of Pharmacological Sciences, 2013. **123**(2): p. 85-101.

217. Nguyen, B.T. and C.W. Dessauer, *Relaxin stimulates protein kinase C zeta translocation: requirement for cyclic adenosine 3',5'-monophosphate production.* Mol Endocrinol, 2005. **19**(4): p. 1012-23.

218. Nguyen, B.T. and C.W. Dessauer, *Relaxin stimulates cAMP production in MCF-7 cells upon overexpression of type V adenylyl cyclase.* Annals of the New York Academy of Sciences, 2005. **1041**: p. 296-299.

219. Göttle, M., et al., *Characterization of Mouse Heart Adenylyl Cyclase.* Journal of Pharmacology and Experimental Therapeutics, 2009. **329**(3): p. 1156.

220. Iwatsubo, K., et al., *Direct Inhibition of Type 5 Adenylyl Cyclase Prevents Myocardial Apoptosis without Functional Deterioration.* Journal of Biological Chemistry, 2004. **279**(39): p. 40938-40945.

221. Okumura, S., et al., *Type 5 Adenylyl Cyclase Disruption Alters Not Only Sympathetic But Also Parasympathetic and Calcium-Mediated Cardiac Regulation.* Circulation Research, 2003. **93**(4): p. 364-371.

222. Efendiev, R. and C.W. Dessauer, *A kinase-anchoring proteins and adenylyl cyclase in cardiovascular physiology and pathology.* J Cardiovasc Pharmacol, 2011. **58**(4): p. 339-44.

223. Defer, N., M. Best-Belpomme, and J. Hanoune, *Tissue specificity and physiological relevance of various isoforms of adenylyl cyclase.* American Journal of Physiology-Renal Physiology, 2000. **279**(3): p. F400-F416.

224. Huang, C., et al., *Organization of G proteins and adenylyl cyclase at the plasma membrane.* Molecular biology of the cell, 1997. **8**(12): p. 2365-2378.

References

225. Leroy, J., G. Vandecasteele, and R. Fischmeister, *Cyclic AMP signaling in cardiac myocytes.* Current Opinion in Physiology, 2018. **1**: p. 161-171.

226. Di Benedetto, G., et al., *Mitochondrial Ca2+ Uptake Induces Cyclic AMP Generation in the Matrix and Modulates Organelle ATP Levels.* Cell Metabolism, 2013. **17**(6): p. 965-975.

227. Kuschel, M., et al., *Ser16 prevails over Thr17 phospholamban phosphorylation in the β-adrenergic regulation of cardiac relaxation.* American Journal of Physiology-Heart and Circulatory Physiology, 1999. **276**(5): p. H1625-H1633.

228. Zarain-Herzberg, A., D.H. MacLennan, and M. Periasamy, *Characterization of rabbit cardiac sarco(endo)plasmic reticulum Ca2(+)-ATPase gene.* Journal of Biological Chemistry, 1990. **265**(8): p. 4670-4677.

229. Sayadi, M. and M. Feig, *Role of conformational sampling of Ser16 and Thr17-phosphorylated phospholamban in interactions with SERCA.* Biochimica et Biophysica Acta (BBA) - Biomembranes, 2013. **1828**(2): p. 577-585.

230. Marks, A.R., *Calcium and the heart: a question of life and death.* The Journal of clinical investigation, 2003. **111**(5): p. 597-600.

231. Kern, A. and G.D. Bryant-Greenwood, *Characterization of relaxin receptor (RXFP1) desensitization and internalization in primary human decidual cells and RXFP1-transfected HEK293 cells.* Endocrinology, 2009. **150**(5): p. 2419-28.

232. Penela, P., et al., *Mechanisms of regulation of G protein-coupled receptor kinases (GRKs) and cardiovascular disease.* Cardiovascular Research, 2006. **69**(1): p. 46-56.

233. Cong, M., et al., *Regulation of Membrane Targeting of the G Protein-coupled Receptor Kinase 2 by Protein Kinase A and Its Anchoring Protein AKAP79.* Journal of Biological Chemistry, 2001. **276**(18): p. 15192-15199.

234. Kamal, F.A., et al., *Simultaneous adrenal and cardiac g-protein-coupled receptor-gβγ inhibition halts heart failure progression.* Journal of the American College of Cardiology, 2014. **63**(23): p. 2549-2557.

235. Naga Prasad, S.V., et al., *Agonist-dependent Recruitment of Phosphoinositide 3-Kinase to the Membrane by β-Adrenergic Receptor Kinase 1: A ROLE IN RECEPTOR SEQUESTRATION.* Journal of Biological Chemistry, 2001. **276**(22): p. 18953-18959.

236. Beckendorf, J., M.M.G. van den Hoogenhof, and J. Backs, *Physiological and unappreciated roles of CaMKII in the heart.* Basic research in cardiology, 2018. **113**(4): p. 29-29.

237. Yano, M., Y. Ikeda, and M. Matsuzaki, *Altered intracellular Ca2+ handling in heart failure.* J Clin Invest, 2005. **115**(3): p. 556-64.

238. Fabiato, A., *Calcium-induced release of calcium from the cardiac sarcoplasmic reticulum.* Am J Physiol, 1983. **245**(1): p. C1-14.

239. Bers, D.M., *Cardiac excitation-contraction coupling.* Nature, 2002. **415**(6868): p. 198-205.

240. Bassani, J.W., R.A. Bassani, and D.M. Bers, *Relaxation in rabbit and rat cardiac cells: species-dependent differences in cellular mechanisms.* J Physiol, 1994. **476**(2): p. 279-93.

241. Mattiazzi, A. and E.G. Kranias, *The role of CaMKII regulation of phospholamban activity in heart disease.* Frontiers in pharmacology, 2014. **5**: p. 5-5.

242. Grimm, M. and J.H. Brown, *Beta-adrenergic receptor signaling in the heart: role of CaMKII.* Journal of molecular and cellular cardiology, 2010. **48**(2): p. 322-330.

243. Joiner, M.-l.A. and O.M. Koval, *CaMKII and stress mix it up in mitochondria.* Frontiers in Pharmacology, 2014. **5**(67).

126

244. Zhang, T., S. Miyamoto, and J.H. Brown, *Cardiomyocyte calcium and calcium/calmodulin-dependent protein kinase II: friends or foes?* Recent Prog Horm Res, 2004. **59**: p. 141-68.

245. Burgos, J.I., et al., *Nitric oxide and CaMKII: Critical steps in the cardiac contractile response To IGF-1 and swim training.* Journal of Molecular and Cellular Cardiology, 2017. **112**: p. 16-26.

246. Sethi, A., et al., *The complex binding mode of the peptide hormone H2 relaxin to its receptor RXFP1.* Nature communications, 2016. **7**: p. 11344-11344.

247. Scott, D.J., et al., *Identification and characterization of the mouse and rat relaxin receptors as the novel orthologues of human leucine-rich repeat-containing G-protein-coupled receptor 7.* Clin Exp Pharmacol Physiol, 2004. **31**(11): p. 828-32.

248. Overbeek, P.A., et al., *A transgenic insertion causing cryptorchidism in mice.* Genesis, 2001. **30**(1): p. 26-35.

249. Hsu, S.Y., S.G. Liang, and A.J. Hsueh, *Characterization of two LGR genes homologous to gonadotropin and thyrotropin receptors with extracellular leucine-rich repeats and a G protein-coupled, seven-transmembrane region.* Mol Endocrinol, 1998. **12**(12): p. 1830-45.

8   Acknowledgements